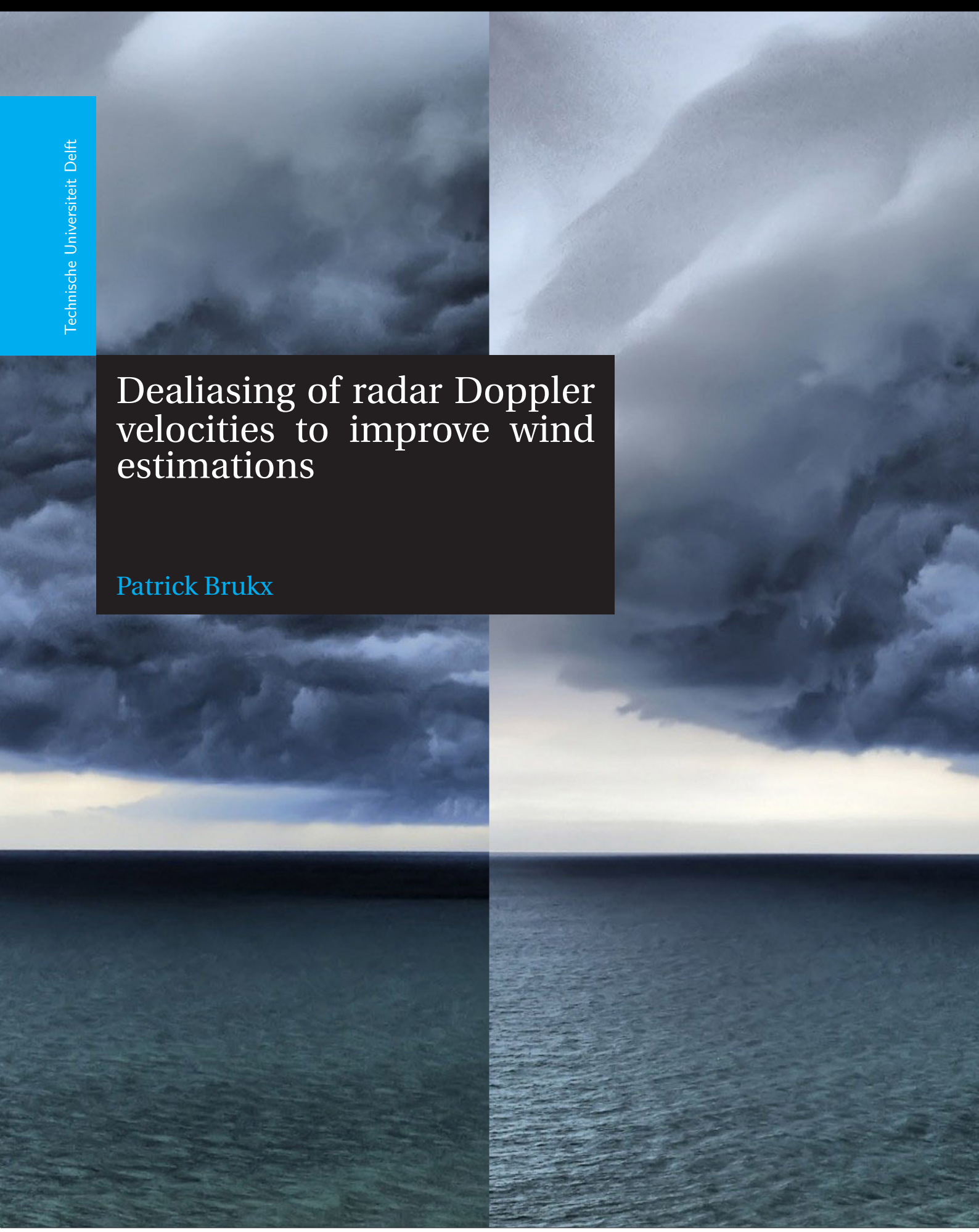

Technische Universiteit Delft

Dealiasing of radar Doppler velocities to improve wind estimations

Patrick Brukx

TU Delft Delft University of Technology

Challenge the future

DEALIASING OF RADAR DOPPLER VELOCITIES TO IMPROVE WIND ESTIMATIONS

by

Patrick Brukx

in partial fulfillment of the requirements for the degree of

Master of Science
in Electrical Engineering

at the Delft University of Technology,
to be defended publicly on Friday August 28, 2015 at 14:00h.

Supervisor:	Prof. dr. ir. Herman Russchenberg
Thesis committee:	Dr. Tim Vlemmix
	Dr. Oleg Krasnov
	Ir. Christine Unal

An electronic version of this thesis is available at http://repository.tudelft.nl/.

TU Delft Delft University of Technology

ABSTRACT

With its three beams in different directions, the Transportable Atmospheric RAdar system (TARA) can provide a wind field estimation. These estimations are inaccurate when the Doppler velocities in one or more of the three beams are aliased. Amongst different approaches to solve aliasing are a continuity check up to four dimensions, staggering PRT (Pulse Repetition Time) technique and a method using polarimetric information. The staggering PRT technique is not applicable, because it requires altering the radar system itself. For the main beam of TARA the method using polarimetric information is used, but for the offset beams no polarimetric information is available. The research presented in this thesis focuses on the dealiasing of the offset beams using a continuity check in one dimension. The assumed correctly dealiased main beam is used as a reference to compare the offset beams with.

The first step towards correct Doppler velocities is unfolding every individual Doppler spectrum. Then, a reference spectrum is searched for in the main beam. The first spectrum in the offset beam that is placed in the right Doppler velocity interval, is the one that is at the same height as the reference spectrum. From there on a continuity check is performed. First away from the radar and then towards the radar. Comparison is done by using the mean Doppler velocities of every Doppler spectrum.

The algorithm proposed in this thesis shows significant improvement in performance, compared with the old algorithm. In case of very wide Doppler spectra, a large difference between the reference and the current spectrum and clutter, the algorithm can fail.

ACKNOWLEDGEMENTS

The completion of this thesis would not have been possible without the support of many people. First of all I would like to thank my thesis supervisor Christine Unal for helping me manage my thesis, ranging from the content of my thesis to preparing me for the presentation. She has been a great motivator during this period and I really liked our discussions about the subject. I also like to thank Professor Russchenberg for his advice and feedback on my work.

I would like to thank my friends, Ed, Huub, Niek, Rens, Rik, Simon, Thomas and Wossos, for helping me to relax during the many Tepske weekends and vacations. This way I could continue to work with new energy.

Last but not least, I like to thank my parents for believing in me and supporting me all the way to the end.

CONTENTS

List of Figures

List of Tables

List of Abbreviations

FFT	Fast Fourier Transform
FM-CW	Frequency Modulated Continuous Wave
KNMI	Royal Netherlands Meteorological Institute
MB	Main Beam of TARA
OB1	Offset Beam 1 of TARA
OB2	Offset Beam 2 of TARA
PRT	Pulse Repetition Time
SNR	Signal-to-Noise Ratio
TARA	Transportable Atmospheric RAdar system
VAD	Vertical Azimuth Display

List of Symbols

α	elevation angle of the radar beams	°
α_w	wind direction in the local coordinate system (x,y)	°
λ	wavelength	m
ρ_{co}	cross-correlation coefficient	
σ_d	Doppler spectrum width	Hz
τ	delay	s
ϕ_r	phase of received signal	rad
ϕ_t	phase of transmitted signal	rad
c	speed of light	m s^{-1} (299,792,458)
f_b	beat frequency	Hz
f_d	Doppler frequency	Hz
n	number of intervals	
v_d	mean Doppler velocity	m s^{-1}
B	bandwidth	Hz
C_a	averaged cosine of the wind direction	
D_a	averaged wind direction	°
D_i	wind direction at time t_i	°
L_{dr}	Linear depolarization ratio	dB
N_d	Doppler bins in each Doppler spectrum	512
P_{tot}	total power	W
R	rainfall rate	mm h^{-1}
R	range	m
R_{xcorr}	result of the cross correlation function	
$S(v)$	Doppler power spectrum as function of Doppler velocity	
S_a	averaged sine of the wind direction	
T_m	measurement time	s
T_s	sweep time	s
V_a	averaged wind velocity	m s^{-1}
V_i	mean Doppler velocity of the current spectrum	m s^{-1}
V_i	wind velocity at time t_i	m s^{-1}
V_m	measured Doppler velocity	m s^{-1}
V_r	radial velocity	m s^{-1}
V_ref	mean Doppler velocity of a reference spectrum	m s^{-1}
V_t	true Doppler velocity	m s^{-1}
V_x	wind vector in x direction	m s^{-1}
V_y	wind vector in y direction	m s^{-1}
V_z	wind vector in z direction	m s^{-1}
$V_{D,max}$	Nyquist velocity	m s^{-1}
V_{MB}	measured Doppler velocity of the MB	m s^{-1}
V_{OB1}	measured Doppler velocity of OB1	m s^{-1}
V_{OB2}	measured Doppler velocity of the OB2	m s^{-1}
W	Doppler width	m s^{-1}
Z	reflectivity	mm^6 m^{-3}
Z_{dr}	differential reflectivity	dB

1

INTRODUCTION

Climate change is a hot topic. And for a reason. It will affect everyone in the world. Also, the world population grows and concentrates itself more and more in urban areas. Especially in urban areas the impacts of extreme weather events such as heavy rainfall and strong winds, resulting in inland flooding, are significant. Because of the combination of increasing extreme weather events, growing world population and increasing urbanization there is a need for tools to battle the effects of climate change. One of the most important instruments in this battle is information. When is it going to rain and how much? Is there going to be a strong wind and from what direction?

Rainfall rate and wind estimates are important components in weather forecasting. Meteorologic instruments, for example weather balloons and anemometers, can provide these components. But because of limited time and/or spatial resolutions these instruments can only be used for normal weather forecasts. However, short-term forecasting (nowcasting) is necessary to provide the information needed to battle the effects of climate change. For automated nowcasting a radar is the designated device. It can provide a high resolution forecast, nearly real-time. This can be used for example in warning systems (flooding, hurricane), safer landing of airplanes at airports, and in agriculture to protect crops from the weather.

Another utilization of the high resolutions provided by radar is for research purposes. For example to study the dynamics inside a rain cloud, the wind estimates has to be accurate and of high resolution. With more information on the dynamics inside rain clouds the weather forecast models can be updated, resulting in a better forecast.

In this thesis a method is discussed to improve wind estimates from the TU Delft radar TARA (section 1.3). The 3.3 GHz transmit frequency means TARA is especially suited for estimation of wind during rain and the presence of clouds. The displacement of precipitation can be retrieved by a Doppler measurement (section 1.2). Consequently the wind (direction and velocity) can be estimated. The reflectivity (Z) measured by weather radars can be used to estimate the rainfall rate (R) via a $Z-R$ power law [11]: $Z = aR^b$. The coefficients a and b vary due to changes in drop size distributions and terminal fall velocity. Often used as a first approximation is $a = 200$ and $b = 1.6$.

In short, better wind estimates can decrease the (economical) damage caused by climate change.

1.1. AIMS OF THE PROJECT

In radar technology, a well-known difficulty is to deal with ambiguity. Both in range and Doppler velocity. In this report a method is discussed/proposed to process aliased Doppler velocities in a Doppler FM-CW (Frequency Modulated Continuous Wave) radar. This results in better wind speed and wind direction estimation. The purpose of this project is to improve dealiasing of the offset beams of TARA on the basis of the following questions:

- How can the dealiasing of the offset beams be improved?
- Can the main beam be used as a reference?

This will be further explained in the next sections.

1.2. DOPPLER FM-CW RADAR

In figure 1.1 a visualization of the FM-CW principle is depicted.

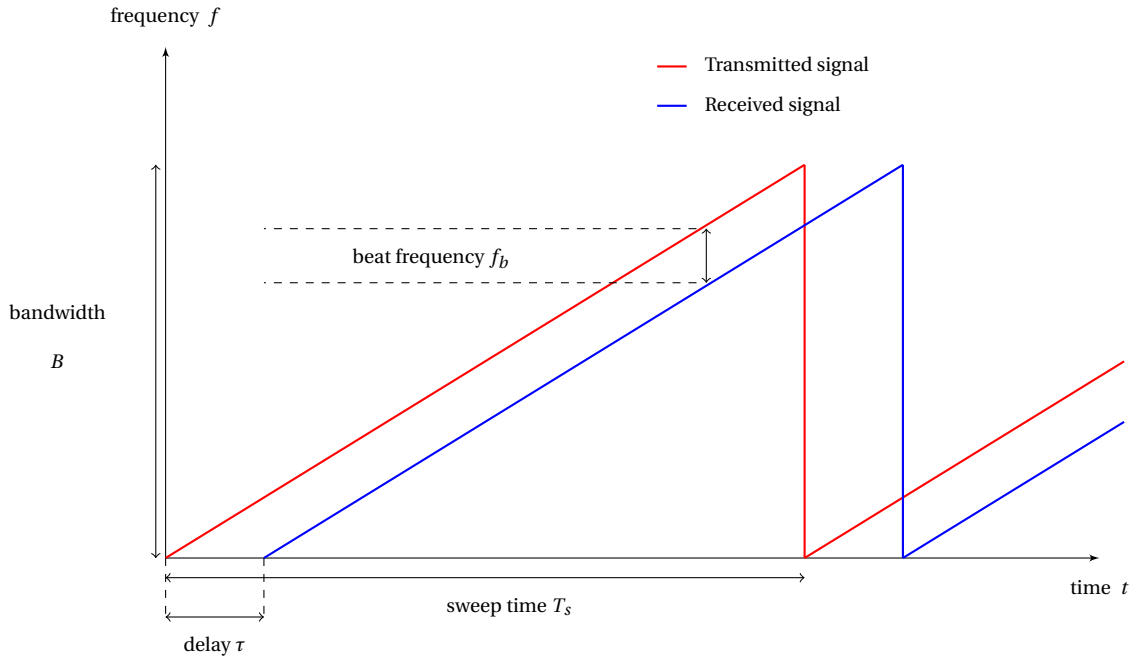

Figure 1.1: Visualization of the FM-CW principle.

The relation between the delay τ and the distance (range) between the antenna and the target is

$$\tau = \frac{2R}{c}, \tag{1.1}$$

where c is the speed of light and R is the range. In a FM-CW system the beat frequency contains information about the range, and can be calculated using equation 1.1 in

$$\frac{\tau}{T_s} = \frac{f_b}{B}, \tag{1.2}$$

where T_s is the sweep time, f_b is the beat frequency and B is the bandwidth. This results in

$$R = \frac{cT_s f_b}{2B}, \tag{1.3}$$

Doppler information is retrieved by using phase differences between successive measurements of the same targets (at fixed range). The phase of the received signal is

$$\phi_r = \phi_t + 2R\frac{2\pi}{\lambda}, \tag{1.4}$$

with ϕ_t the phase of the transmitted signal and λ the wavelength. The change of the phase of the received signal over time is given by

$$\frac{d\phi_r}{dt} = \frac{4\pi}{\lambda}\frac{dR}{dt} = \frac{4\pi}{\lambda}V_r, \tag{1.5}$$

with V_r is the radial velocity of the target. And the change of the phase of the received signal from sweep to sweep is given as

$$\frac{\Delta\phi_r}{T_s} = \frac{4\pi}{\lambda}V_r \longrightarrow V_r = \frac{\Delta\phi_r}{T_s}\frac{\lambda}{4\pi}, \tag{1.6}$$

Aliasing occurs when the change in phase is more than $\pm\pi$ from sweep to sweep. The maximum detectable Doppler velocity, the Nyquist velocity, is given by

$$V_{D,max} = \pm\frac{\lambda}{4T_s}, \tag{1.7}$$

where $V_{D,max}$ can be a positive or negative velocity. Thus a velocity away from or towards the radar. All targets detected by the radar are placed in the Doppler velocity measuring interval $-V_{D,max}$ to $V_{D,max}$, called the Nyquist co-interval. Aliasing occurs when the true velocity of a target is outside this interval. When the velocity of a target is in a different Doppler velocity interval, it is aliased $2nV_{D,max}$ to a velocity inside the Nyquist co-interval, where n is the number of intervals (positive or negative) away from the Nyquist co-interval, i.e. the Nyquist number. The measured Doppler velocity (V_m) is related to the true Doppler velocity (V_t) as follows:

$$V_m = V_t + 2nV_{D,max} \tag{1.8}$$

We have seen that the radial velocity of a single target at fixed range R can be calculated from two consecutive measurements of the phase of the received signal. When several targets are present at range R, like raindrops, a Fourier transform is carried out on a time series of the received signal to obtain a Doppler spectrum. The full processing of the Doppler FM-CW radar is shortly explained next.

A two dimensional FFT (Fast Fourier Transform) is used to calculate Doppler spectra from the received signal. In figure 1.2 a visualization of the process is depicted. Per sweep 1024 samples are taken. A first FFT per sweep is done and 512 range spectra are accumulated. These spectra contain the reflectivity per range resolution cell. After 512 sweeps a second FFT is calculated per range bin. The result is a Doppler spectrum of 512 (N_d) Doppler bins in each of the 512 range bins. Each Doppler spectrum represents the reflectivity weighted radial velocity distribution of all particles in the associated range resolution volume.

In many cases the Doppler spectrum of atmospheric particles is assumed to be Gaussian shaped [9]. In figure 1.3 a typical Doppler spectrum is depicted. In this figure the Doppler frequency spectrum is shown. To convert this into a Doppler velocity spectrum equation 1.9 is used.

$$f_d = \frac{2V_r}{\lambda} \longrightarrow V_r = \frac{f_d\lambda}{2}, \tag{1.9}$$

where f_d is the Doppler frequency. From the Doppler velocity spectrum the first three spectral moments are determined; total power, mean Doppler velocity and Doppler spectrum variance, using the following equations:

0th moment, total power

$$P_{tot} = \int S(v)dv, \tag{1.10}$$

where $S(v)$ denotes the Doppler power spectrum as function of Doppler velocity.

1st moment, mean Doppler velocity

$$v_d = \frac{1}{P_{tot}}\int vS(v)dv, \tag{1.11}$$

2nd moment, Doppler spectrum variance

$$\sigma_d^2 = \frac{1}{P_{tot}}\int (v - v_d)^2 S(v)dv \tag{1.12}$$

The Doppler spectrum width σ_d follows from the square root of the Doppler spectrum variance.

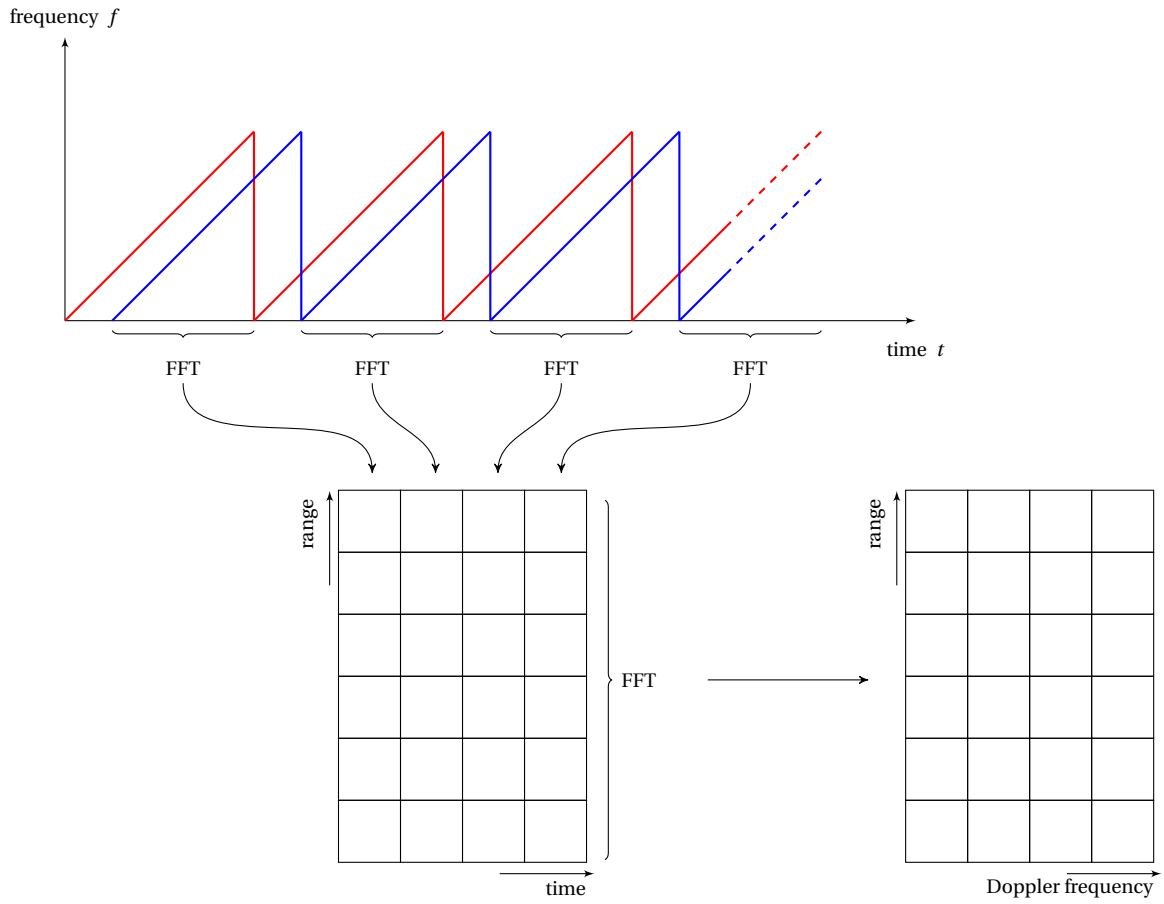

Figure 1.2: Visualization of the FM-CW principle and Doppler processing.

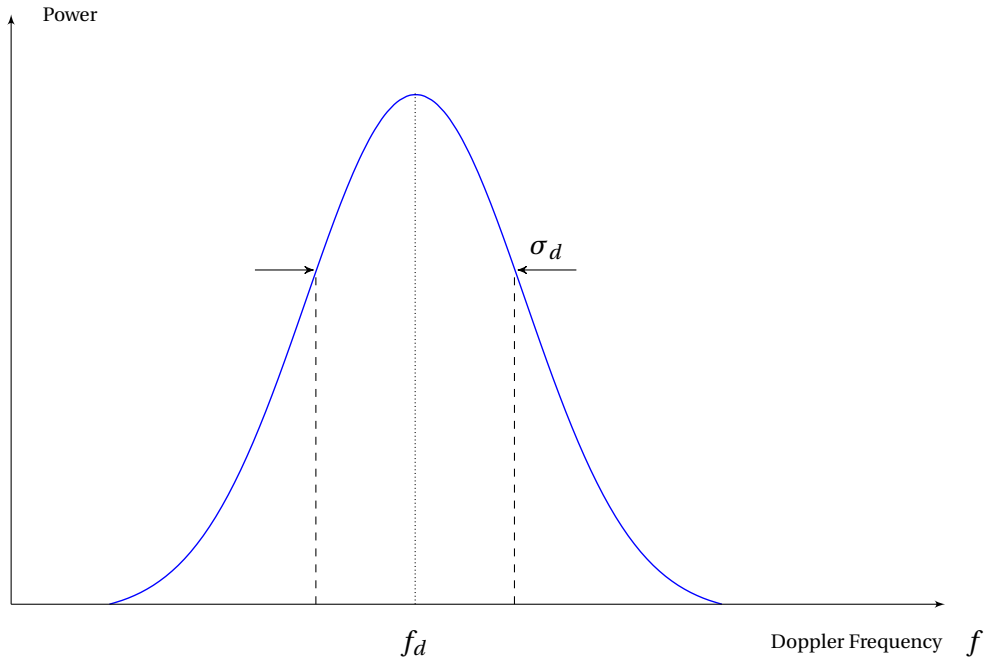

Figure 1.3: Typical Doppler spectrum with mean Doppler frequency f_d and Doppler width σ_d.

1.3. TARA

The radar used for this report is TARA (Transportable Atmospheric RAdar system). TARA has been developed at the Delft University of Technology (TUD) [7]. Recently, in 2011, there has been an update of the system [16]. TARA measures precipitation and ice/mixed-phased clouds. The radar provides height-time displays of different observables measured in real time: reflectivity (Z), differential reflectivity (Z_{dr}), linear depolarization ratio (L_{dr}), Doppler velocity (V_d) and Doppler width (W). TARA uses a digitized linear frequency sweep with a bandwidth that can be changed between 5 and 50 MHz. In this report all the results are obtained using a bandwidth of 5 MHz, which corresponds to a range resolution of 30 m. The maximum range is 15 km. These are the default specifications of TARA. The transmit frequency is 3.3 GHz. A sweep time (T_s) of 0.5 ms is used. There is a cycle of five measurements so that a total of 2.5 ms (T_m) is needed for one sequence. The extension of the measurement cycle time from 0.5 ms to 2.5 ms implies a drastic reduction of the maximum unambiguous Doppler velocity by a factor of five. Replacing T_s with T_m in equation 1.7 reduces $V_{D,max}$ from roughly 45 m s^{-1} to 9 m s^{-1}.

Three of the five sweeps are from the polarimetric main beam (MB), using polarizations vv, hv and hh. The other two measurements are from the single-polarized (vv) offset beams (OB1,OB2), that are 15° away in two orthogonal directions. In figure 1.4 the local coordinate system of TARA, based on its three beams, is depicted. Z is the vertical axis and (X,Y) is the horizontal plane. The main beam is located in the plane (X,Z) and has an elevation angle α, measured from the X axis. The X axis gives the azimuth angle of TARA related to the North. The offset beam OB1 is 15° away from the main beam, towards the Z axis, and it is thus also in the plane (X,Z). The offset beam OB2 is 15° away from the main beam in the Y direction. The plane MB-OB1 is orthogonal to the plane MB-OB2.

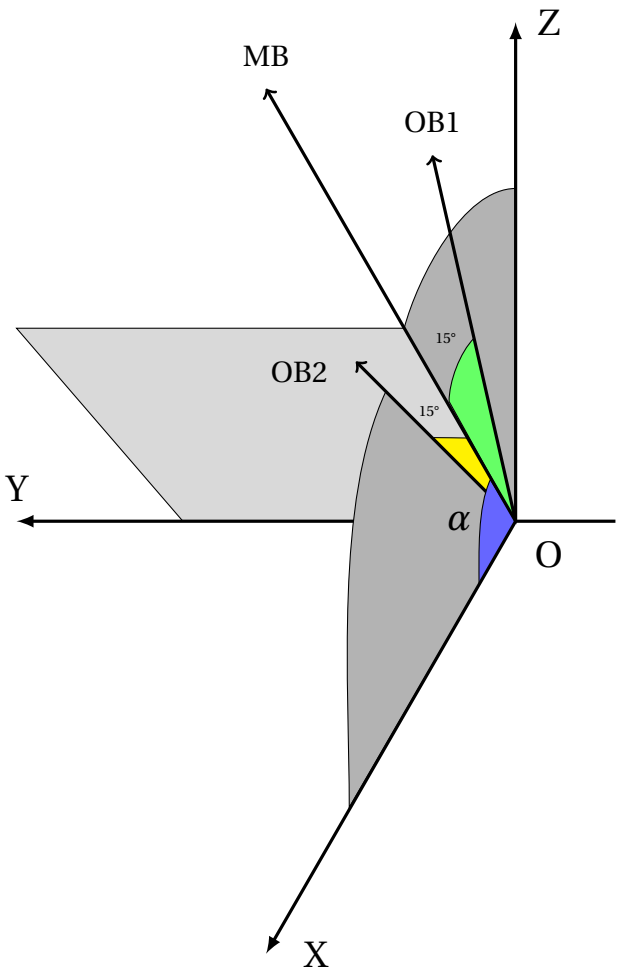

Figure 1.4: Local coordinate system of TARA, where X is the azimuth direction of the main beam and Z the vertical direction. α is the elevation angle of the main beam.

1.4. PREVIOUS WORK

In this section a small review is given on three different approaches to dealing with aliasing in Doppler radars.

1.4.1. DEALIASING SCHEMES FOR SCANNING RADARS

Since the late 1970s many dealiasing techniques have been developed for scanning weather radars. Starting with one-dimensional dealiasing, where along every radial, the velocity of a range gate is compared with the previous ones in order to determine discontinuities, caused by aliasing. This is done for every position in azimuth of the radar separately. A disadvantage here is that one wrongly placed velocity causes all consecutive velocities to be incorrect as well, for a particular position in azimuth. Ray and Ziegler [13] developed a technique that is more robust, where it is assumed each radial has a mean velocity and all range gates together follow a normal distribution. This method is unreliable when there is severe weather. An other one-dimensional technique was proposed by Bargen and Brown [1], where the velocity at each range gate is compared with an average of a number of previous range gates that are considered dealiased correctly. Two-dimensional techniques, along radials and azimuth [2, 5] up to four-dimensional techniques, along radials, azimuth, elevations and in time [8], all deal with discontinuities in velocity fields.

The common factor in these methods is the use of external sources to provide an initial reference and references for error checking. The previous methods make use of a human operator and/or information provided by an additional source, such as a radiosonde or wind profile. This wind profile can be obtained via a sounding (anemometer) or from a VAD (Vertical Azimuth Display, [3]) analysis. In a traditional VAD it is assumed the horizontal wind is uniform and its components vary linearly. However, when this is not the case, a correctly dealiased VAD is more difficult to produce. Various methods have improved the way a VAD is obtained and therefore have a better reference for a continuity check on aliased wind fields [6, 14, 19].

1.4.2. STAGGERING PRT TECHNIQUE

The techniques mentioned in 1.4.1 are all on the processing side, building algorithms to achieve unambiguous velocities. Another approach is focusing on the hardware side of the radar, preventing aliasing from occurring. According to equation 1.7 decreasing the radar frequency or the sweep time is the easiest way to increase the Nyquist velocity, so less aliasing will occur. Furthermore, staggering the Pulse Repetition Time (PRT) is a good way to decrease aliasing. A staggered PRT is a technique, for a pulse radar, where two alternating pulse spacings (T_1 and T_2) are used. In a FM-CW radar, the sweep time T_s is the equivalent of the pulse spacing. A velocity estimate $\hat{v}$ is made from the phase difference between the autocovariance estimates $\hat{R}_1$ at lag T_1 and $\hat{R}_2$ at lag T_2 [4]:

$$\hat{v} = \frac{\lambda}{4\pi(T_1 - T_2)} \arg\left(\frac{\hat{R}_1}{\hat{R}_2}\right). \tag{1.13}$$

Now $\hat{v}$ becomes ambiguous when the phase difference, $\arg\hat{R}_1 - \arg\hat{R}_2$, is larger than $\pm\pi$. Thus, the difference between T_1 and T_2 determines the Nyquist velocity, or unambiguous velocity, given by

$$V_{D,max} = \pm\frac{\lambda}{4(T_2 - T_1)}; \qquad T_1 < T_2. \tag{1.14}$$

The smaller the difference between T_1 and T_2, the larger $V_{D,max}$ will be. However, the errors in $\hat{v}$ are inversely proportional, due to statistical fluctuations in $\hat{R}_1$ and $\hat{R}_2$, to this difference [20].

1.4.3. USING POLARIMETRIC INFORMATION

The third method is the one used to dealiase the Doppler velocities of the main beam of TARA and is discussed by Unal and Moisseev [17]. It makes use of the different polarizations of the main beam (vv, hv and hh). When dealiasing, the focus is on the phase of the cross spectrum (hh, vv). This is basically the difference in phase between two consecutive sweeps (hh and vv). With the assumption of Rayleigh scattering and no propagation effect, the phase of the cross spectrum is zero when no aliasing is present. Before determining if aliasing occurred and what the Nyquist number is, a phase compensation is carried out in the Doppler velocity domain. This Doppler phase compensation is necessary to nullify the effect of nonsimultaneous polarimetric measurements. After phase compensation, the resulting cross spectrum phase is nonzero when aliasing is present. It depends on the offset time (the time between measurements of hh and vv) and the time between two measurements (or samples) with the same polarization setting (T_m), how large the cross spectrum phase is when aliasing occurs. Also the ability to deal with multiple aliasing depends on these

settings. It is shown that this dealiasing technique based on the cross spectrum phase is successful when no averaging is used, but for robustness an average on two Doppler spectra is recommended.

1.5. BRIEF DESCRIPTION OF METHODOLOGY

Since the main beam of TARA is already dealiased, using the method described above, only the offset beams need dealiasing. Because there is no polarimetric information in the offset beams, the method used to dealiase the main beam cannot be used for the offset beams. Also the staggering PRT technique cannot be used, because a change in the radar system itself is undesirable. All that remains are the techniques for scanning radars. Although TARA is stationary, some of the ideas for scanning radars are applicable to dealiase the offset beams of TARA. But for example it is impossible to produce a VAD or check for continuity in multiple dimensions.

The method described in this report uses a one-dimensional continuity check for each beam (OB1 and OB1) separately. An initial reference is taken from the main beam, which is dealiased already. This reference is compared with a range gate, at similar height, of the offset beam under evaluation. After this first range gate is dealiased correctly, a continuity check is executed on the other range gates, first away from and secondly towards the radar.

1.6. THESIS OUTLINE

In Chapter 2 the complete dealiasing process is explained. This starts with the unfolding of a Doppler spectrum, then the finding of a reference from the main beam, and finally the dealiasing by means of a continuity check.

Chapter 3 is used to discuss the results and an overview is given of factors that play a role when the dealiasing algorithm fails.

A validation of the results is given in chapter 4, where the wind velocity and wind direction of TARA after processing are compared with the outcome of other sensors.

Chapter 5 contains the conclusions of the complete research and recommendations for further research.

2

DEALIASING

After the data is obtained from the radar and is processed (figure 1.2) the Doppler velocity may be incorrect due to aliasing. To demonstrate this, the processed data can be presented as a 3D-plot with spectral reflectivity as a function of height and Doppler velocity, a spectrogram. A raw data spectrogram is a spectrogram of the processed data before dealiasing, noise clipping and clutter suppression. An example of a raw data spectrogram of the main beam of TARA is depicted in figure 2.1. In figures 2.2 and 2.3 the corresponding raw data spectrograms of the offset beams 1 and 2 are depicted. As mentioned in chapter 1, the interval, in which the atmospheric targets are placed, is between $-V_{D,max}$ and $V_{D,max}$. Or in our case, between -9.096 and 9.096 m s^{-1}. In these raw data spectrograms there is a significant part aliased at heights around 1000 m and between Doppler velocities 2.5 m s^{-1} to $V_{D,max}$.

In this chapter a method is explained to dealiase the offset beams. The dealiasing starts with the unfolding of individual Doppler spectra, explained in section 2.1. In section 2.2 the dealiasing process is explained, where each unfolded Doppler spectrum is placed in the right Doppler velocity interval.

2.1. UNFOLDING

A raw data spectrogram, like the one in figure 2.1, is built from 512 Doppler spectra. Each spectrum represents a range gate. When there is aliasing, most of the time only a part of the spectrum is aliased, while the other part is correct. An example of a spectrum which is partly aliased is depicted in figure 2.4a. This is the spectrum that belongs to the range gate around 1500 m of figure 2.1. It is assumed that the Doppler power spectra of atmospheric targets are Gaussian shaped [9], so the separated parts should be placed together to form a Gaussian. This is called the unfolding of a Doppler spectrum. Although a lot of Doppler spectra are not perfectly Gaussian shaped, it is not a problem for the unfolding. The result of the unfolding of the spectrum in figure 2.4a is depicted in figure 2.4b. It depends on the method of unfolding, which Doppler bins are filled with data, but every data point is in the same Doppler bin or 512 Doppler bins shifted.

After unfolding, all the relevant parts (atmospheric targets) in the spectrum are the same number of intervals (n) away from the right Doppler velocity interval. This number can also be zero, which means the spectrum is not aliased.

In this section the unfolding of a Doppler spectrum is explained. First, the unfolding process is explained which is implemented in TARA. Secondly, an alternative method to unfold a Doppler spectrum is presented.

Before the unfolding process there is a notch filter applied to remove all data around a Doppler velocity of 0 m s^{-1}. The width of this filter can be adapted. Also there is an attempt to remove some of the non-stationary clutter.

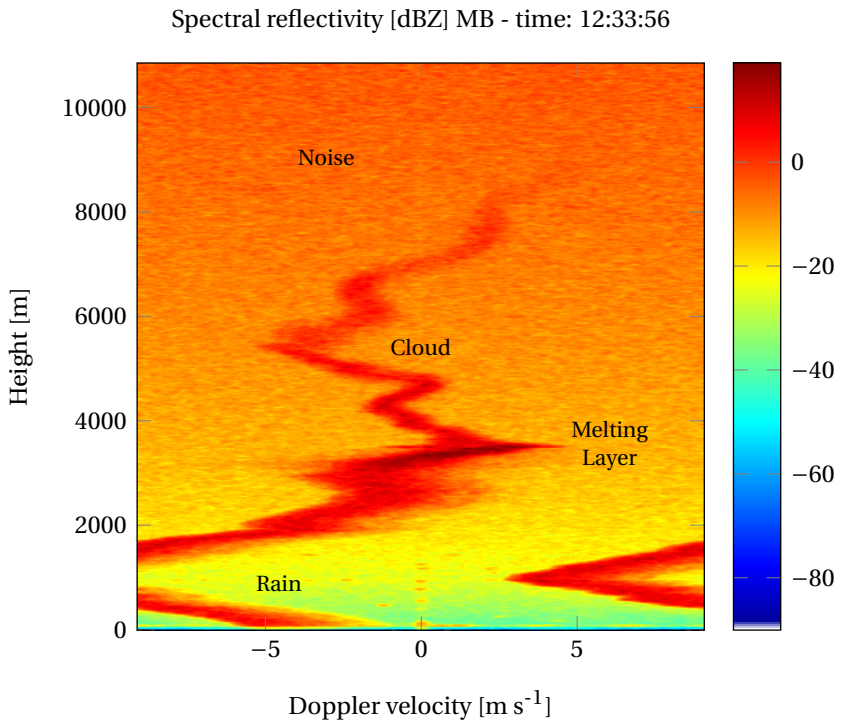

Figure 2.1: Example of a raw data spectrogram of the main beam of TARA on June 20, 2013. The Doppler velocity is in the interval $-V_{D,max}$ to $V_{D,max}$, where $V_{D,max} = 9.096$ m s^{-1}. At height around 1000 m it can be seen that a part of the spectrogram is placed at a positive Doppler velocity, where it should be at a large negative velocity. In this figure the melting layer is at height 3400 m. Above the melting layer is a precipitating cloud and below the melting layer is rain.

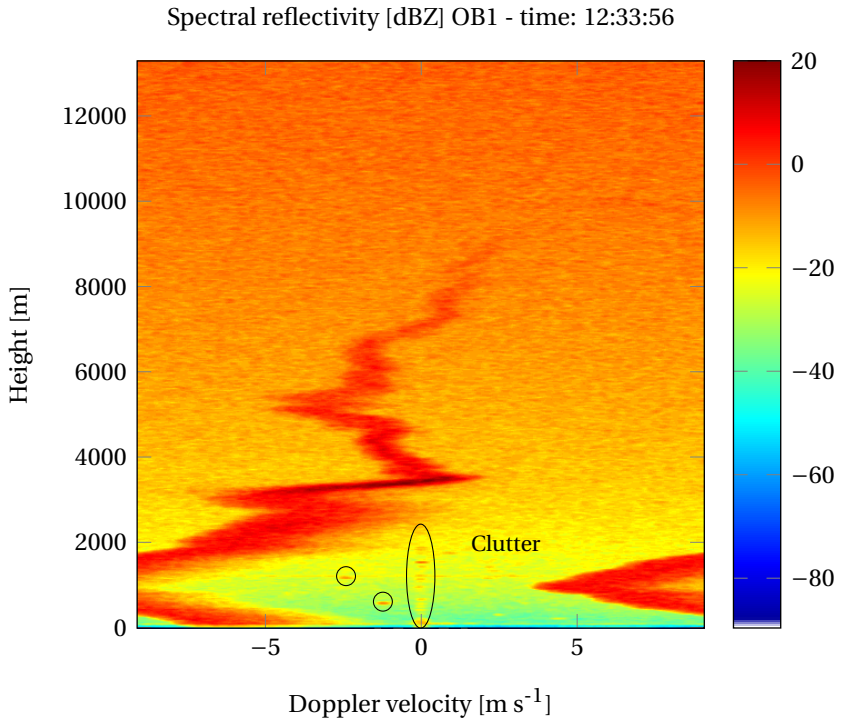

Figure 2.2: Raw data spectrogram of the offset beam 1 of TARA. With clutter encircled.

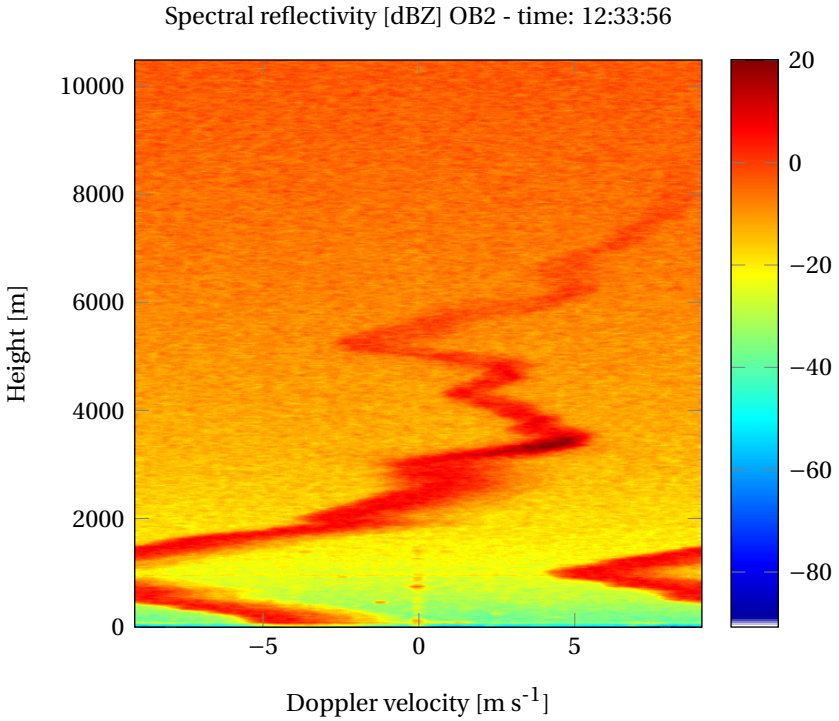

Figure 2.3: Raw data spectrogram of the offset beam 2 of TARA.

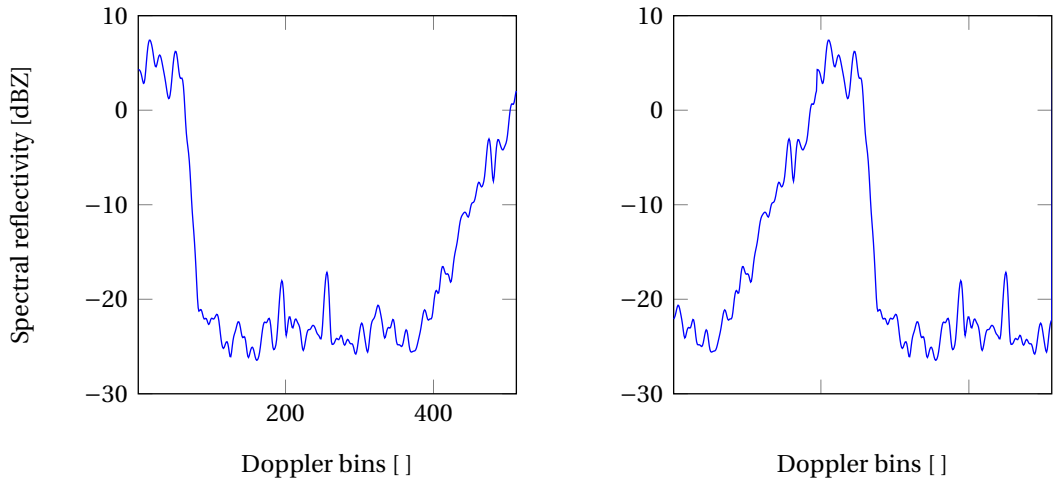

(a) Folded spectrum

(b) Unfolded spectrum

Figure 2.4: The spectrum around height 1500 m (range bin 57) of the raw data of offset beam 1 on June 20, 2013 at 12:33:56, with (a) the raw spectrum and (b) an unfolded form of this spectrum. This is a Doppler spectrum of rain and it is clearly not Gaussian shaped. But for the unfolding this is not a problem.

2.1.1. STANDARD UNFOLDING PROCESS

For every range gate, it may be necessary to unfold the Doppler spectrum. The unfolding is only necessary when the atmospheric data is on the edges of the Doppler velocity interval. When a Doppler spectrum is folded as shown in figure 2.4a, it is unfolded around its maximum. Each Doppler spectrum has 512 (N_d) Doppler bins of width 0.0355 m s^{-1}. To unfold a Doppler spectrum, first, the location of the maximum is determined. Then, when the maximum is to the left of the middle of the spectrum (position 256, $N_d/2$), the

part of the spectrum after maximum + 256 is moved to the front of the spectrum. When the maximum is to the right of the middle, a part at the start of the spectrum is moved to the end. In figure 2.5 there is a visualization of the unfolding process on the spectrum of figure 2.4a.

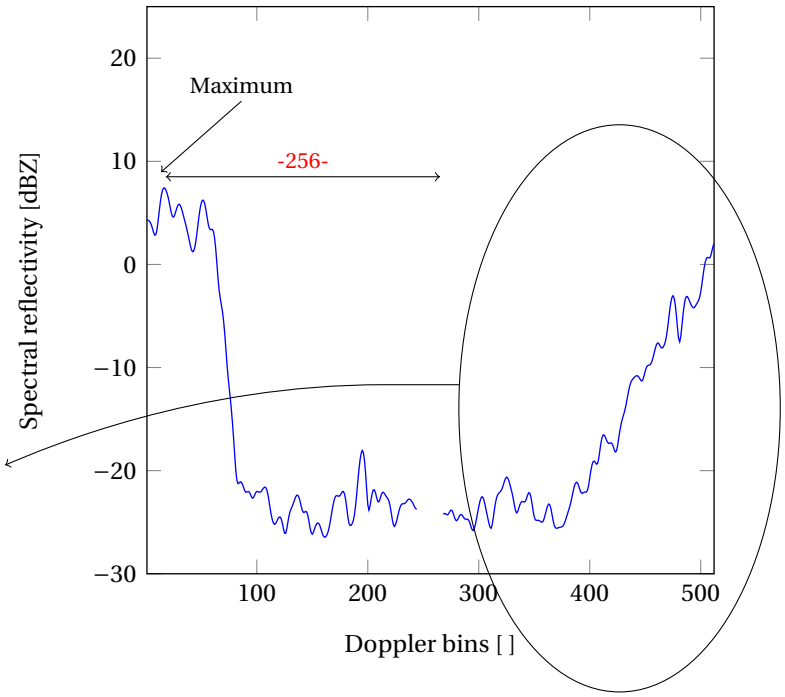

Figure 2.5: The unfolding process on the spectrum from figure 2.4a, where first the maximum is determined. Then, depending on the position of the maximum, data points are moved so there are 256 Doppler bins filled with data to the left of the maximum and 256 (including the maximum itself) to the right. Note the removal of Doppler bins 245 to 267 by a notch filter around 0 m s^{-1}.

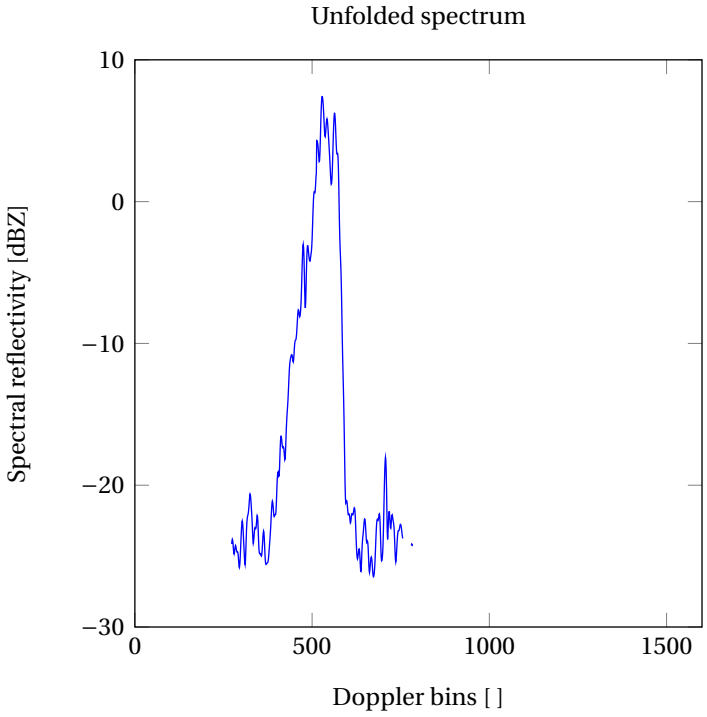

Figure 2.6: Unfolded Doppler spectrum as a result of applying the standard unfolding process on the spectrum from figure 2.4a.

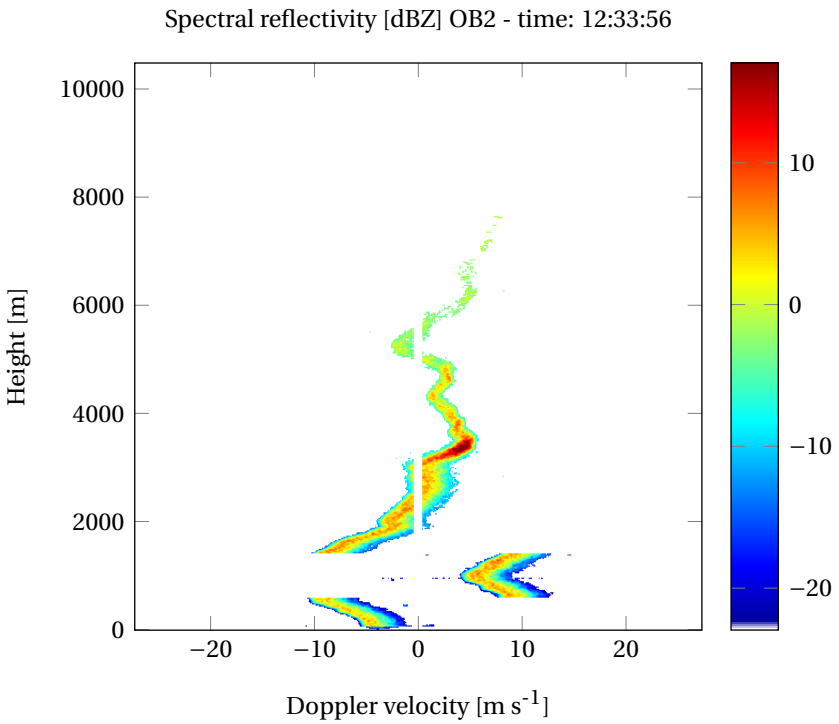

Figure 2.7: The result of the unfolding process on the raw spectrogram of figure 2.3 of offset beam 2. A notch filter around 0 m s^{-1} and noise clipping have been applied.

The result of unfolding this single spectrum is depicted in figure 2.6. After unfolding, every data point is in the same position or shifted 512 (N_d) points. The result is stored as a vector of 1536 points ($3N_d$), including 1024 zeros. Here the interval $-V_{D,max}$ to $V_{D,max}$ is in Doppler bins 513 to 1024 and the maximum is always in this interval.

The spectrogram of OB2 after the unfolding process and after clipping is depicted in figure 2.7. The dealiasing process, explained in section 2.2, will place all spectra in the correct Doppler interval.

2.1.2. ALTERNATIVE UNFOLDING PROCESS

An other way to unfold a Doppler spectrum is the opposite of the method described above. Instead of unfolding around the maximum, the minimum is used to unfold around. The minimum is defined as the middle between two parts of the Doppler spectrum that are above the noise clipping level. The noise clipping level is determined by a noise file and a desired signal-to-noise ratio (SNR) added to it. In the noise file the background noise is stored for every range bin. The farther in range the larger the background noise is. For OB1 the SNR is set at 7 dB and for OB2 it is 5 dB. In figure 2.8 a visualization of the alternative unfolding process is depicted.

This method works as follows: first the Doppler spectrum is copied and the two identical spectra are put next to each other. Secondly, parts of the spectrum below the clipping level are replaced by zeros. Thirdly, the minimum is determined by taking the middle of the longest sequence of zeros. Lastly, starting at the minimum, 512 Doppler bins are taken.

When no notch filter is applied and the reflectivity in every Doppler bin is above clipping level, the true minimum is used to unfold around. An example of this is showed in section 3.3.

Similar to the previous method the result is stored as a vector of $3N_d$ points, adding 1024 zeros. The difference is that the maximum now is not always put in the original interval of $-V_{D,max}$ to $V_{D,max}$. Therefore most of the time the spectrogram after unfolding is worse using the alternative method compared to the standard method. However, after dealiasing this evens out. In figure 2.9 the spectrogram, after unfolding using the alternative method and before dealiasing, is depicted.

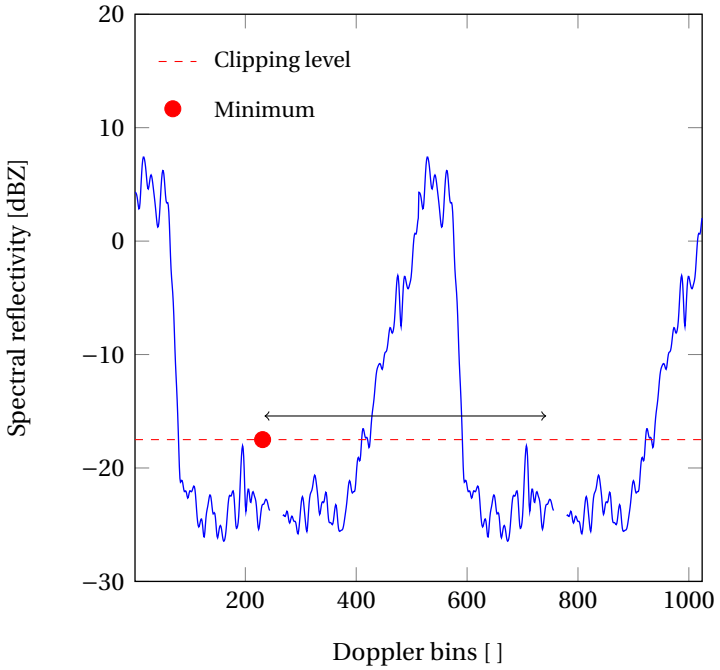

Figure 2.8: Visualization of the alternative unfolding process on the spectrum from figure 2.4a. The original spectrum is copied and the two identical spectra are put next to each other. Then the minimum is determined and starting from the minimum 512 Doppler bins are taken.

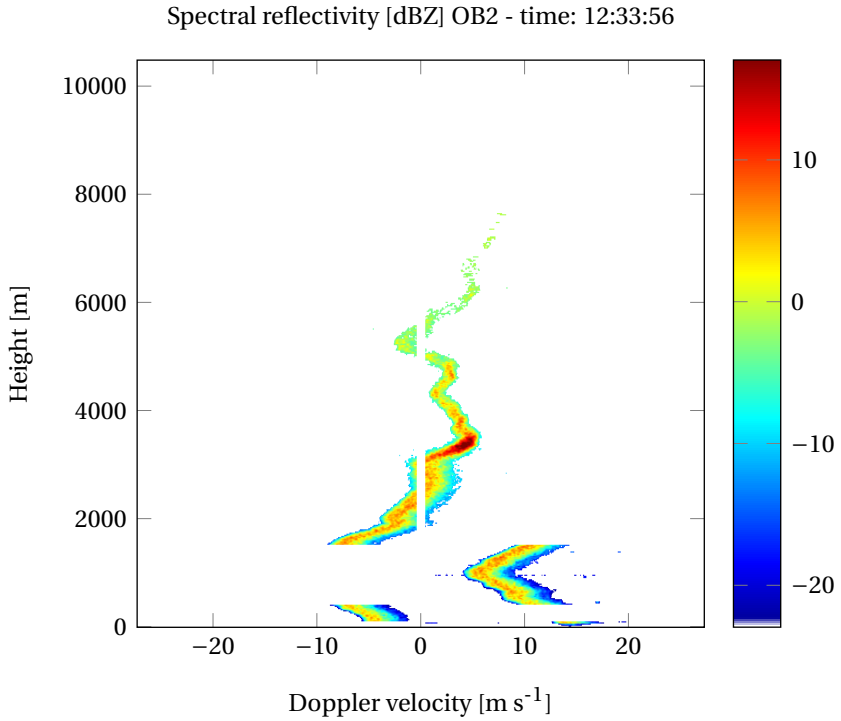

Figure 2.9: The result of the alternative unfolding process on the raw spectrogram of figure 2.3 of offset beam 2. A notch filter around 0 m s^{-1} and noise clipping have been applied.

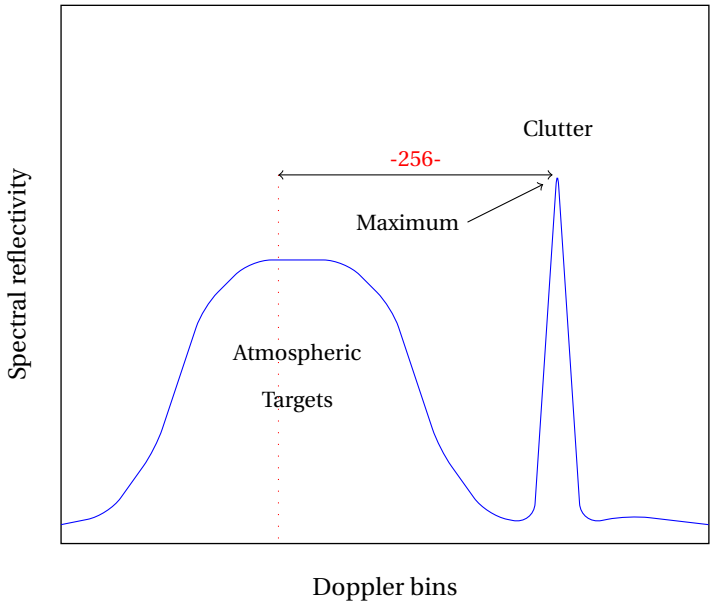

Figure 2.10: Schematic of a case where dominant clutter causes the standard unfolding process to fail. By taking 256 Doppler bins on each side of the maximum, the part of the spectrum with atmospheric targets is split up.

2.1.3. ADVANTAGES OF THE ALTERNATIVE UNFOLDING PROCESS

There are two typical cases in which the alternative unfolding process performs better than the standard one. The first case is when clutter is present that has a larger reflectivity than the maximum of the atmospheric targets. This means, using the standard unfolding process, that the spectrum is unfolded around the clutter. Figure 2.10 shows that dominant clutter can cause the spectrum to be unfolded incorrectly, when using the standard unfolding process. Here the part with atmospheric targets will be split in half, causing the opposite of what the unfolding process is supposed to do. Most of the time dominant clutter is stationary clutter and is removed by the notch filter. However, if the notch filter becomes adaptive in the future, it is possible some clutter around 0 m s^{-1} will not be removed. This means the advantage of the alternative unfolding process over the standard unfolding process will increase.

The second case is when a spectrum is very wide, the unfolding is not perfect using the standard unfolding process. In a very wide spectrum, the part of the spectrum above clipping level has a width larger than half ($N_d/2$) of the total spectrum (N_d). In figure 2.11 the spectra around 5000 m (range bins 191, 192, 195, 196 and 197) are not unfolded correctly. In figure 2.12 the wrongly unfolded spectrum at height 4936 m is depicted. Two factors play a role in this failure. First, the maximum, around which the unfolding is performed, is not in the middle of the part of the spectrum above clipping level. The spectrum is bimodal [18] and therefore not Gaussian shaped as assumed. Secondly, the number of Doppler bins containing atmospheric targets on one side of the maximum is larger than $N_d/2$. This means all Doppler bins further than 256 bins away from the maximum are folded to the other side of the spectrum. Although this problem does not influence the outcome of the dealiasing process, it changes the outcome of follow up calculations that for example make use of the mean Doppler velocity. Using the alternative unfolding process here makes the unfolding correct.

The only time the standard unfolding process can outperform the alternative one is when there is no part of the spectrum below clipping level, except where the notch filter is applied. Using the notch filter, the minimum is chosen at 0 m s^{-1}. This can be a problem when the atmospheric targets also concentrate around 0 m s^{-1}. That way part of the unfolding fails. An example of this is in figure 3.8 in section 3.3.

Because the advantages of the alternative unfolding process outweigh the small disadvantage described above, this method is implemented.

After unfolding the spectrum of each range gate is built from $5N_d$ Doppler bins, of which only 512 are filled with the raw data. The rest is zero. $5N_d$ Doppler bins equal a Doppler velocity from -45 to 45 m s^{-1}. This is a large enough interval to cover any severe weather event. In a worst case scenario -45 m s^{-1} of the offset beam 2 will be exceeded when the horizontal wind speed is larger than 52.3 m s^{-1}. The relations between the three measured Doppler velocities along the three beams (V_{MB}, V_{OB1} and V_{OB2}) and the wind (V_x, V_y and

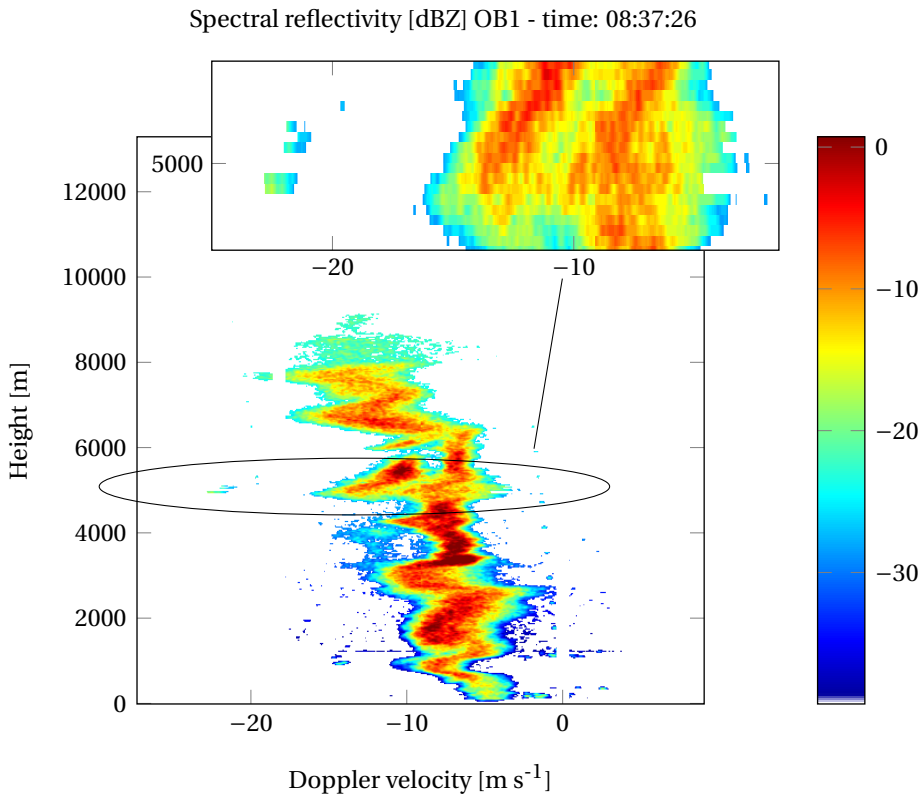

Figure 2.11: Example of a spectrogram with spectra around height 5000 m that are not unfolded correctly. These spectra are bimodal and thus not Gaussian shaped. The spectrogram is from July 26, 2013.

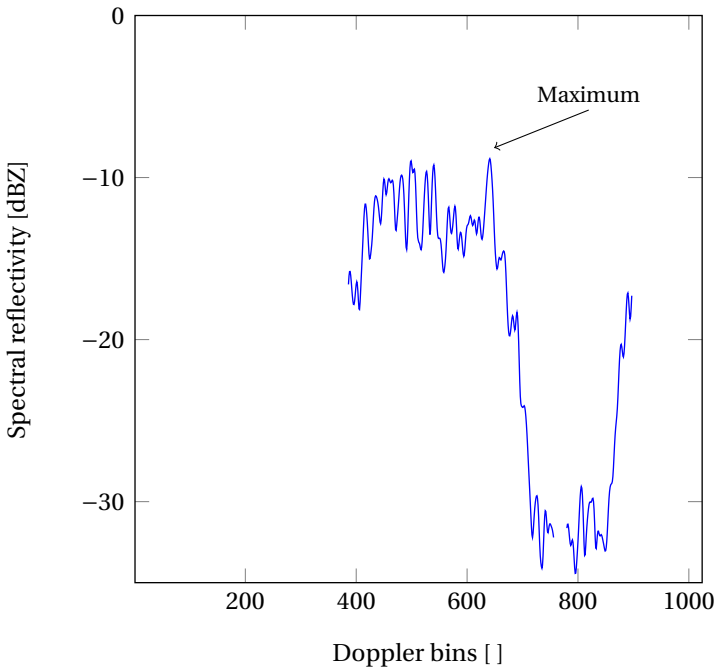

Figure 2.12: Spectrum at height 4936 m (range bin 191) from figure 2.11 that is unfolded incorrectly.

V_z) are in equation 2.1, assuming that the atmospheric particles are perfect tracers of the wind. In this worst case scenario the elevation angle (α) of the main beam of TARA is 45°, the direction from which the wind blows is 21° from the x-axis of TARA (267.5° from the north) and a fall velocity (V_z) of -10 m s^{-1} is taken. Note the convention that the velocities towards the pointing direction of the radar are negative. In appendix A the maximum allowed horizontal wind speed (before $V_{OB1,OB2}$ exceeds ± 45 m s^{-1}) for different directions and fall velocities is calculated. This is the maximum Doppler velocity that can be displayed in the spectrogram. It is also the maximum the mean Doppler velocity can be for dealiasing. Two things must be considered here.

1. Using the alternative unfolding method, the **mean** Doppler velocity never reaches -9 m s^{-1} before dealiasing (see figure 2.9). Depending on the width of the Doppler spectrum the limit for the mean Doppler velocity ranges from -36 to almost -45 m s^{-1}. When the tail end of the spectrum will reach -45 m s^{-1} that is.

2. On the other side of the velocity spectrum, the mean Doppler velocity can reach larger values than +45 m s^{-1}. But as a consequence of a limit of 5 N_d for a spectrum, every part of a spectrum larger than +45 m s^{-1} will be removed.

There is an easy solution to increase the maximum allowed horizontal wind speed. It only requires the spectrum size to be increased from $5N_d$ to $7N_d$ (or even much larger if necessary). This is not done, because it will increase size of the code unnecessary and it slows down the software. It is not expected a horizontal wind speed larger than 52 m s^{-1} from a specific direction happens a lot.

$$\begin{aligned} V_{MB} &= V_x \cos\alpha + V_z \sin\alpha \\ V_{OB1} &= V_x \cos(\alpha + 15) + V_z \sin(\alpha + 15) \\ V_{OB2} &= V_x \cos\alpha \cos(15) + V_y \sin(15) + V_z \sin\alpha \cos(15) \end{aligned} \tag{2.1}$$

Equation 2.1 is expressed in the TARA coordinate system (figure 1.4), where the azimuth direction of the x-axis of TARA is 246.5° related to the north.

2.2. DEALIASING PROCESS

During the dealiasing process each spectrum, of the total of 512 spectra, is considered separately and tested to be in the right velocity interval. Two methods to test this are discussed next; making use of the cross correlation between the current spectrum and a reference, or calculate the mean Doppler velocity of the current spectrum and compare it with a reference. Although both methods can be used to dealiase correctly, the mean Doppler velocity method is preferred. The reasons for this are that it is easier to implement, adjust and explain. It is easier to put constraints on the mean Doppler velocity whether it can be used as reference, than on a spectrum. The mean Doppler velocity is already available and can be used for dealiasing simultaneously.

In section 2.2.3 the finding of an initial reference is described. And in section 2.2.4 the dealiasing algorithm is explained, after a reference is found. During the whole process offset beam 1 and offset beam 2 are processed individually.

2.2.1. CROSS CORRELATION

By using the cross correlation function 'xcorr' in Matlab, the current spectrum and a reference spectrum are correlated. An example of both the current and reference spectrum are in figure 2.13. It is clear the current spectrum should be shifted one interval of 512 Doppler bins (N_d, the FFT length) to be aligned with the reference spectrum. The correlation of the two spectra results in a cross correlation graph as depicted in figure 2.14. In this example the maximum is at position 2006, where the maximum of an autocorrelation function would be at position 2560 ($5N_d$, number of Doppler bins in a spectrum before dealiasing). This means the current spectrum and the reference are on average 554 Doppler bins from each other. If the current spectrum is shifted this number of bins to the right, it is placed in the same Doppler bins as the reference. However only shifts of $n \times N_d$ are possible. In this example $n = 1$ and the current spectrum is shifted 512 Doppler bins to the right. To determine whether a spectrum needs to be shifted, the difference between 2560 (result of the autocorrelation function) and the result of the cross correlation function (R_{xcorr}) is rounded to the nearest n times N_d.

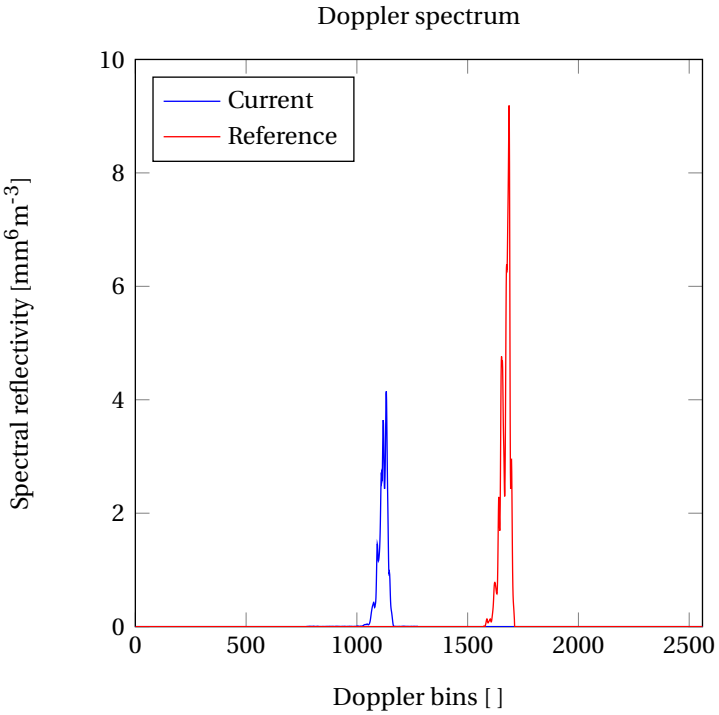

Figure 2.13: Current Doppler spectrum and a reference spectrum before dealiasing. The current spectrum is the spectrum at range bin 50 (corresponds to a height of 1004 m) of offset beam 2 on June 20, 2013 at 12:33:56. The reference spectrum is from the main beam at the same height.

$$\text{if} \quad |5N_d - R_{xcorr}| \leq \frac{N_d}{2} \quad \rightarrow \quad n = 0, \tag{2.2a}$$

$$\text{if} \quad 5N_d - R_{xcorr} > \frac{N_d}{2} \quad \rightarrow \quad n = 1, \tag{2.2b}$$

$$\text{if} \quad R_{xcorr} - 5N_d > \frac{N_d}{2} \quad \rightarrow \quad n = -1, \tag{2.2c}$$

In the example of figure 2.13 no clipping has been applied to the current spectrum before correlation. The noise can influence the outcome of the cross correlation function. This influence increases when the SNR decreases. In this case it is not a problem, because the reflectivity of the atmospheric targets is large compared with the noise. However, when spectra that only contain noise are correlated with each other, after a number of spectra in range an unwanted interval shift can occur. This is explained in the next example.

After unfolding the spectra are in different Doppler bins. See figure 2.15 for a generated example. When the reflectivity of the atmospheric targets is smaller than approximately 5 dB above noise level, the result of the cross correlation function depends on the position of all data. For example, a spectrum with data (noise or atmospheric targets within 5 dB of the noise level) in Doppler bins 1 to 512 is cross correlated with a spectrum with Doppler bins 124 to 635 filled with data. The result will be a shift of 123 bins (124 - 1). The largest possible shift happens when Doppler bins 2-513 of one spectrum and Doppler bins 511-1022 of the consecutive spectrum are filled with noise. Problems can occur when a number of consecutive spectra are only filled with noise or weak atmospheric targets and the filled bins of these spectra gradually shift, as depicted in figure 2.15. In this case not one of the spectra is shifted, which eventually leads to an unwanted shift of 512 bins between the first and last displayed spectrum. If one of the next spectra contains atmospheric targets, for example the start of a precipitating cloud, and it is cross correlated with the noise spectrum, the complete cloud can be placed in the wrong Doppler velocity interval.

To prevent problems, using cross correlation with spectra that contain mainly noise, clipping is applied in advance. By using the alternative unfolding process the clipping is already done. Another solution is to prevent these spectra from being used as a reference.

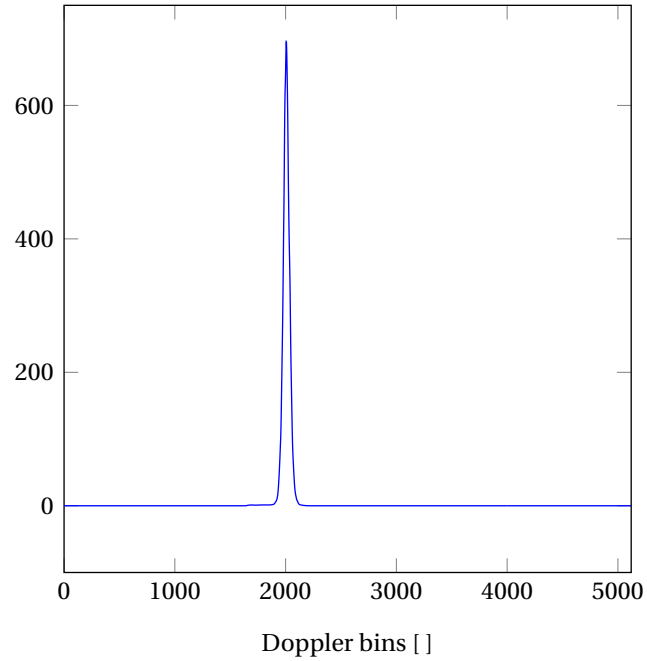

Figure 2.14: Result of the cross correlation between the spectra in figure 2.13. The maximum is at 2006, which means the current spectrum is aliased.

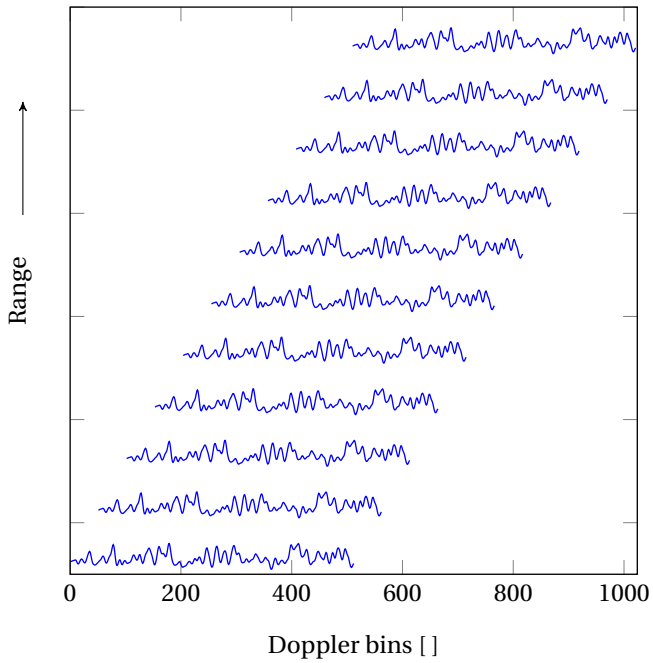

Figure 2.15: Generated example of a situation noise causes a failure in dealiasing, using the standard unfolding process without noise clipping. In this example any spectrum in range is cross correlated with the previous one. Because the outcome of these cross correlations is not a shift, every spectrum stays in its original interval. This eventually leads to an unwanted shift of 512 bins. This situation can only occur when the reflectivity of all Doppler bins in the spectra is within 5 dB of the noise level.

2.2.2. MEAN DOPPLER VELOCITY

Another method to test if the current spectrum is in the right velocity interval, is using the mean Doppler velocity. First, the mean Doppler velocity is calculated for every spectrum, remembering equation 1.11

$$v_d = \frac{1}{P_{tot}} \int v S(v) dv, \tag{2.3}$$

The problem with spectra that mainly contain noise, as mentioned in the previous section, is nullified. Because noise clipping and a notch filter are applied to obtain $S(v)$ free from noise and stationary clutter, in the case of the offset beams (non-polarimetric). Then, the mean Doppler velocity of every spectrum is compared with the mean Doppler velocity of a reference spectrum. Here the following algorithm is used:

$$\text{if} \quad V_{ref} + V_{D,max} \geq V_i \geq V_{ref} - V_{D,max} \quad \rightarrow \quad n = 0, \tag{2.4a}$$
$$\text{if} \quad V_i > V_{ref} + V_{D,max} \quad \rightarrow \quad n = -1, \tag{2.4b}$$
$$\text{if} \quad V_i < V_{ref} - V_{D,max} \quad \rightarrow \quad n = 1, \tag{2.4c}$$

where V_i is the mean Doppler velocity of the current spectrum and V_{ref} the mean Doppler velocity of a reference spectrum. Equation 2.4 can be extended to $n = \pm 2$ as follows:

$$\text{if} \quad V_{ref} + V_{D,max} \geq V_i \geq V_{ref} - V_{D,max} \quad \rightarrow \quad n = 0, \tag{2.5a}$$
$$\text{if} \quad V_{ref} + 3V_{D,max} \geq V_i > V_{ref} + V_{D,max} \quad \rightarrow \quad n = -1, \tag{2.5b}$$
$$\text{if} \quad V_{ref} - 3V_{D,max} \leq V_i < V_{ref} - V_{D,max} \quad \rightarrow \quad n = 1, \tag{2.5c}$$
$$\text{if} \quad V_i > V_{ref} + 3V_{D,max} \quad \rightarrow \quad n = -2, \tag{2.5d}$$
$$\text{if} \quad V_i < V_{ref} - 3V_{D,max} \quad \rightarrow \quad n = 2, \tag{2.5e}$$

2.2.3. INITIAL REFERENCE

A reference spectrum is needed to know where to place a spectrum. Looking at the raw data spectrogram in figure 2.1, it is clear using for example the spectrum at height 1000 m as a reference for the spectrum at height 3500 m is wrong. The reference spectrum should be relevant to the spectrum under consideration. At the start of processing the offset beams, none of the spectra are guaranteed to be in the correct Doppler velocity interval. Therefore an initial reference spectrum is chosen from the main beam. The main beam uses polarimetry for the dealiasing procedure and shows very good performance in Doppler dealiasing [17].

For the initial reference a spectrum with good atmospheric properties is searched for in the main beam. Good atmospheric properties are:

1. Doppler width W between 0.2 and 2 m s^{-1}.
2. Cross-correlation coefficient ρ_{co} larger than 0.8.
3. Linear depolarization ratio L_{dr} smaller than -10 dB.
4. Differential reflectivity Z_{dr} between 0 and 3 dB.
5. Spectral reflectivity Z larger than 0.02 mm^{6}m^{-3}

Typically, the spectra with only clutter (especially stationary clutter around 0 m s^{-1}) have a Doppler width smaller than 0.2 m s^{-1}. Spectra with both clutter and atmospheric targets usually have a larger Doppler width than 2 m s^{-1}. A cross-correlation coefficient ρ_{co} larger than 0.8 means the spectra with mainly noise and unwanted targets in the side lobes of the antenna patterns are ignored. A linear depolarization ratio L_{dr} smaller than -10 dB means the spectra with clutter are ignored [15]. Also spectra with only noise have a L_{dr} larger than -10 dB. A spectrum with a differential reflectivity Z_{dr} smaller than 0 dB is noisy and one larger than 3 dB contains unwanted targets like bugs, birds etc.

To avoid a large spatial difference between the location of the reference spectrum from the main beam and the spectrum of the offset beam, it is best to find a reference as close to the radar as possible. Starting at the radar (range = 0 m) and going further in range, but skipping the near field (~300 m), the range bin of the first applicable spectrum is stored as 'nref'.

When no nref is found in a first sweep, the lower bound of the Doppler width (0.2 m s^{-1}) is lowered to the Doppler velocity resolution (velres = 0.0355 m s^{-1}) and the threshold for the spectral reflectivity is lowered to

0.01 mm^6m^{-3}. Then, a new search for nref is done. If there is still no nref found it means there is very little precipitation in the main beam. Dealiasing of the offset beams will not be carried out.

The spectra of the main beam are already filtered and clipped. As a result nref is the range bin of a clean spectrum to be used for the cross correlation function or mean Doppler velocity method. During the testing of the dealiasing program, the choice for a particular nref was never the cause of a failure in dealiasing. Except when the mean Doppler velocity of the spectrum of nref was significantly different than the mean Doppler velocity of the spectrum from the offset beam. This is explained in section 3.4.

2.2.4. DEALIASING ALGORITHM

The version of the dealiasing algorithm implemented in TARA uses the mean Doppler velocity method. Before dealiasing the mean Doppler velocity of every spectrum of the main beam and the offset beams is calculated. In this section the dealiasing algorithm is explained. It starts with correcting (if necessary) a first mean Doppler velocity from the offset beam. Then it is explained if and how this newly corrected mean Doppler velocity can be used as a next reference and how the algorithm continues from there. Finally, the need for a second reference from the main beam (nref2) is explained, as well as the procedure to determine this.

Note that every time $n \neq 0$ in equation 2.5 not only the mean Doppler velocity is changed, but the corresponding spectrum is shifted accordingly. This is not needed for the dealiasing nor for the final wind estimation, but placing the Doppler spectra in the right velocity interval is necessary to carry out retrievals directly on the Doppler power spectra (for example raindrop size distribution).

FIRST CORRECTED MEAN DOPPLER VELOCITY

The horizontal wind speed may change significantly versus the height. Therefore comparing two mean Doppler velocities of spectra roughly at the same height, gives the best result. Because the main beam and the offset beams are different in angle of elevation, spectra at the same range are not at the same height. The mean Doppler velocity of the spectrum in the offset beam closest to the height of nref is chosen to compare with first. It is compared with the average of six mean Doppler velocities from spectra of the main beam; the mean Doppler velocity of the spectrum of nref plus the mean Doppler velocities of the five spectra immediately following in range. Averaging makes the reference more robust. It is unnecessary to average here, because the spectrum of nref is expected to have good atmospheric properties and therefore this mean Doppler velocity is a good reference on its own. However, the mean Doppler velocities from the main beam spectra are used later on in the algorithm as well. For the sake of convenience, the mean Doppler velocities of all spectra from the main beam are averaged at the start of the algorithm. It is not expected the quality of the first reference deteriorates much, since it is unlikely to have just a 'good' spectrum surrounded by 'bad' spectra. Because nref corresponds to the first spectrum in range which meets the requirements, only the mean Doppler velocities of the spectra after nref are taken into the averaging. Using equation 2.5 on the reference and the mean Doppler velocity of the current spectrum of the offset beam results in a first correct mean Doppler velocity of the offset beam.

NEW REFERENCE

In an ideal situation the first correct mean Doppler velocity of the offset beam can function as a reference for the next mean Doppler velocity in range. However, a spectrum with good atmospheric properties in the main beam does not guarantee the spectrum of the offset beam at the same height to be good as well. The following constraints have been put on the spectrum in order to consider the mean Doppler velocity of that spectrum as a reference: reflectivity Z is not NaN and Doppler width W between 0.4 and 2.5 m s^{-1}. Because the offset beams are non-polarimetric, the quantities used to find nref are not available. If the mean Doppler velocity is allowed to be used as a reference, it is added to the reference vector 'OUTrefer'. This vector has six entries and the average of OUTrefer is always used as the reference to compare with. The first five entries are filled with the latest corrected mean Doppler velocities from the offset beam, that are allowed to be used as a reference. When there are not yet five accepted references, one entry is filled with the averaged mean Doppler velocity at nref ($v_d$nref), and the remaining entries are empty. The sixth entry of OUTrefer is always the average of six mean Doppler velocities from the main beam at the same height as the current mean Doppler velocity. This is done because sometimes there is no reference from the offset beam available and the averaged mean Doppler velocity at nref will stay in OUTrefer too long. In table 2.1 an example of the filling of OUTrefer is displayed. In this table, 112 is the range bin of the first spectrum of the offset beam, at the same height as nref. When the mean Doppler velocity of the spectrum of range bin 112 is considered as a reference it is added to OUTrefer. Also from this point on, the sixth entry of OUTrefer contains the average reference from the main beam at the same height as the current mean Doppler velocity.

Table 2.1: The six entries of OUTrefer, where entry six is filled with an average of mean Doppler velocities from the main beam at the same height as the current mean Doppler velocity. The other entries are filled when a mean Doppler velocity of the offset beam is accepted as reference. An average of the six entries is used as a reference to compare with the current mean Doppler velocity. In this example it is unnecessary to add MB112 in the first column, because MB112 is equal to $v_d$nref.

	112 ✓ →	113 ✗ →	114 ✓ →	115 ✓ →	
	112	113	114	115	116
1	NaN	NaN	NaN	NaN	NaN
2	NaN	NaN	NaN	NaN	$v_d$nref
3	NaN	NaN	NaN	$v_d$nref	v_d112
4	NaN	$v_d$nref	$v_d$nref	v_d112	v_d114
5	$v_d$nref	v_d112	v_d112	v_d114	v_d115
6	NaN	MB113	MB114	MB115	MB116

After the first mean Doppler velocity from the offset beam is added to OUTrefer an extra constraint is added; the difference between the mean Doppler velocity of the current spectrum and the mean Doppler velocity in entry no.5 (most recent added velocity) of OUTrefer can not be larger than 2 m s^{-1}. This constraint will be removed after five times in a row a mean Doppler velocity is declined only because of this constraint. When this happens it is likely entry no.5 is not a good reference. This typically happens when this mean Doppler velocity is added as the first one from the offset beam.

CONTINUING THE ALGORITHM

First, working away from the radar, every mean Doppler velocity in the offset beam above nref is dealiased. This is done by using the average of OUTrefer to compare with. After that the five mean Doppler velocities first added to OUTrefer are now again placed in OUTrefer. These five velocities are the mean Doppler velocities of the five spectra closest to nref which are accepted as a good reference. Now, working towards the radar, every mean Doppler velocity in the offset beam below nref is dealiased.

A SECOND NREF

The procedure above describes the dealiasing process when there are substantial atmospheric targets in every range bin, resulting in a continuous spectrogram. In figure 2.16 an example of a continuous spectrogram is depicted. And the raw data spectrogram of this continuous spectrogram is in figure 2.17. If the spectrogram is discontinuous, some spectra in between do not have good atmospheric targets and the mean Doppler velocities of these spectra cannot be used as a reference.

In figure 2.18 an example of a spectrogram of the main beam with a gap is depicted. In figure 2.19 the corresponding spectrogram from offset beam 1 is depicted. In the example of figure 2.18, nref is chosen in the part of the spectrogram close to the radar (height 255 m). Without a second nref, the mean Doppler velocity of the bottom spectrum of the large continuous part starting at height 1450 m (in figure 2.19) is compared with previous 'good' velocities (stored in OUTrefer). Because the previous spectra are not very clean, it is possible OUTrefer is not a good reference for the mean Doppler velocity of the spectrum at height 1450 m. Two things can be the reason for this. First, the difference in height between the velocities in OUTrefer and the current mean Doppler velocity means different atmospheric properties. Therefore the mean Doppler velocities can be completely different. Secondly, OUTrefer can be filled with the mean Doppler velocities of noisy spectra. This means the mean Doppler velocity of those spectra can be faulty.

When the mean Doppler velocity of the spectrum at height 1450 m is dealiased incorrectly, all the mean Doppler velocities above this will also be incorrectly. To prevent this, the raw data spectrogram with a gap is cut at the location of the gap. The two parts are considered as two separate spectrograms, with each an own nref, and put together after dealiasing.

In this example dealiasing is not a problem without a second nref, because the Doppler velocity change between the two parts of the spectrogram is not large. When the gap is larger the Doppler velocity change is more likely to become a problem and nref2 is necessary. A second nref is searched for when a gap of twenty or more range bins is detected. The same atmospheric properties are valid as for nref (see section 2.2.3). With a

gap of less than twenty range bins it is not expected the change in mean Doppler velocity is larger than $V_{D,max}$ and therefore will not fail the dealiasing. However, even when the gap in the main beam is small, there can be a large gap in the offset beams. This is demonstrated in figures 2.20 and 2.21. Here the gap in the main beam is too small to search for a second nref. The gap in offset beam 2 is so large, the entries in OUTrefer are not a good reference anymore once the algorithm reaches the spectrum at height 7270 m.

To prevent a possible failure described above, there is searched for a gap of minimum 10 range bins in the offset beams when there is no nref2. A gap of minimum 10 range bins is taken to be on the safe side. When a gap is detected the first three entries of OUTrefer are filled with averaged mean Doppler velocities from the main beam. This will be the dominant factor to use as a reference. The fourth entry is filled with an average of OUTrefer before the gap. This entry insures a reference when there is no data available in the main beam, but is inferior when there is. The fifth and sixth entry are NaN and filled when the algorithm progresses in the same way as described before.

Lastly, when there is no nref at all, the mean Doppler velocity is not shifted. Except when the mean Doppler velocity is larger than 3 m s^{-1}, then it is shifted $-2V_{D,max}$. Because the convention that the velocity towards the radar is negative not many positive velocities are expected. It means the mean Doppler velocity is probably aliased when it is larger than 3 m s^{-1}. Therefore it is shifted. Although it is not a guarantee it is correct, it is not important since there is not much data in the main beam and therefore impossible to calculate a wind field.

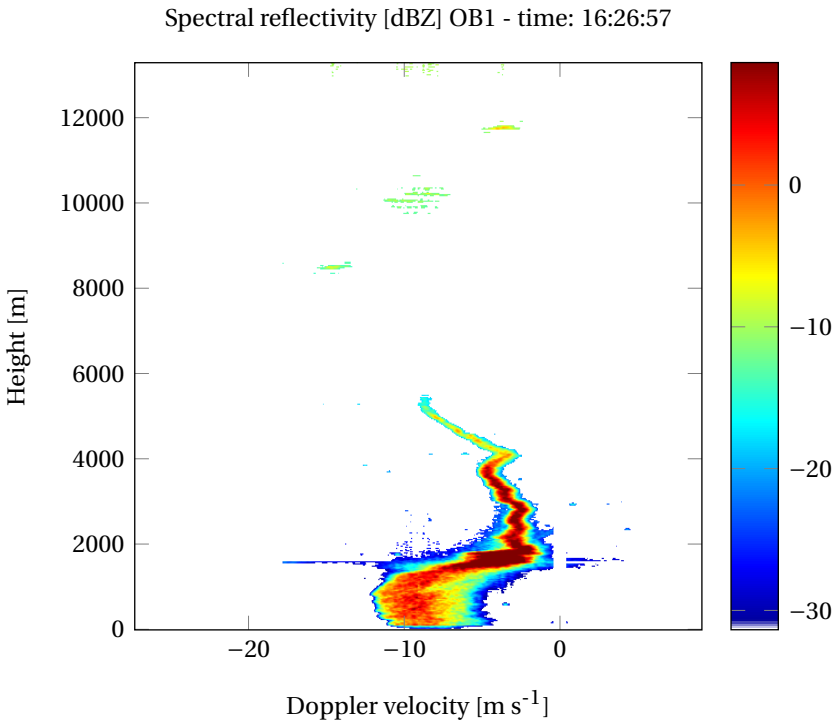

Figure 2.16: Example of a continuous spectrogram of the offset beam 1 on September 9, 2013. This is the final result after unfolding and dealiasing.

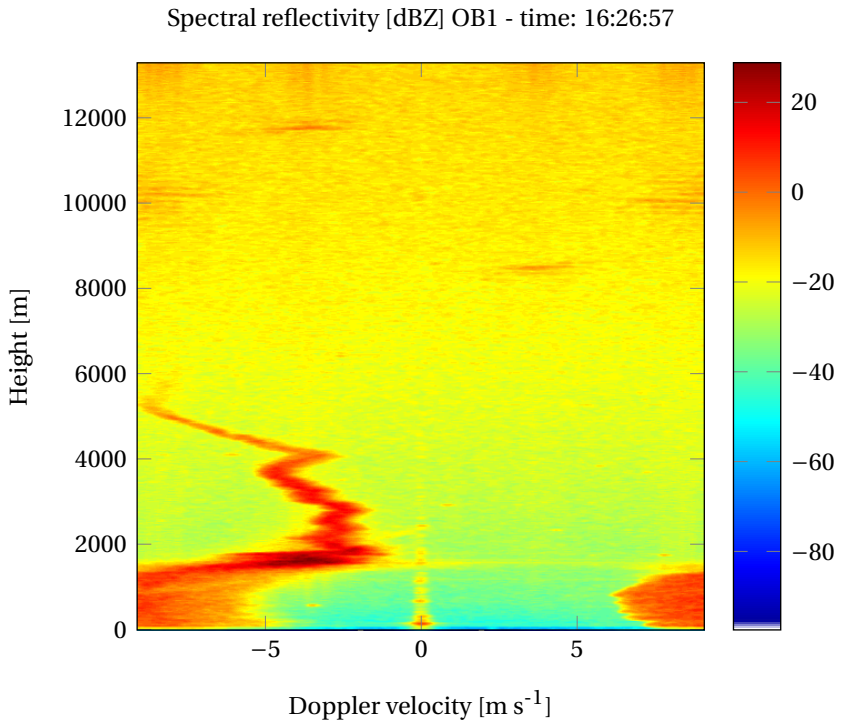

Figure 2.17: Raw data spectrogram of the result in figure 2.16. Note that the echoes above 8000 m are related to a small saturation of the radar receiver.

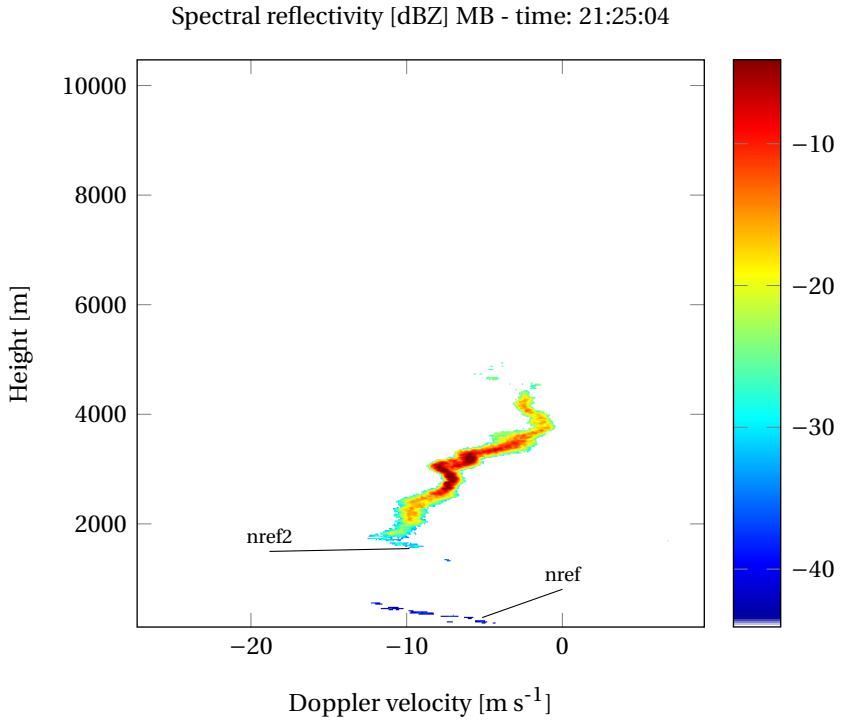

Figure 2.18: Example of a spectrogram with a gap between two parts of it. This is the spectrogram of the main beam on October 14, 2012. At height 255 m nref is chosen and at height 1591 m is nref2.

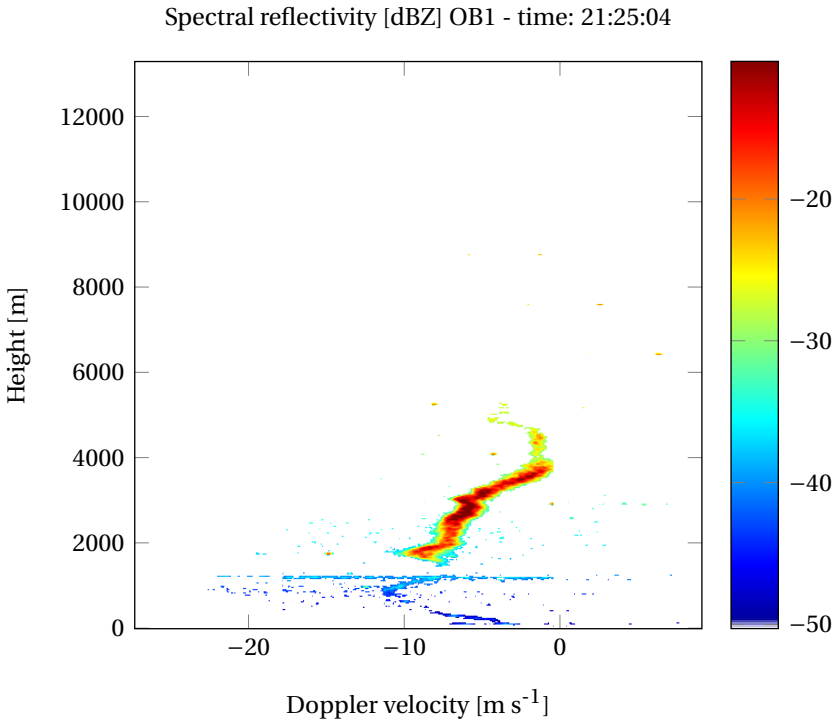

Figure 2.19: Corresponding spectrogram from offset beam 1 of the spectrogram in figure 2.18 with a gap on October 14, 2012. Without nref2, the spectrum at height around 1500 m is compared with the previous spectra. It is possible this results in a wrongly placed spectrum, because the previous spectra are noisy with some remaining clutter.

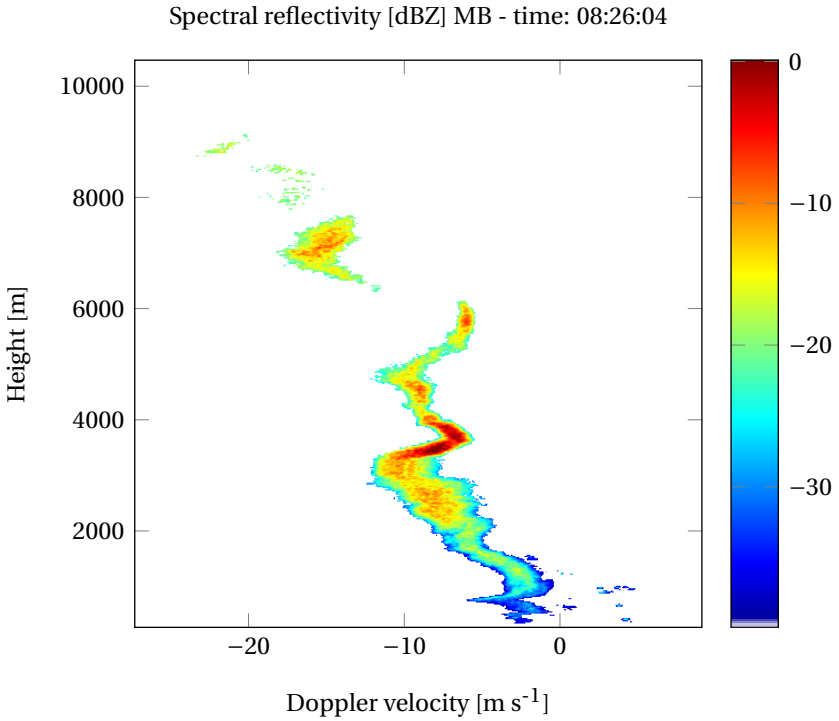

Figure 2.20: Example of a spectrogram with such a small gap it is not recognized as a gap in the algorithm. Therefore no nref2 is determined. This is the spectrogram of the main beam on July 26, 2013.

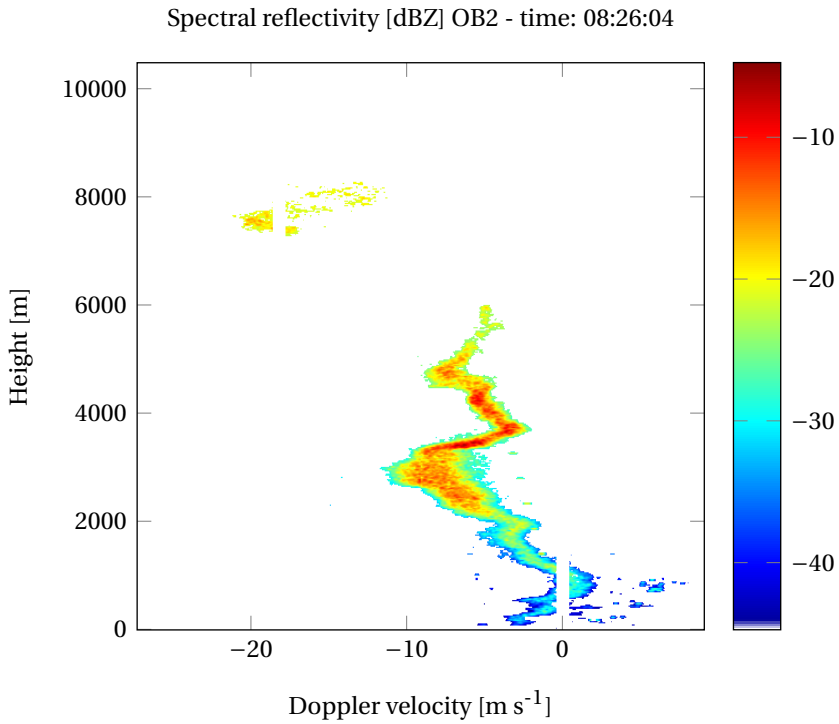

Figure 2.21: Corresponding spectrogram from offset beam 2 of the spectrogram in figure 2.20 on July 26, 2013. Without nref2, the spectra at height around 8000 m are compared with the spectra at 6000 m. This results in wrongly placed spectra. In this figure the spectra are well located using the procedure in absence of nref2.

3

RESULTS AND UNSOLVED PROBLEMS

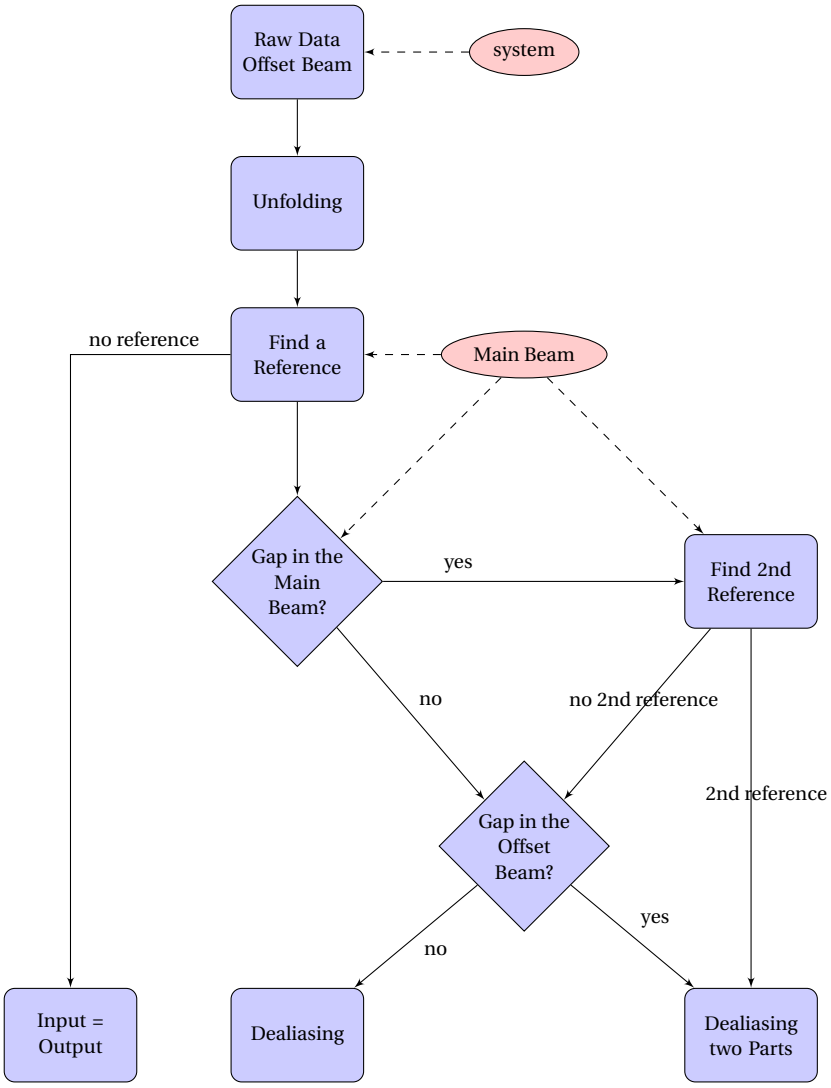

Figure 3.1: Flowchart of the decision making during the process from raw data to the final spectrogram. When there is no reference, every spectrum with a mean Doppler velocity larger than 3 m s^{-1} is shifted one Doppler interval into negative velocities.

In this chapter a summary of the implemented unfolding process and dealiasing process is given. After that, a comparison is made between a few raw data files processed by using the new algorithm described in this report and processed by using the old algorithm. The old algorithm did not use data from the main beam at all and the first reference was chosen in the offset beam itself.

The last sections of this chapter explain some encountered difficulties. In section 3.3 an example is given where the Nyquist interval ($-V_{D,max}$ to $V_{D,max}$) is not sufficient for the spread of the Doppler velocity. Section 3.4 shows what happens when the mean Doppler velocity of the main beam is significantly different than that of the offset beams. The last section, section 3.5, points out that clutter can be a problem during the dealiasing process.

3.1. SUMMARY OF DEALIASING

In figure 3.1 a flowchart of the dealiasing of raw data is depicted. First, every spectrum of the offset beam is unfolded using the alternative unfolding process, explained in section 2.1.2. After unfolding, a reference is searched for in the main beam (section 2.2.3). If no reference is found the dealiasing is skipped. The only thing that is done is shifting spectra that have a mean Doppler velocity of at least three meters per second one Doppler interval into negative velocities. Lastly, the dealiasing process is executed (section 2.2.4) using the mean Doppler velocity (section 2.2.2) to compare spectra.

The dealiasing process basically comes down to a continuity check on every range gate and when a gap is detected in the data from the main beam and/or the offset beam, a continuity check is performed on two separate sets of spectra, with the division at the level of the gap.

The final spectrogram of offset beam 2, from the raw data spectrogram of figure 2.3, after the unfolding process and dealiasing process is depicted in figure 3.2.

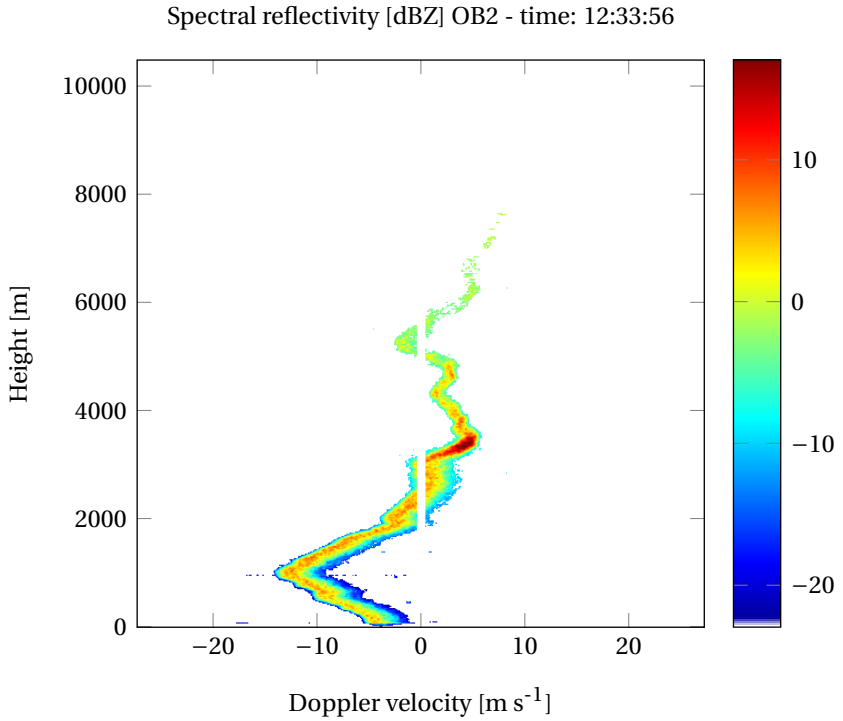

Figure 3.2: Final spectrogram of the offset beam 2. After unfolding and dealiasing the raw data spectrogram from figure 2.3.

3.2. PROCESSING RESULTS

In this section mean Doppler velocity profiles are shown of offset beam 1 and offset beam 2. A profile is generated by combining all the spectrograms from one raw data file. A standard raw data file produces 120 spectrograms. The time resolution is just over 2.5 seconds per spectrogram. In figures 3.3 (OB1) and 3.5 (OB2) the profiles processed with the old algorithm are depicted. Aliasing is still occurring here. In figures 3.4 and

3.6 the depicted profiles are the same profiles except processed with the new algorithm. Here the aliasing is solved. The first time slot in these profiles contains the mean Doppler velocities generated from the raw data spectrograms in figures 2.2 and 2.3. In appendix B more mean Doppler velocity profiles are shown. These profiles are from a variety of different days containing different weather conditions.

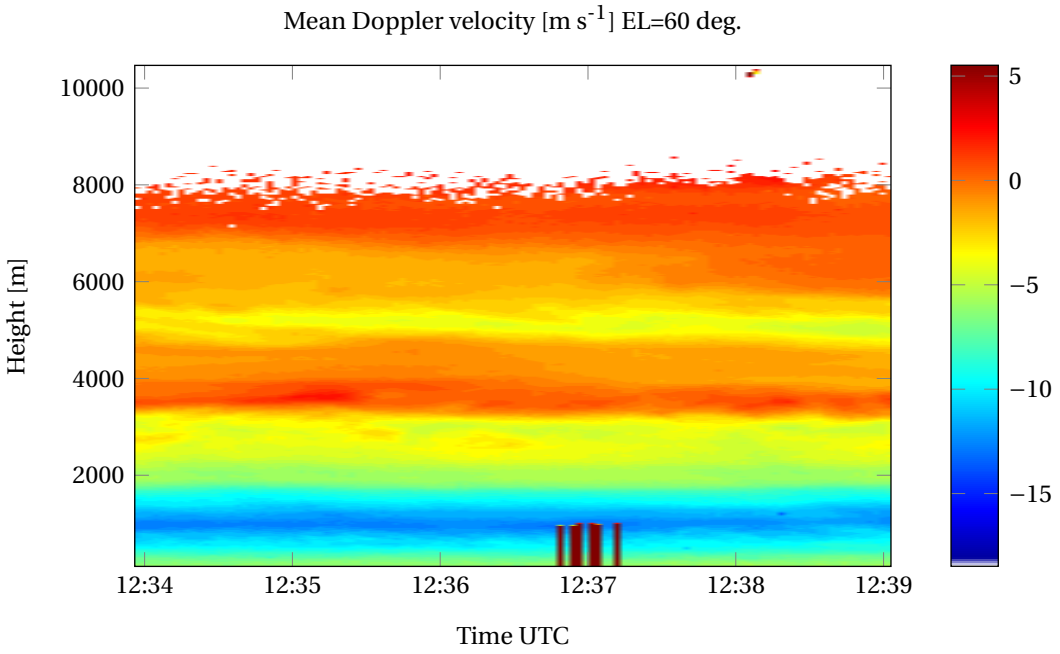

Figure 3.3: Profiles of the mean Doppler velocity of offset beam 1 on June 20, 2013. These are the profiles generated with the old dealiasing algorithm. Because the main beam is at an elevation of 45 degrees, offset beam 1 is at 60 degrees. It is clear aliasing occurs around 12:37 at low altitude. In figure 3.4 the profiles generated with the new algorithm are depicted.

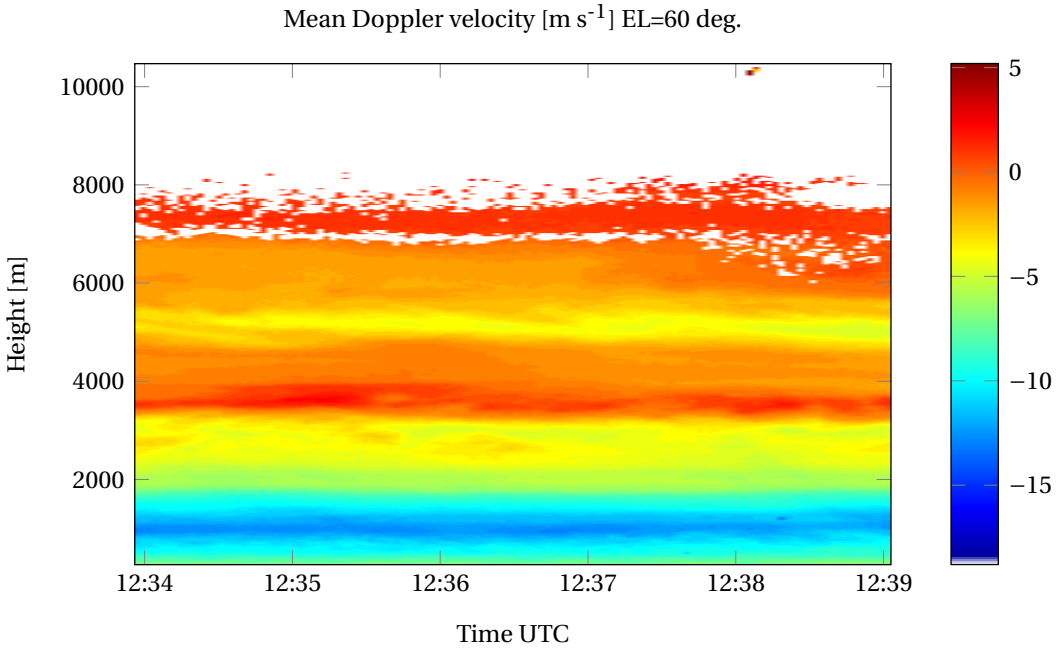

Figure 3.4: Profiles of the mean Doppler velocity of offset beam 1 on June 20, 2013. These are the profiles generated with the new dealiasing algorithm. In figure 3.3 the profiles generated with the old algorithm are depicted. The aliasing around 12:37 is solved. The missing data around 7000 m are because of the notch filter around 0 m s^{-1} and the narrow spectra at that height.

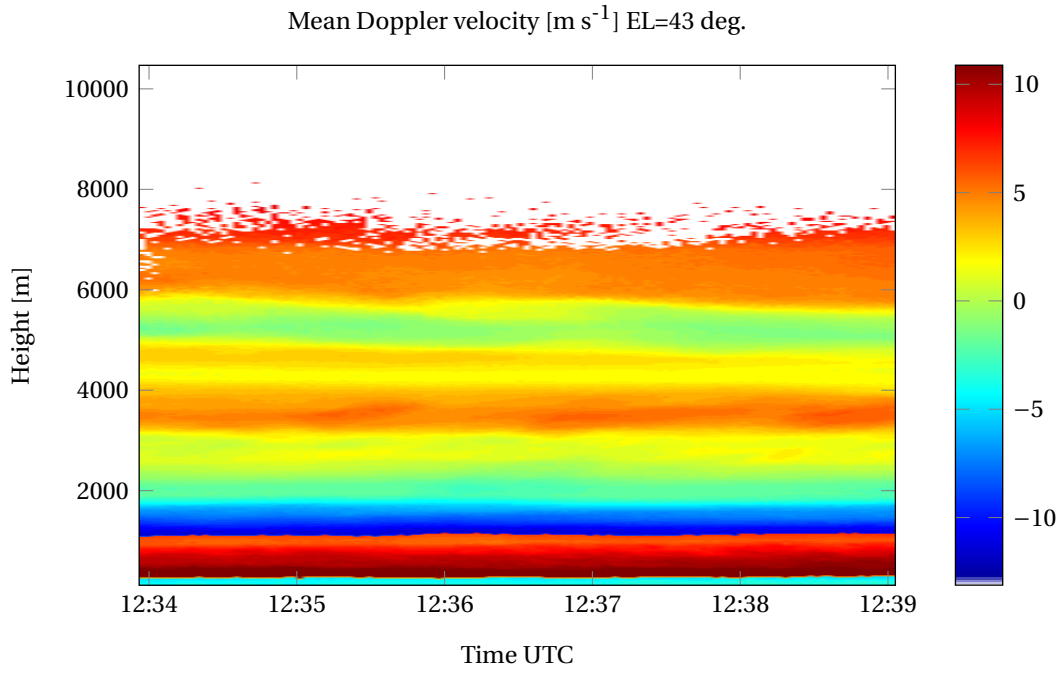

Figure 3.5: Profiles of the mean Doppler velocity of offset beam 2 on June 20, 2013. These are the profiles generated with the old dealiasing algorithm. Because the main beam is at an elevation of 45 degrees, offset beam 2 is at 43 degrees. It is clear aliasing occurs at low altitude for every spectrogram. In figure 3.6 the profiles generated with the new algorithm are depicted.

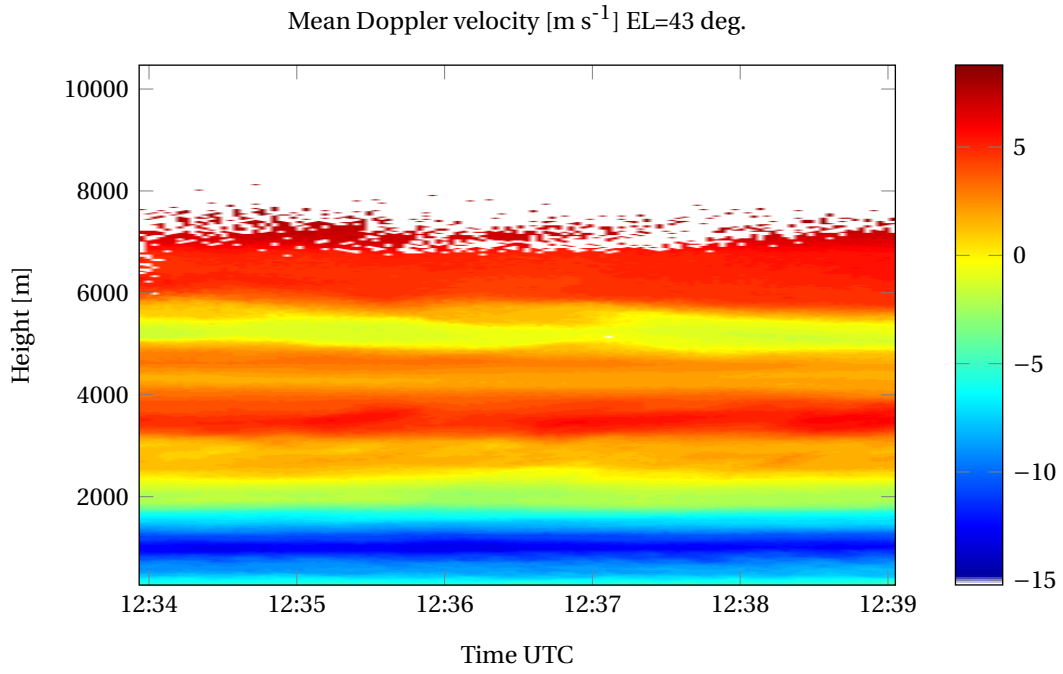

Figure 3.6: Profiles of the mean Doppler velocity of offset beam 2 on June 20, 2013. These are the profiles generated with the new dealiasing algorithm. In figure 3.5 the profiles generated with the old algorithm are depicted. The aliasing at low altitude is solved.

3.3. OVERLAPPING SPECTRA

In this section an example is given of a case where all the 512 Doppler bins of a raw spectrum have been taken up by atmospheric targets. The raw data spectrogram of this case is depicted in figure 3.7. Here the spectra at height 4100 to 4500 m are so wide it is difficult to determine the start and end of the spectrum because it is

slightly overlapping. Problems arise during the unfolding process. Especially by using a notch filter around 0 m s^{-1} all the wide spectra are unfolded around this notch filter. The result after unfolding and dealiasing is depicted in figure 3.8 and the result when not applying a notch filter is in figure 3.9. With an adaptive notch filter or an unfolding algorithm that includes the possibility of a notch filter it might be possible to unfold the spectra as if no notch filter was applied (figure 3.9).

The only way to dealiase truly overlapping spectra (between 4100 and 4500 m in this example) is changing the radar measurement specifications. The Doppler sampling time, T_m should be reduced.

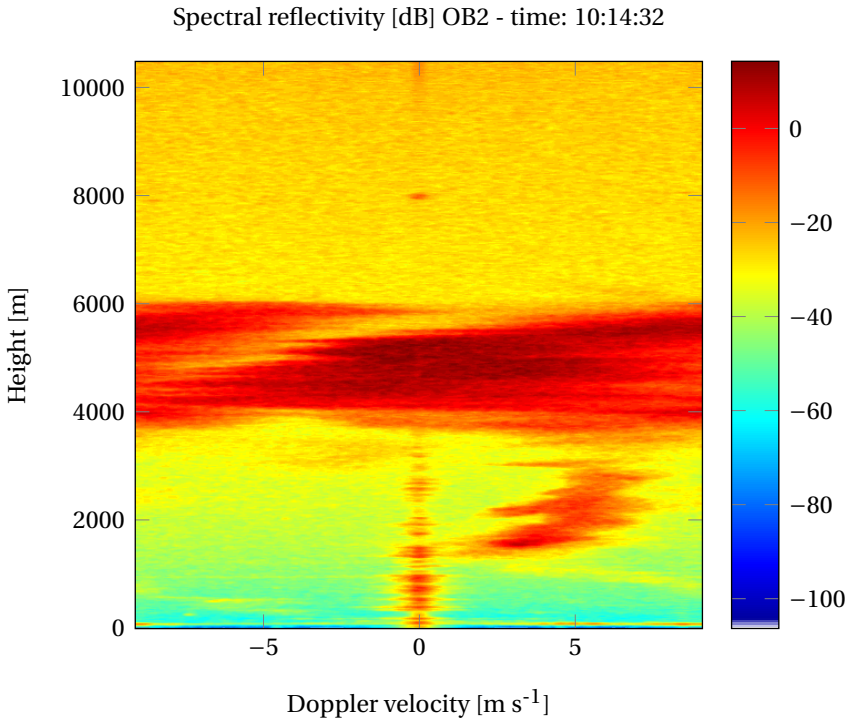

Figure 3.7: Raw data spectrogram of the offset beam 2 of TARA on October 7, 2014. Overlapping spectra between 4100 and 4500 m.

3.4. LARGE DIFFERENCE BETWEEN MEAN DOPPLER VELOCITIES

Taking the main beam as reference is only valid when the difference in mean Doppler velocity between the main beam and an offset beam is smaller than $V_{D,max}$(9.096 m s^{-1}). Remembering equation 2.1:

$$
\begin{aligned}
V_{MB} &= V_x \cos\alpha + V_z \sin\alpha \\
V_{OB1} &= V_x \cos(\alpha + 15) + V_z \sin(\alpha + 15) \\
V_{OB2} &= V_x \cos\alpha \cos(15) + V_y \sin(15) + V_z \sin\alpha \cos(15),
\end{aligned}
$$

the difference in velocity between the main beam (V_{MB}) and offset beam 1 (V_{OB1}) is small when the wind direction is perpendicular to the direction of the x-axis of TARA. This difference is large when the wind direction is the same as the x-axis of TARA. The difference between V_{MB} and V_{OB2} is almost the opposite, large when perpendicular and small when in the same direction. Mainly due to the factor $V_y \sin(15)$ in the formula for V_{OB2}. If there is a strong horizontal wind, with a direction perpendicular to the x-axis of TARA, the difference between V_{MB} and V_{OB2} could exceed $V_{D,max}$. On October 13, 2013, this happened a few times during a storm in the Netherlands. In figure 3.10 the raw spectrograms of the main beam and offset beam 2, at one time this occurred , are depicted. In this case nref was chosen at range bin 19 (height 381 m), where, unfortunately, the difference in velocity between the main beam and the offset beam 2 is larger than the limit. The mean Doppler velocity for the main beam is -7.03 m s^{-1} and for offset beam it is 3.18 m s^{-1}. Here -7.03 m s^{-1} is an average of range bin 19 to 24 of the main beam. But even only taken range bin 19 (nref) would cause a failure, because the mean Doppler velocity of nref is -5.98 m s^{-1}. Looking at the resulting spectrograms of the main

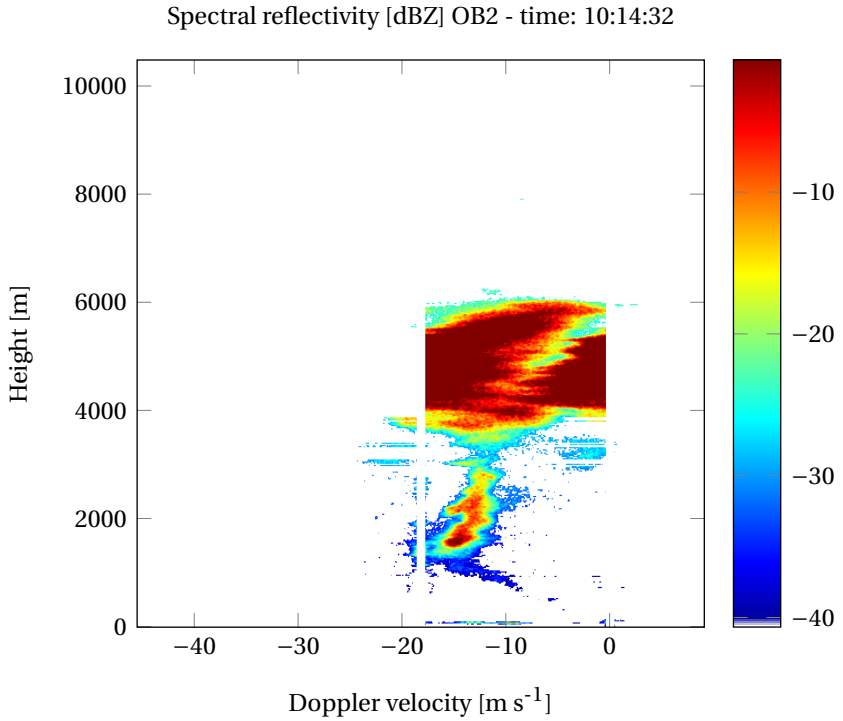

Figure 3.8: Spectrogram after unfolding and dealiasing the raw data spectrogram from figure 3.7. The wide spectra are unfolded around the notch filter, which is incorrect.

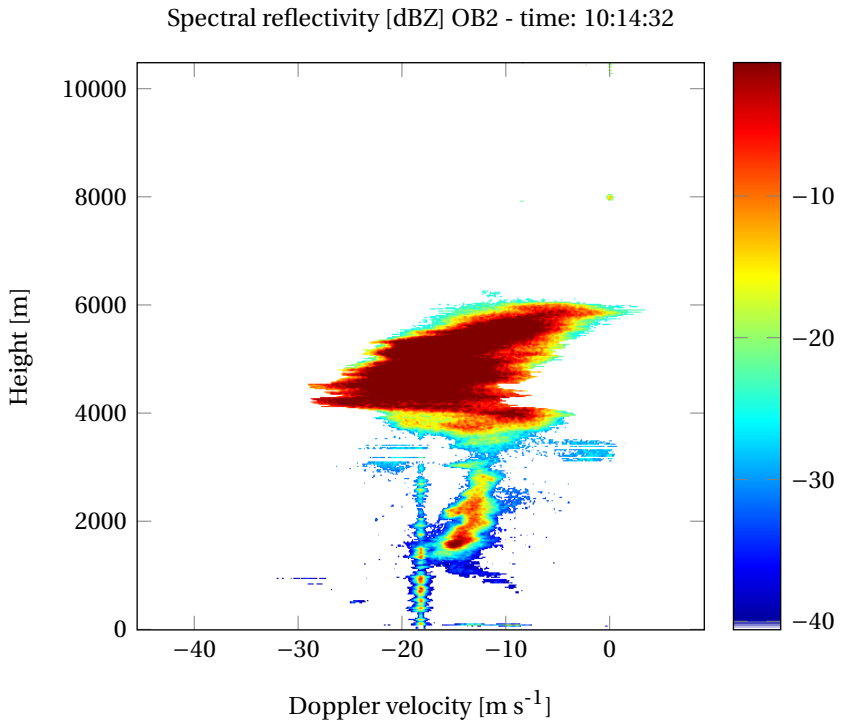

Figure 3.9: Spectrogram after unfolding and dealiasing the raw data spectrogram from figure 3.7. Without a notch filter unfolding is much better compared with figure 3.8.

beam and offset beam 2 (figure 3.11) it is clear the whole spectrogram of offset beam 2 is placed one Doppler interval to the left.

Because nref is at low range, the volumes both beams are looking at, are close to each other. Therefore the difference in weather condition is negligible. The deviation in velocity comes from the direction both beams are in. The graph in figure 3.12 shows the velocity difference versus the wind direction, calculated using equation 2.1, with $\alpha = 45°$, $V_z = -7$ m s^{-1} and horizontal wind speed (V_H) = 34.3 m s^{-1} (OB2) and V_H = 38.5 m s^{-1} for OB1. V_x and V_y are defined as

$$\begin{aligned} V_x &= V_H \cos(\alpha_w) \\ V_y &= V_H \sin(\alpha_w), \end{aligned} \tag{3.1}$$

with α_w the wind direction in the local coordinate system (x,y). In this graph it can be seen the largest difference between V_{MB} and V_{OB2} is when the wind direction is 95° and 275° (nearly orthogonal to x). And by using V_H = 34.3 m s^{-1} the difference just stays within the limits. So when V_H exceeds 34.3 m s^{-1} and the wind direction is 275° the dealiasing fails. For other wind directions a larger V_H is necessary to fail the dealiasing for OB2. The largest difference between V_{MB} and V_{OB1} is when the wind direction is 0° or 180°. Using V_z = -7 m s^{-1} and V_H = 38.5 m s^{-1} the difference just stays within the limits. So when V_H exceeds 38.5 m s^{-1} and the wind direction is 180° the dealiasing fails for OB1.

According to the Royal Netherlands Meteorological Institute (KNMI) website [www.knmi.nl] on October 13, 2013, a maximum gust of 19.0 m s^{-1} was measured in Cabauw, and the prevailing wind direction was 159° (related to the north). Calculating the difference with this wind speed and angle (272.5° from TARA X-axis), gives a -5.1 m s^{-1} difference between V_{MB} and V_{OB2}. As shown in figure 3.10 it is almost doubled. The wind speed from the KNMI is given at ground level (10 m) and at 381 m height the wind speed was much larger that day. Or perhaps the wind speed and direction in both radar resolution volumes are much more diverse than assumed, due to turbulence or other phenomena. A closer look into this is a next step. But the combination of a large wind speed and this least favorable wind direction rarely happens. It is therefore not a priority.

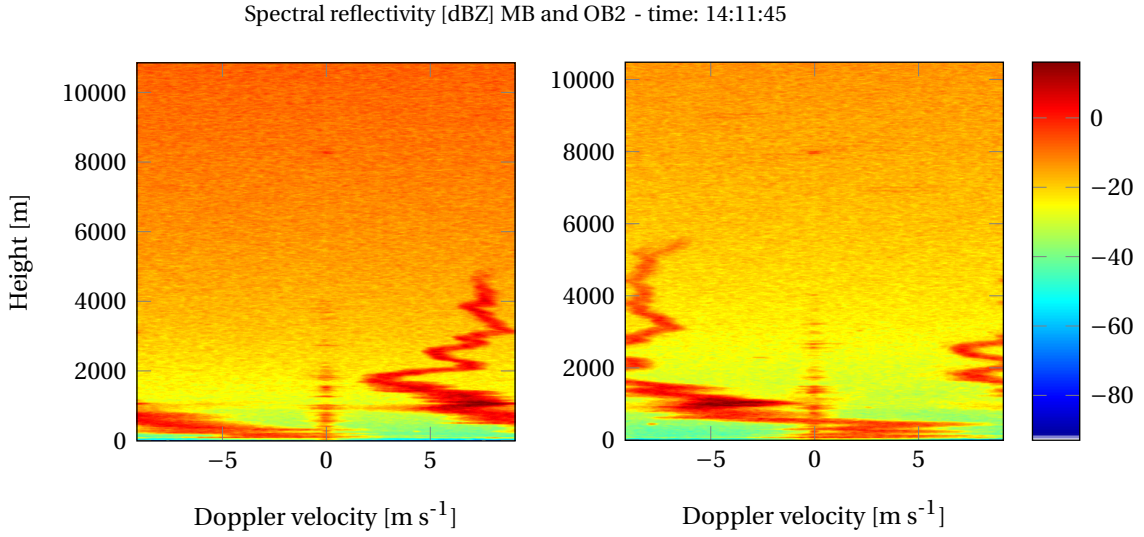

Figure 3.10: Raw data spectrograms of the main beam (left panel) and offset beam 2 (right panel), on October 13, 2013. The difference in Doppler velocity between the reference in the main beam (nref) at height 381 m and the spectrum at the same height in the offset beam, causes a failure in dealiasing when it is larger than 9.096 m s^{-1}.

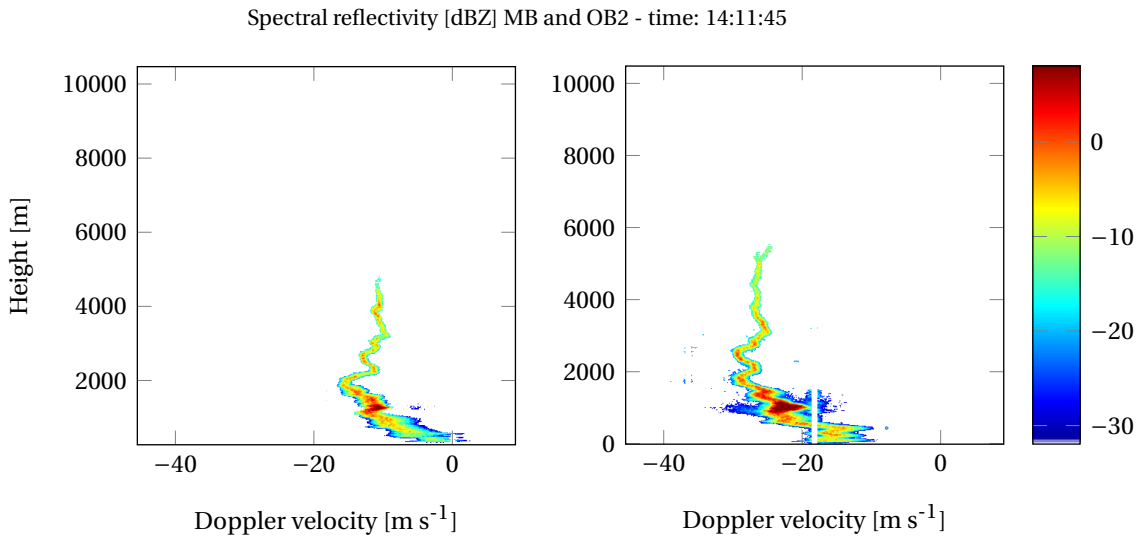

Figure 3.11: Spectrograms of the main beam (left panel) and offset beam 2 (right panel) after unfolding and dealiasing the raw data spectrograms of figure 3.10. The dealiasing has failed due to a large difference in mean Doppler velocity between nref and the spectrum of the offset beam at the same height.

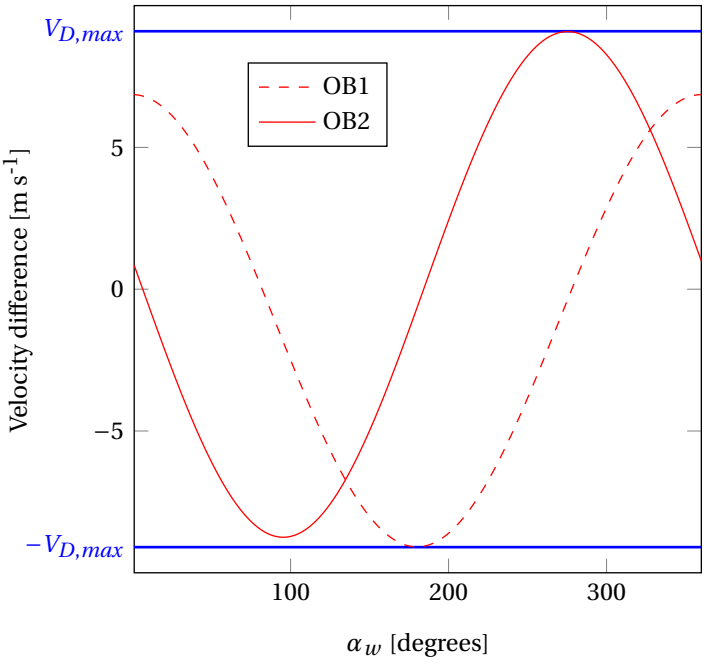

Figure 3.12: Difference in velocity between V_{MB} and V_{OB1} (V_{OB2}) versus wind direction related to the x-axis of TARA (α_w), calculated using equations 2.1 and 3.1. 34.3 m s^{-1} is used for the horizontal wind speed (V_H) to show the difference in velocity between V_{MB} and V_{OB2}. This difference will exceed the limit of $V_{D,max}$ (9.096 m s^{-1}) when V_H is larger than this and the direction is 275°. 38.5 m s^{-1} is used for V_H to show the difference in velocity between V_{MB} and V_{OB1}. This difference will exceed $V_{D,max}$ when V_H is larger than 38.5 m s^{-1} and the wind direction is 180°.

3.5. CLUTTER

It is difficult to remove all of the clutter without removing any atmospheric targets. With the notch filter around 0 m s^{-1} a lot of clutter is removed, but sometimes the filter is too small and some leftover clutter is still present. And on the other hand sometimes the filter removes perfectly fine data. A better clutter suppression method is necessary to improve this.

Although the dealiasing algorithm can deal with some clutter, dealiasing can fail due to the clutter. Next is an example where clutter influences the dealiasing. In this example nref is at height 425 m (range bin 21) and the data in the main beam is limited to height 1400 m. The spectrogram of the main beam is depicted in figure 3.13 and of offset beam 1 in figure 3.14. The part around height 5500 m is aliased, because there is no reference from the main beam and OUTrefer is filled with mean Doppler velocities of spectra only containing clutter. In figure 3.15 the result of dealiasing is depicted when the width of the notch filter is doubled. Now more clutter is removed and the dealiasing works well.

It is not advised to have a wide notch filter applied as a default. Most of the time when there is a precipitating cloud a wide notch filter will do more harm than good. In the case described above it does not matter if dealiasing is correct or not for the part around 5500 m. It cannot be used for the wind estimation, since that requires the mean Doppler velocity from every beam (MB, OB1 and OB2). And the dealiasing mainly fails because there is no mean Doppler velocity information from the main beam at that height.

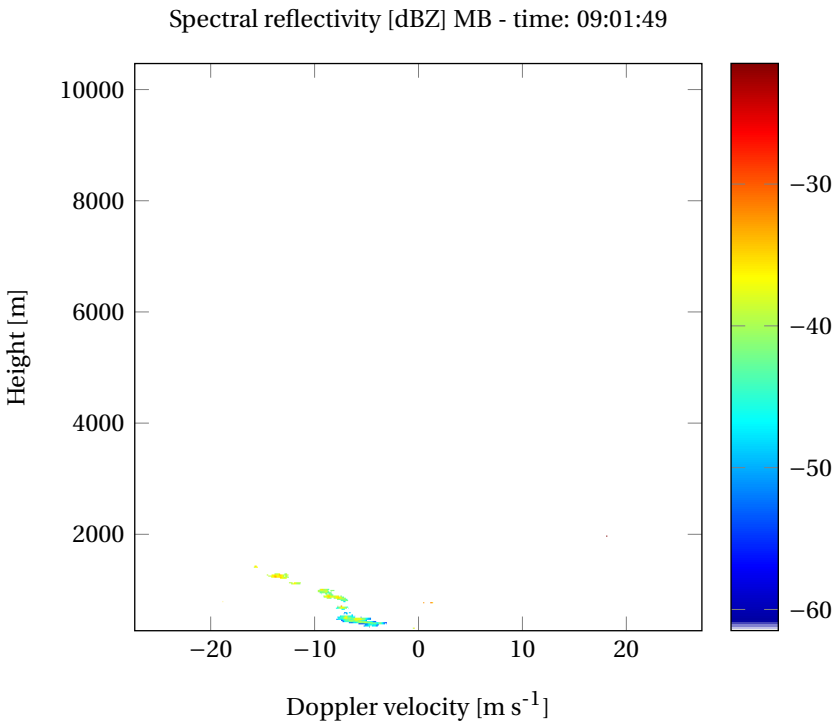

Figure 3.13: Spectrogram of the main beam on October 7, 2014. Because the data in the main beam is limited to a height of 1400 m, clutter influences the dealiasing of parts in the offset beam at higher heights. In figure 3.14 the spectrogram of offset beam 1 is depicted.

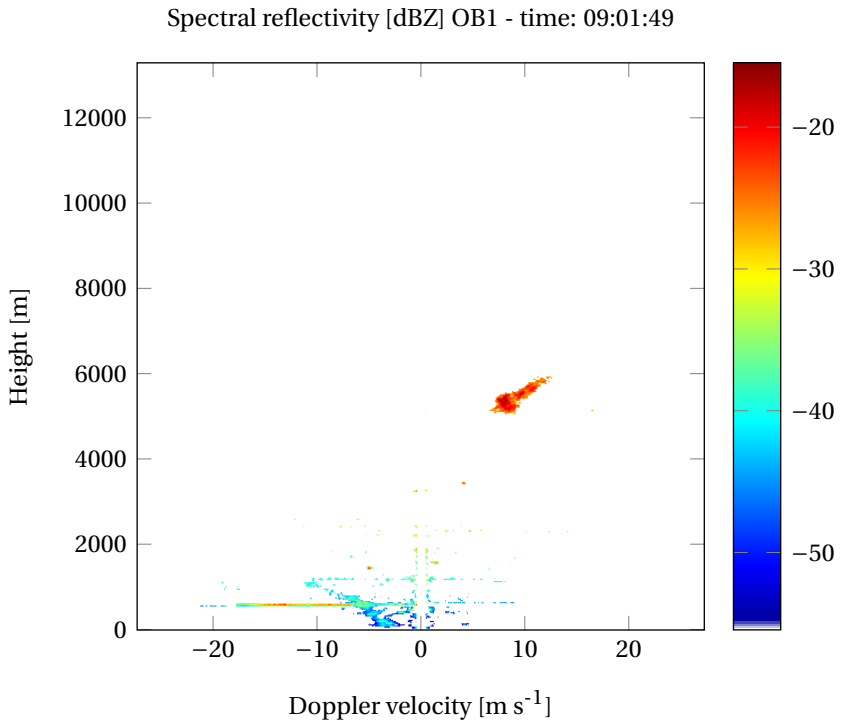

Figure 3.14: Spectrogram of offset beam 1 on October 7, 2014. The part around 5500 m is aliased, because OUTrefer is filled with the clutter around 0 m s^{-1} from range bins higher than 1400 m.

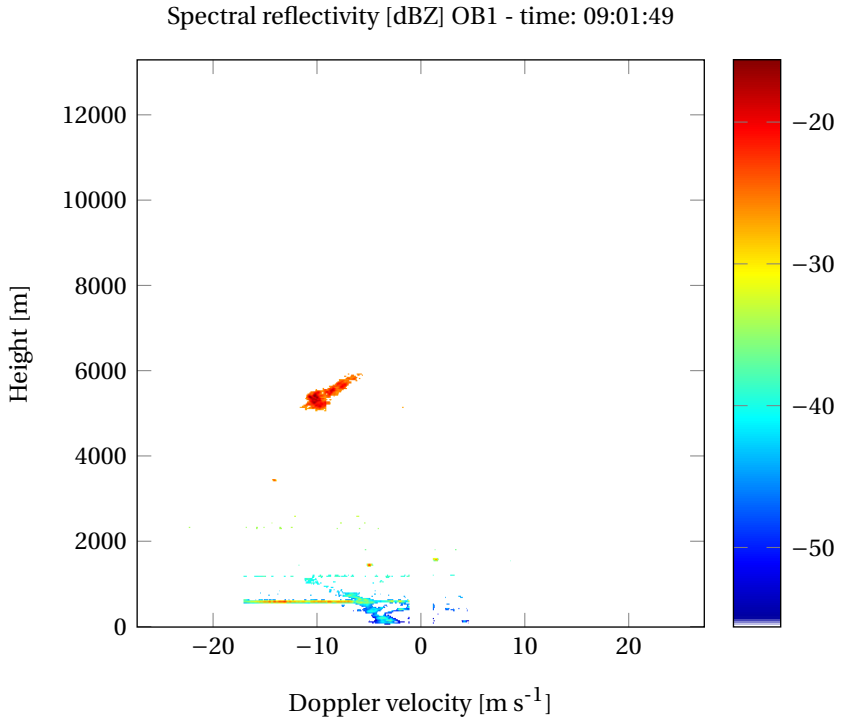

Figure 3.15: Spectrogram of offset beam 1 on October 7, 2014. With the width of the notch filter doubled, OUTrefer is no longer filled with the clutter around 0 m s^{-1}. Therefore the dealiasing works as intended.

4

COMPARISON BETWEEN SENSORS

In this chapter a comparison is made between wind velocities and wind directions generated by TARA and generated by other sensors. The sensors that are standard available at Cabauw Experimental Site for Atmospheric Research (CESAR) are discussed first. Cabauw is the site TARA is usually located at. The sensors discussed first are: Cabauw anemometer, KNMI Lower Atmospheric Profiler LAP3000 and KNMI 35 GHz cloud radar. The anemometer and the wind profiler (LAP3000) have the horizontal wind speed and wind direction as output, while the cloud radar only has the vertical velocity as output. After this two sensors are discussed briefly; a Doppler lidar (HALO Photonics) and a cloud radar (Mira36). These were brought to Cabauw by TROPOS (Leibniz Institute for Tropospheric Research, Leipzig, Germany) during the ACCEPT campaign (Analysis of the Composition of mixed-phase Clouds with Extended Polarization Techniques) between October 6th and November 16th, 2014.

For every sensor a MATLAB m-file is available to produce graphs with a comparison between TARA and that sensor. In each section of this chapter a typical output is given of the m-file for the different sensors. For the examples in this chapter a small interpretation of the results is given. When using the m-files it is up to the user to interpret the results, which can be more in depth than is done here. The user is also able to change the settings in the m-file to have the results more to its liking. These settings are the time resolution of each sensor and at what heights the comparisons should take place. Depending on the sensor the there are different limitations on each setting.

June 20, 2013 is the day the comparisons, between TARA and the sensors that are standard available at Cabauw, are made. Figures 2.1 to 2.3 and 3.2 to 3.6 show some spectrograms and profiles on that day. These only cover a very small part of the day and do not show the wind field calculations. In figures 4.1 to 4.3 the profiles for horizontal wind velocity, direction of the wind and the vertical Doppler velocity are shown for the whole day. Note that the vertical Doppler velocity in an estimate, because TARA profiles slantingly at 45° elevation. The vertical Doppler velocity is the sum of the hydrometeors mean fall velocity and the mean vertical wind. The three dynamics parameters of these figures are generated at the end of each day. Consequently at that time the old algorithm was still in use. Especially in figure 4.1 it can be seen aliasing causes some errors between 12:00 and 14:00h at low altitude.

4.1. SONIC ANEMOMETER

In figure 4.4 the comparison between TARA and the sonic anemometer is shown for the whole day as well. The anemometer is located at a height of 200 m and the time resolution is ten minutes. To best compare the results of TARA the height closest to 200 m is taken, which is 191 m. It is up to the user to select the time resolution for TARA. The resolution in figure 4.4 is chosen at ten minutes. On average every 6.6 seconds a measurement is taken for TARA, so a resolution of ten minutes (600 seconds) results in averaging over 91 measurements. In those measurements V_i is the wind velocity at time t_i and D_i the wind direction. Averaging over the wind velocity is easy using

$$V_a = \frac{\sum V_i}{n}, \tag{4.1}$$

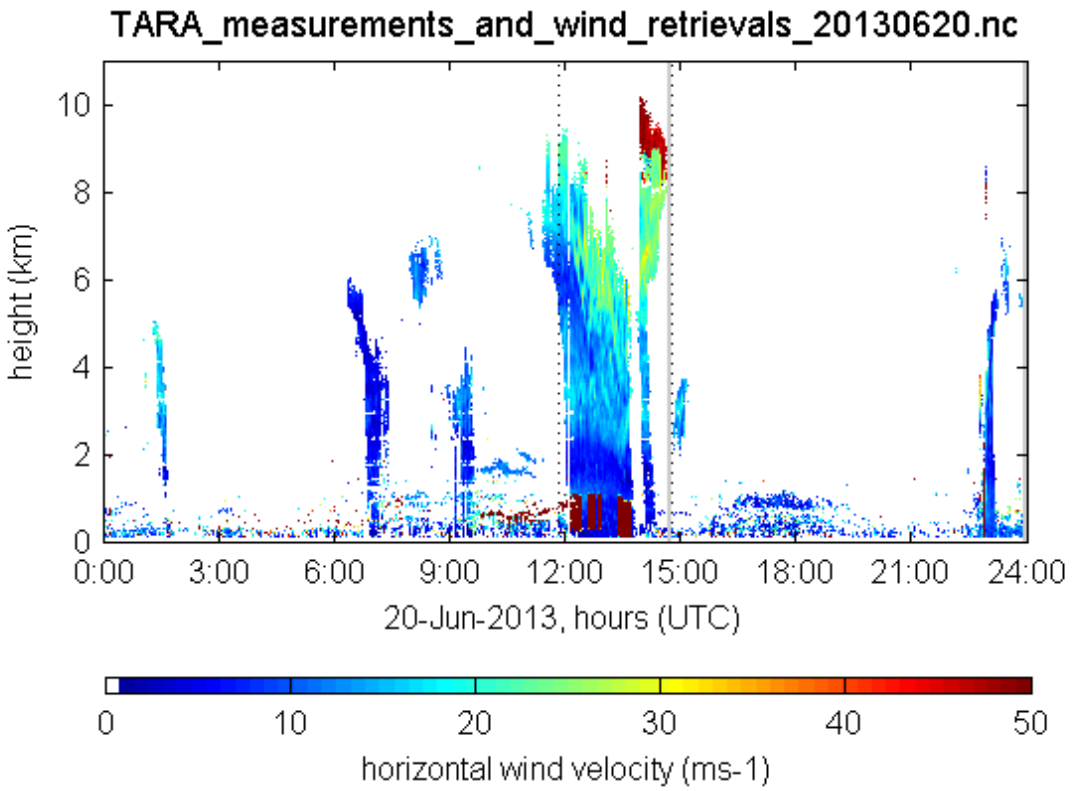

Figure 4.1: Profiles of the horizontal wind velocity generated by TARA on June 20, 2013. The aliasing consequence is clear in the rain the first km between 12:00 and 14:00h. Further the large values at the top of the precipitating cloud around 14:00h between 9 and 10 km are caused by aliasing.

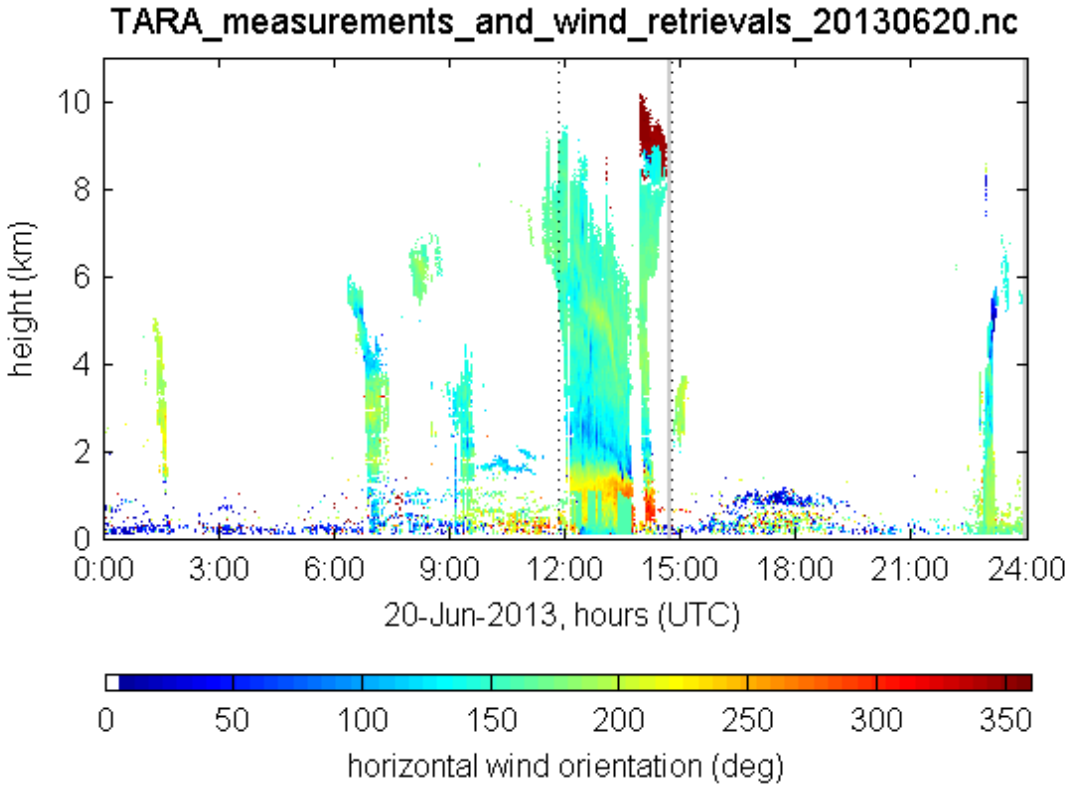

Figure 4.2: Profiles of the orientation of the wind related to the north generated by TARA on June 20, 2013.

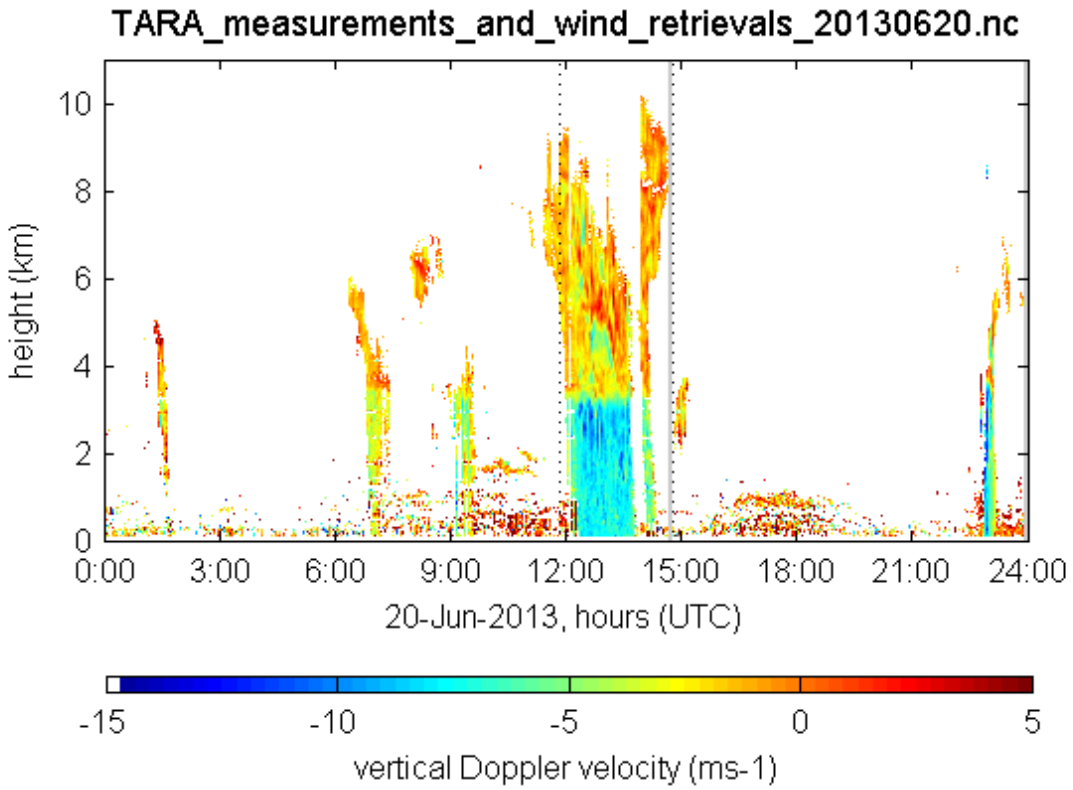

Figure 4.3: Profiles of the vertical Doppler velocity generated by TARA on June 20, 2013.

with n the number of measurements. But averaging over the wind direction is a bit more complicated due to the discontinuity at 360°. Mori [12] shows averaging in direction is done by the following equation:

$$D_a = \tan^{-1}\left(\frac{S_a}{C_a}\right), \tag{4.2}$$

where

$$C_a = \frac{\sum \cos D_i}{n}, \tag{4.3}$$

and

$$S_a = \frac{\sum \sin D_i}{n}, \tag{4.4}$$

Before averaging statistical outliers are removed. Every value of V_i outside the 15th and 85th percentile is removed. Basically every value in the middle 70 % is kept for averaging. Because NaN values are removed beforehand there is often a low amount of measurements to average. In any case the highest and lowest value of the wind velocity is removed. This holds for $n \geq 3$. When $n < 3$ every value is kept for averaging. When values of V_i are removed, also the corresponding values of D_i are removed before averaging the wind direction.

Because the measurements of TARA are unreliable when there is little to no precipitation, it is only useful to look at time periods with precipitation. Looking at figure 4.4, the wind direction of TARA follows more or less the wind direction of the anemometer during the day. The wind velocity for TARA on the other hand is unreliable, when assuming the anemometer indicates the right value of the wind velocity. In figure 4.5 the period with precipitation (between 11:50 and 14:40h) is enlarged. Figure 4.6 shows the same period but with a time resolution of one minute (60 seconds). In these figures the values for TARA and the anemometer are comparable in the period between 12:30 and 13:15h. After that aliasing occurs for TARA. Note that the

wind direction changes just after 14:00h from very high values to very low values. That is the crossing of the discontinuity at 360°. In figure 4.7 the same comparison is shown as in figure 4.5, except the values for TARA are computed using the new dealiasing algorithm. Note that the values for TARA after 13:45h are unreliable, because at height 200 m not much precipitation was present after that time.

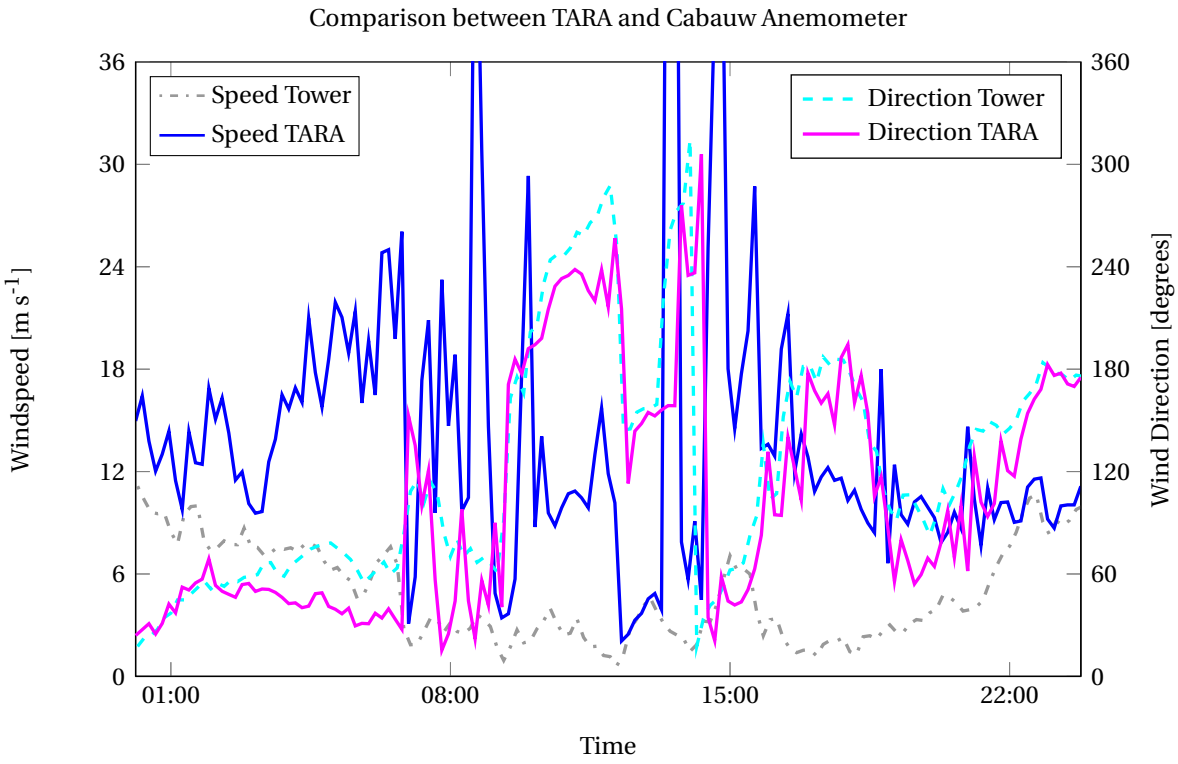

Figure 4.4: Comparison of horizontal wind velocity and wind direction between TARA and the anemometer at Cabauw. The time resolution of TARA is 600 seconds.

4.2. WIND PROFILER

The wind profiler at Cabauw has a time resolution of 30 minutes, and in contrast to the anemometer it has measurements at different heights. With a resolution of 58 m at altitudes below 1500 m and a resolution of 198 m above 1500 m. The default output of the program is made to have a comparison every 1000 m up to 5000 m. This means the height of the wind profiler closest to every 1000 m is taken to compare with the height of TARA closest to the height of the wind profiler. For these comparisons the time resolution of TARA is set at ten minutes. The results are in figures 4.8 to 4.12. At height 1000 m the aliasing still has a lot of influence on the results of TARA. At higher heights there is no aliasing anymore and it shows in the results. At heights 2000 to 5000 m, the horizontal wind velocity and wind direction are quite similar for TARA and the wind profiler. The gap in the data for TARA at time around 14:00h (figure 4.1) causes the results around that time to be missing or averaged over very little data points. In figure 4.13 the same comparison is shown as in figure 4.8, except the values for TARA are computed using the new dealiasing algorithm. Note that the values for TARA after 13:45h are unreliable, because at height 1000 m not much precipitation was present after that time.

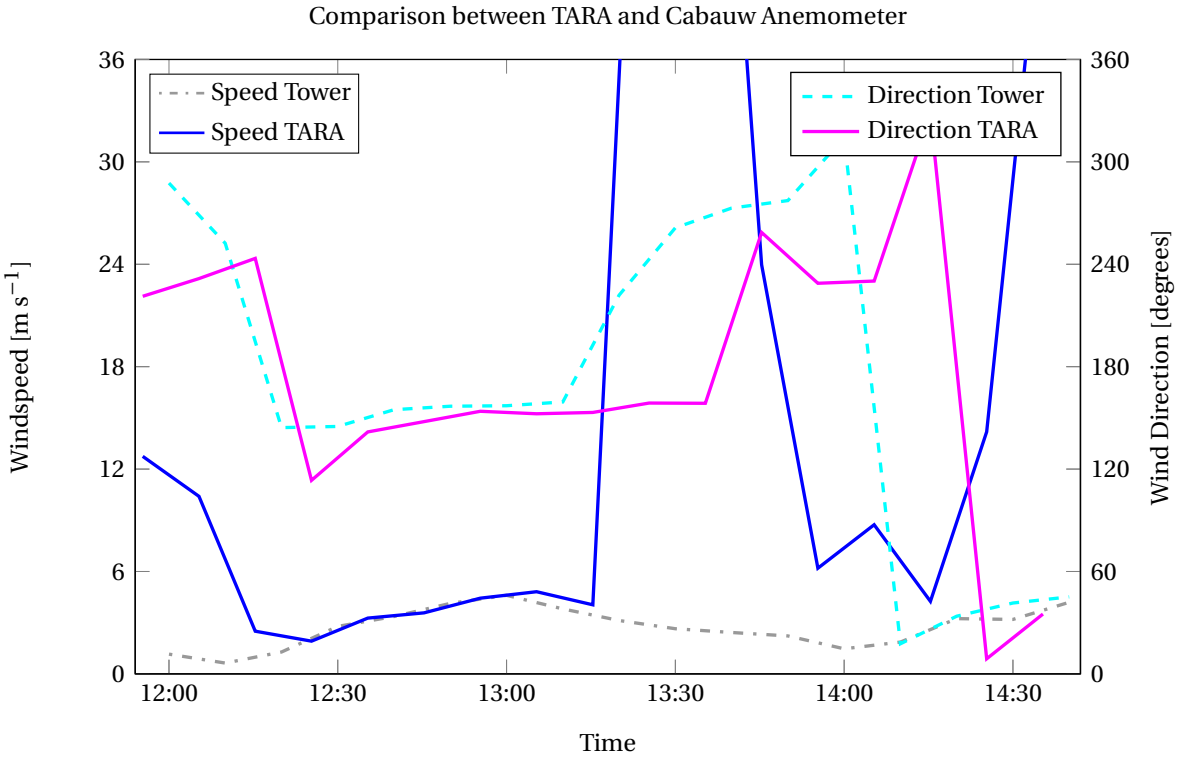

Figure 4.5: Comparison of horizontal wind velocity and wind direction between TARA and the anemometer at Cabauw. The time resolution of TARA is 600 seconds.

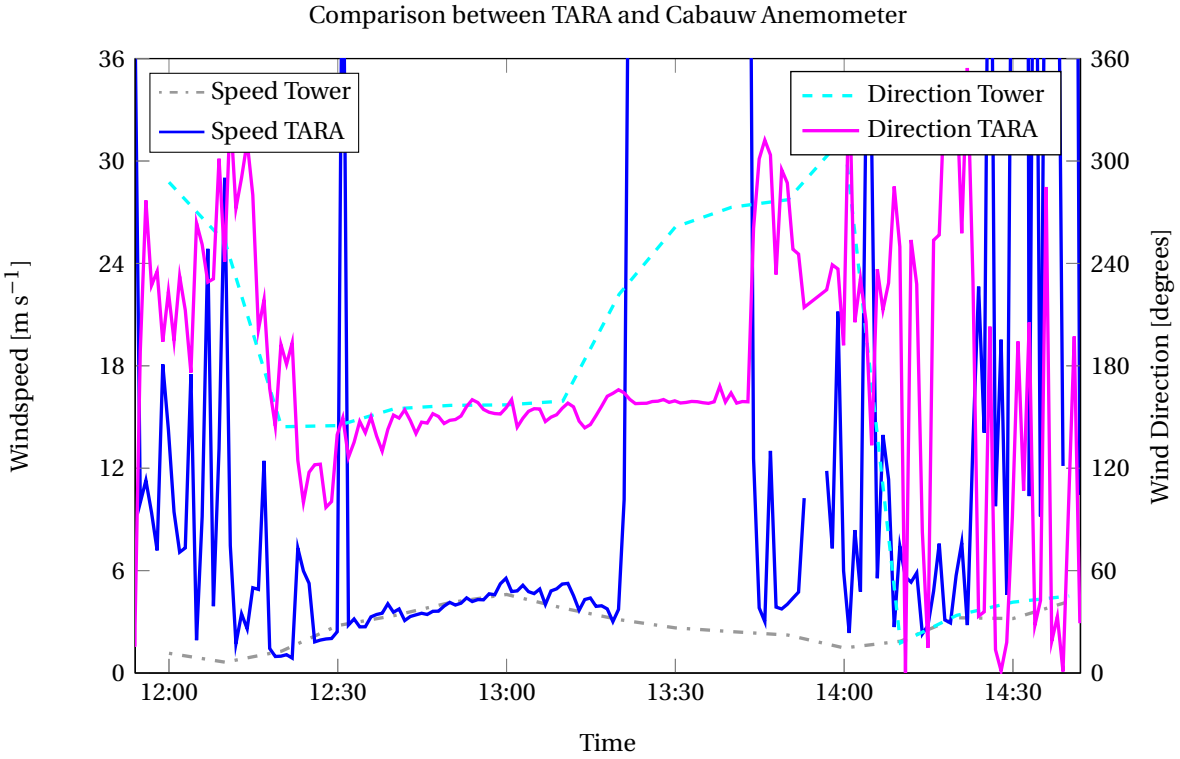

Figure 4.6: Comparison of horizontal wind velocity and wind direction between TARA and the anemometer at Cabauw. The time resolution of TARA is 60 seconds.

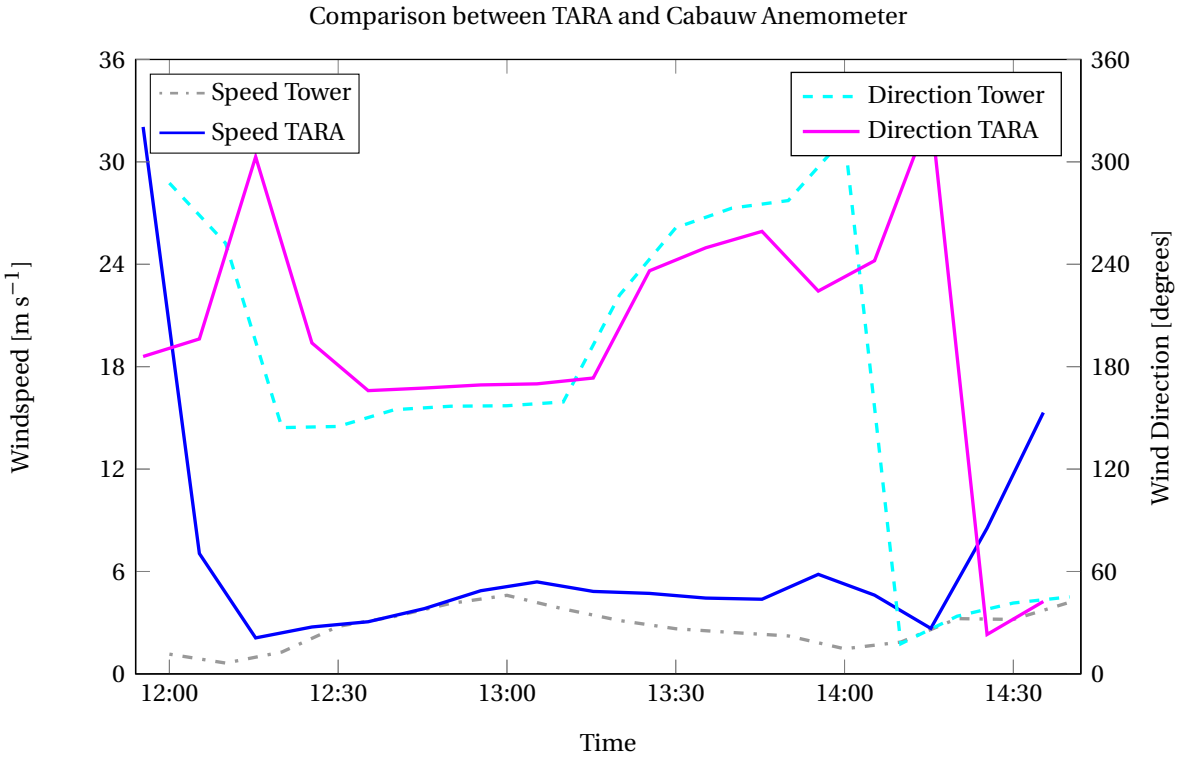

Figure 4.7: Comparison of horizontal wind velocity and wind direction between TARA and the anemometer at Cabauw. The resolution of TARA is 600 seconds. This is after using the new dealiasing technique.

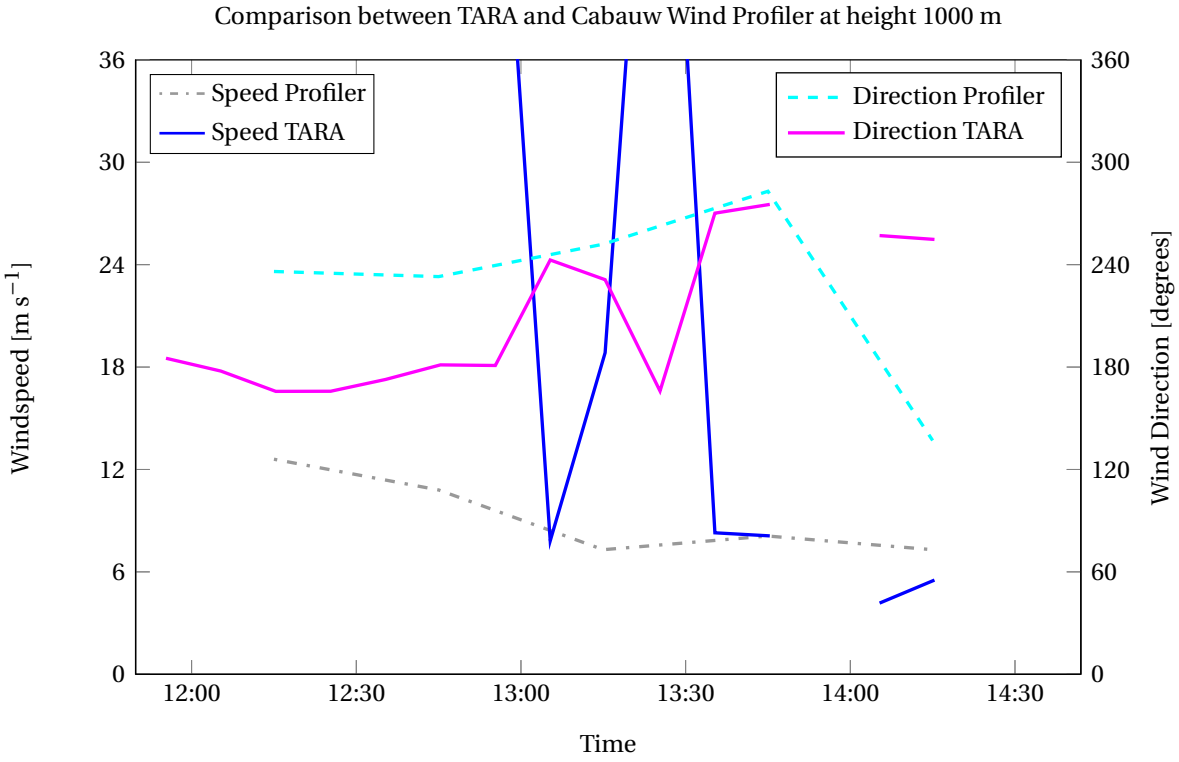

Figure 4.8: Comparison of horizontal wind velocity and wind direction between TARA and the wind profiler at Cabauw at height 1000 m.

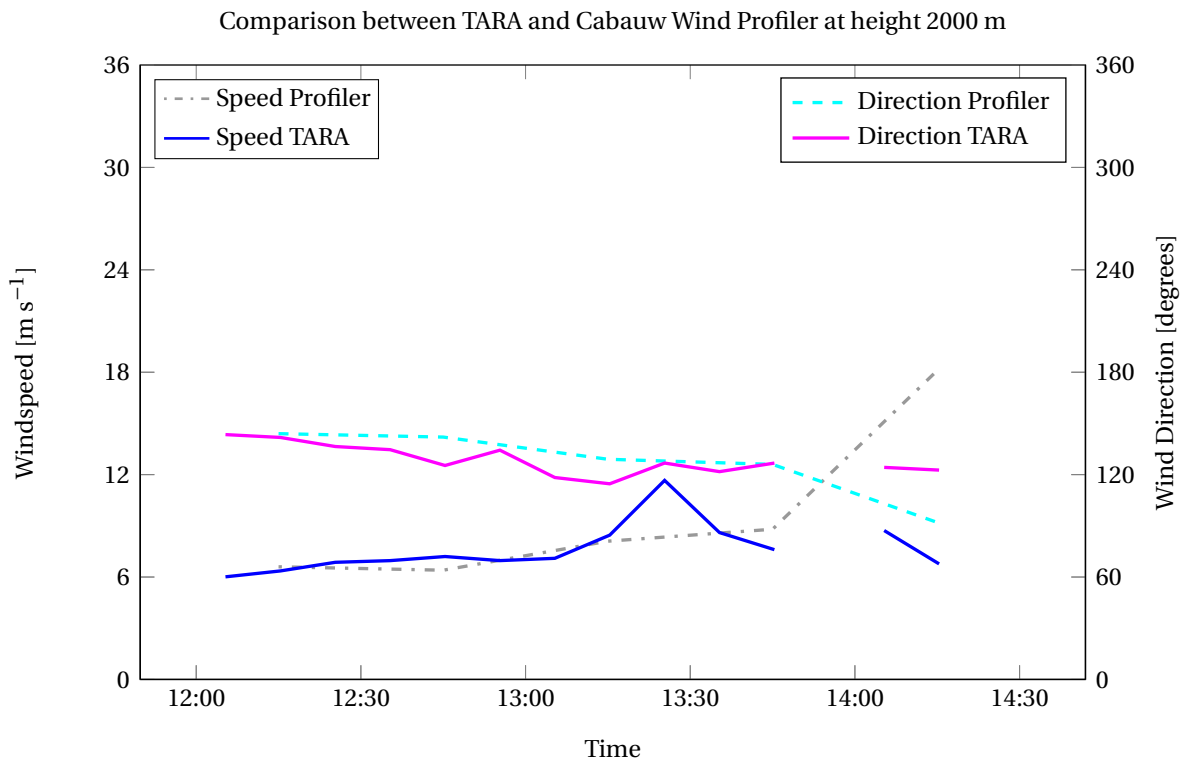

Figure 4.9: Comparison of horizontal wind velocity and wind direction between TARA and the wind profiler at Cabauw at height 2000 m.

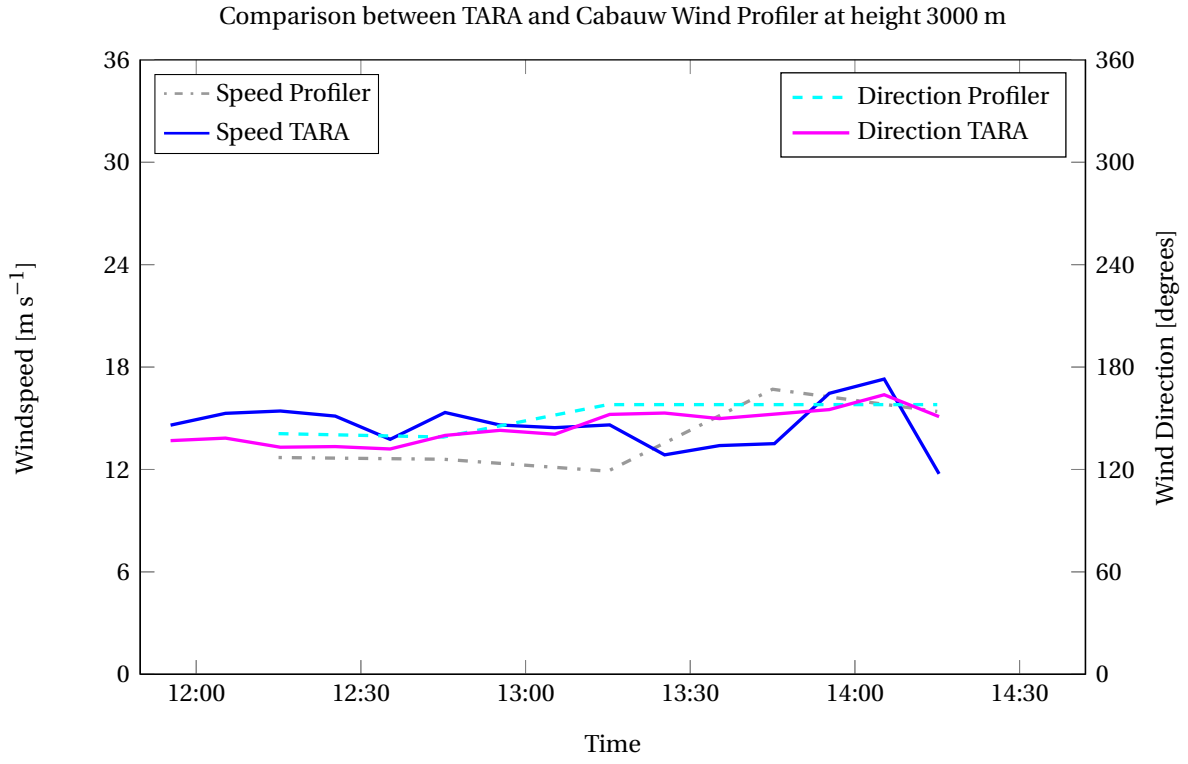

Figure 4.10: Comparison of horizontal wind velocity and wind direction between TARA and the wind profiler at Cabauw at height 3000 m.

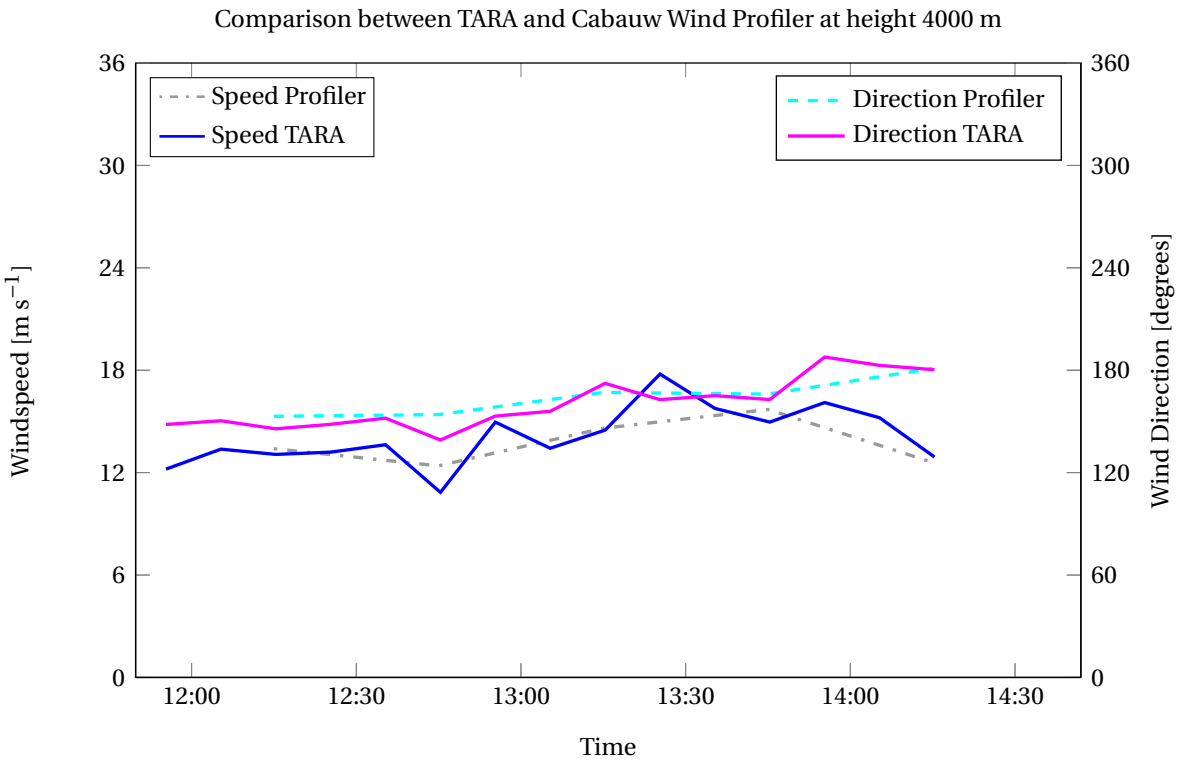

Figure 4.11: Comparison of horizontal wind velocity and wind direction between TARA and the wind profiler at Cabauw at height 4000 m.

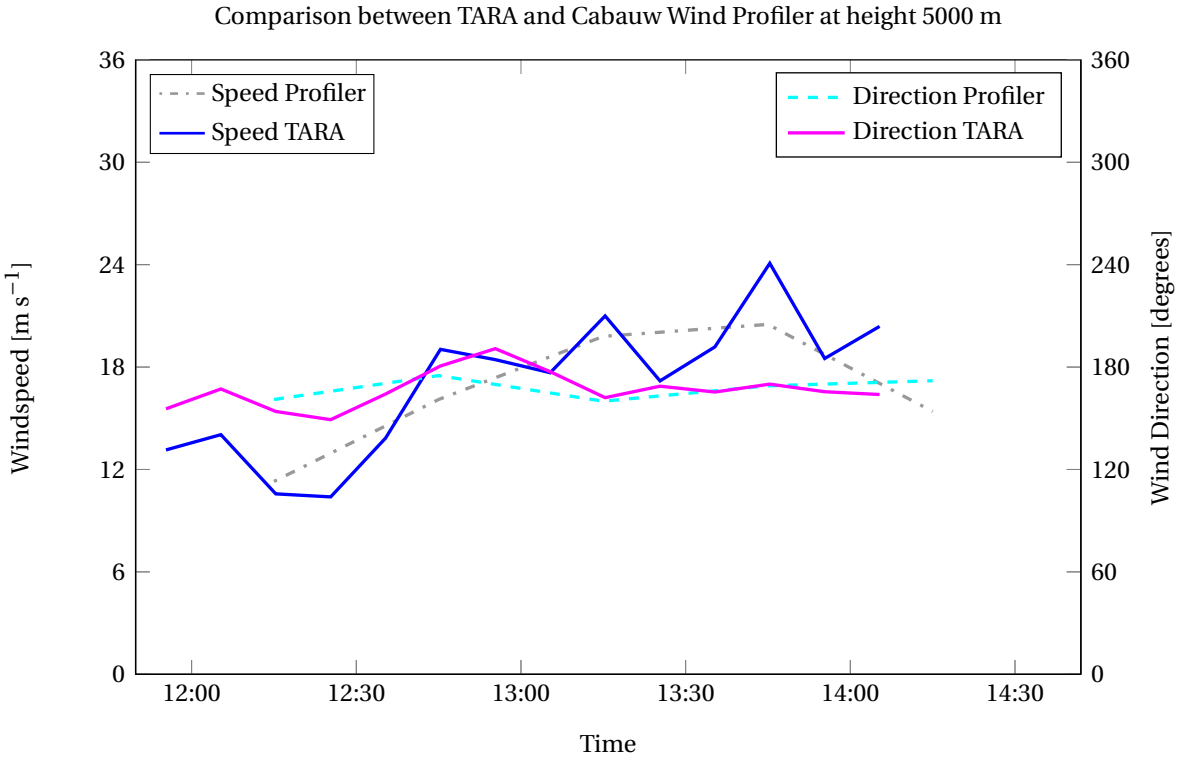

Figure 4.12: Comparison of horizontal wind velocity and wind direction between TARA and the wind profiler at Cabauw at height 5000 m.

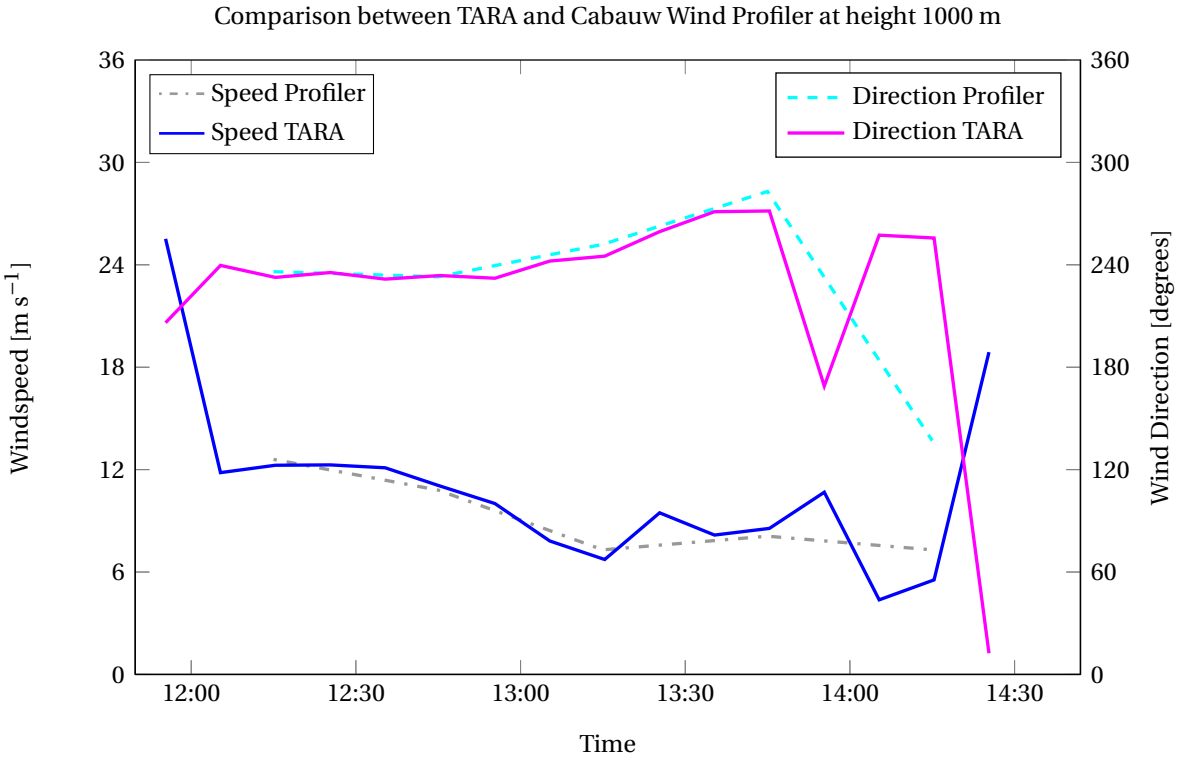

Figure 4.13: Comparison of horizontal wind velocity and wind direction between TARA and the wind profiler at Cabauw at height 1000 m. This is after using the new dealiasing technique.

4.3. CLOUD RADAR 35 GHZ

The cloud radar at Cabauw is a 35 GHz radar that is pointing to the zenith. Therefore only a vertical velocity measured and consequently no wind direction can be calculated. Because the three beams of TARA it is possible to make a calculation of the vertical velocity, besides the horizontal wind velocity and wind direction. The data from the cloud radar goes up to 13 km and, while it is about 10 km for TARA. The default comparison is made similar to the one of the wind profiler. Every 1000 m a comparison is made up to 7000 m. In figures 4.14 to 4.17 a selection of the results is shown for 1000, 3000, 5000 and 7000 m. The time resolution for both the cloud radar and for TARA is ten minutes. Although TARA profiles slantingly at 45°, there is a good agreement in vertical Doppler velocity between both radars with an averaging time of 10 minutes.

4.4. NON-PERMANENTLY STATIONED SENSORS

During the ACCEPT campaign (Oct 6 - Nov 16, 2014) two other sensors were located at Cabauw; a Doppler lidar (HALO Photonics) and a cloud radar (Mira36). Both these sensors are pointing to the zenith. With small adjustments to the m-file of the cloud radar from section 4.3, the vertical velocity of these sensors compared with TARA can be shown. October 12, 2014 is the day the comparisons, between TARA and the Non-permanently stationed sensors, are made. In figure 4.18 the profiles of the vertical Doppler velocity are depicted. The only relevant part of the day is between 15:30 and 24:00h. Again a default of steps of 1000 m in height are used and a time resolution of ten minutes is used for every sensor. A selection of the results are depicted in figures 4.19 to 4.22. The results are from measurements at heights 2000 m and 3000 m, on October 12 between 15:30 and 24:00h. The cloud radar figures 4.19 and 4.20 is very much in agreement with TARA. The lidar, however, has difficulties to penetrate through the rain. Only before 19:00h at 3000 m it shows good results. This is at the bottom of the cloud.

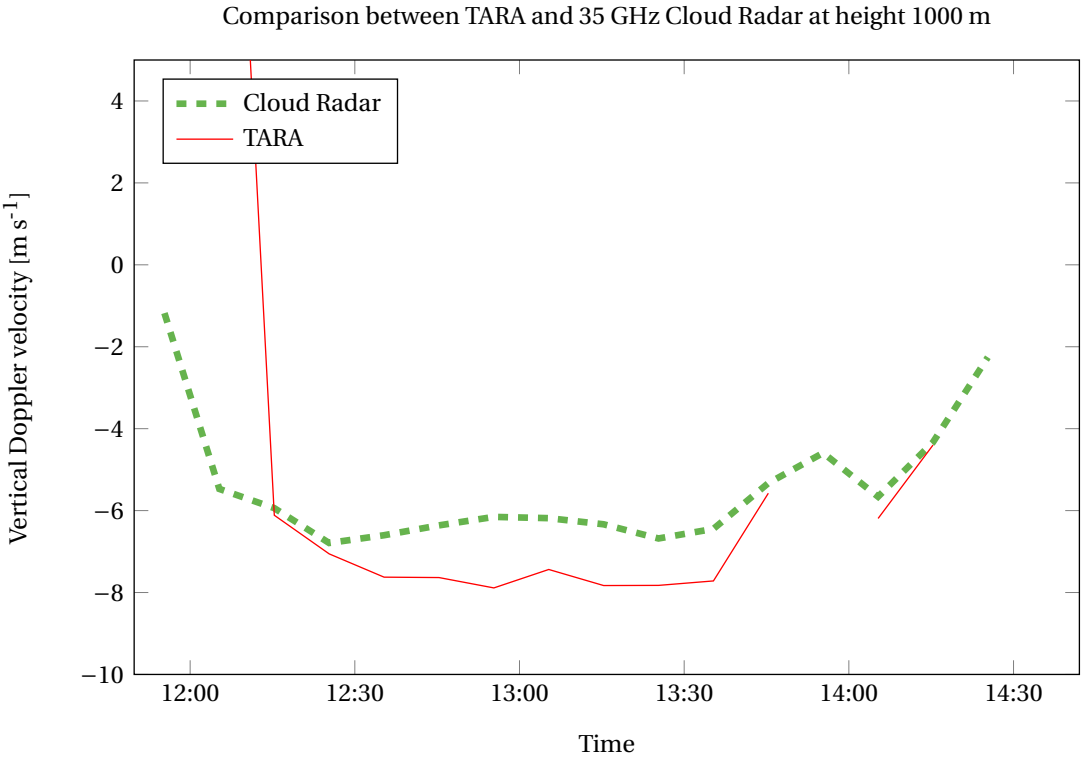

Figure 4.14: Comparison of the vertical velocity between TARA and the cloud radar at Cabauw at height 1000 m.

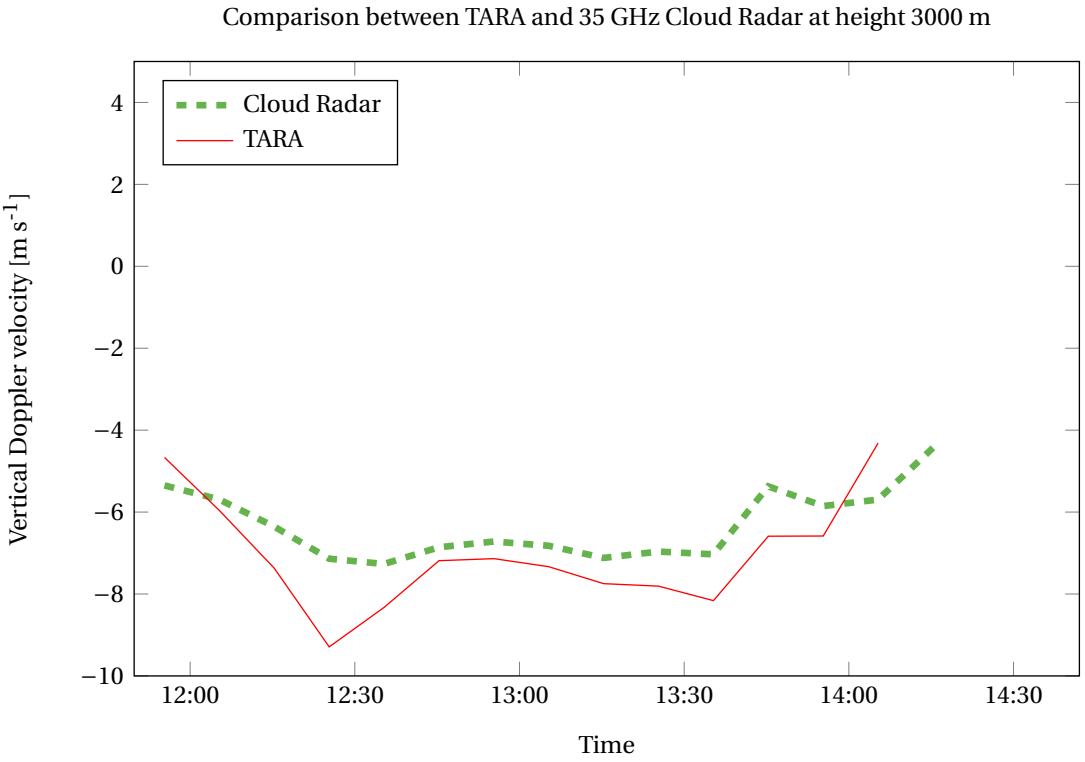

Figure 4.15: Comparison of the vertical velocity between TARA and the cloud radar at Cabauw at height 3000 m.

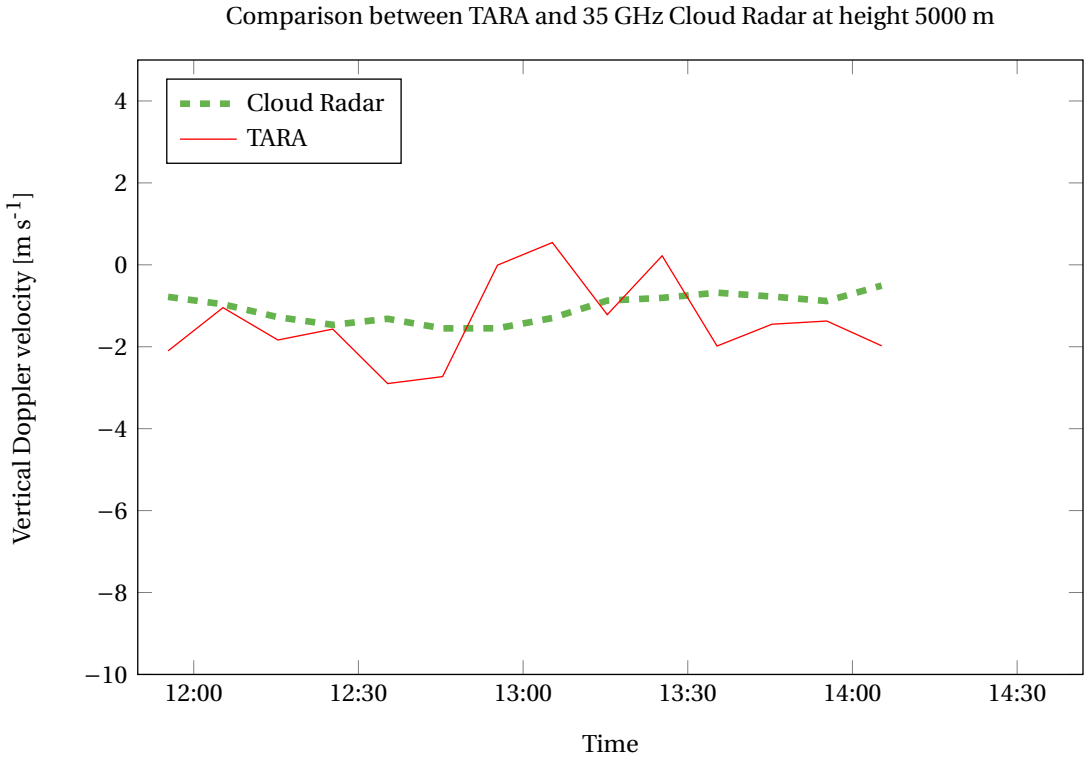

Figure 4.16: Comparison of the vertical velocity between TARA and the cloud radar at Cabauw at height 5000 m.

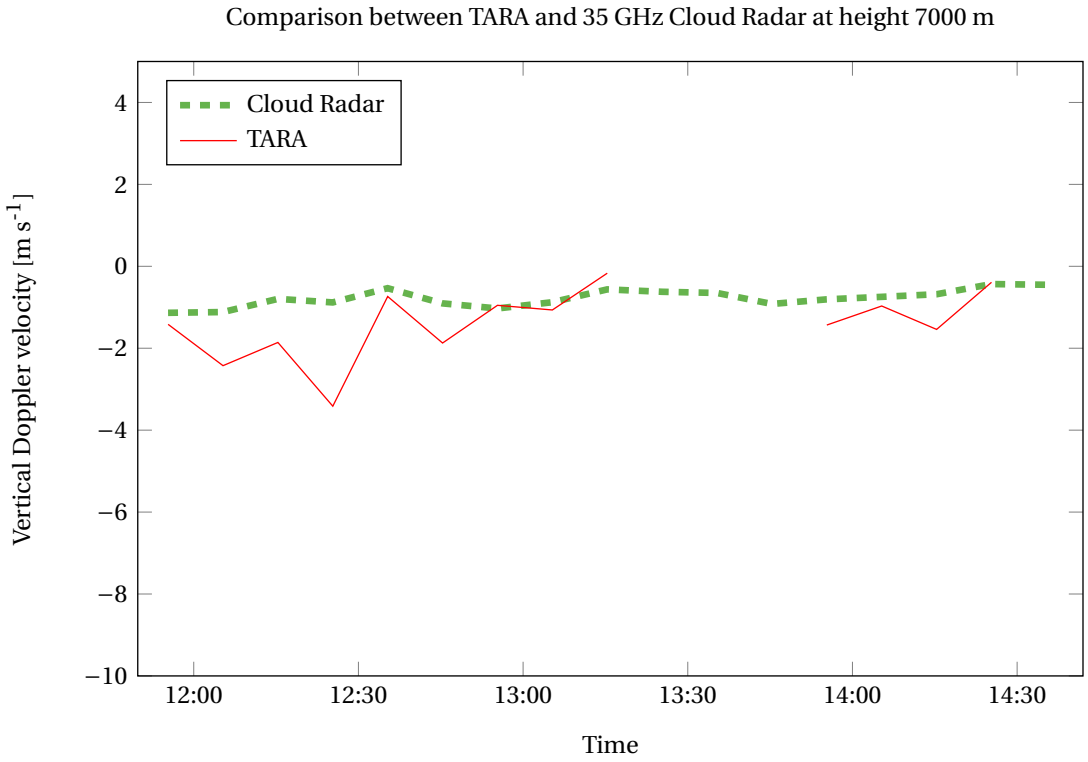

Figure 4.17: Comparison of the vertical velocity between TARA and the cloud radar at Cabauw at height 7000 m.

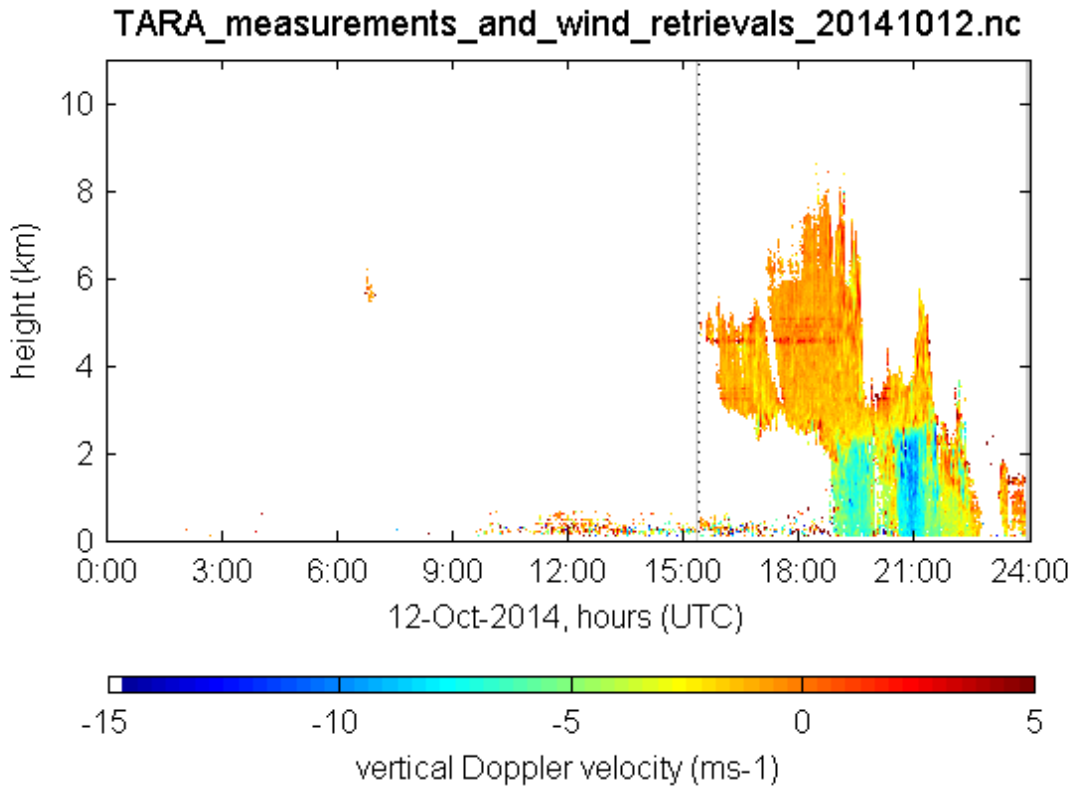

Figure 4.18: Profiles of the vertical Doppler velocity generated by TARA on October 12, 2014.

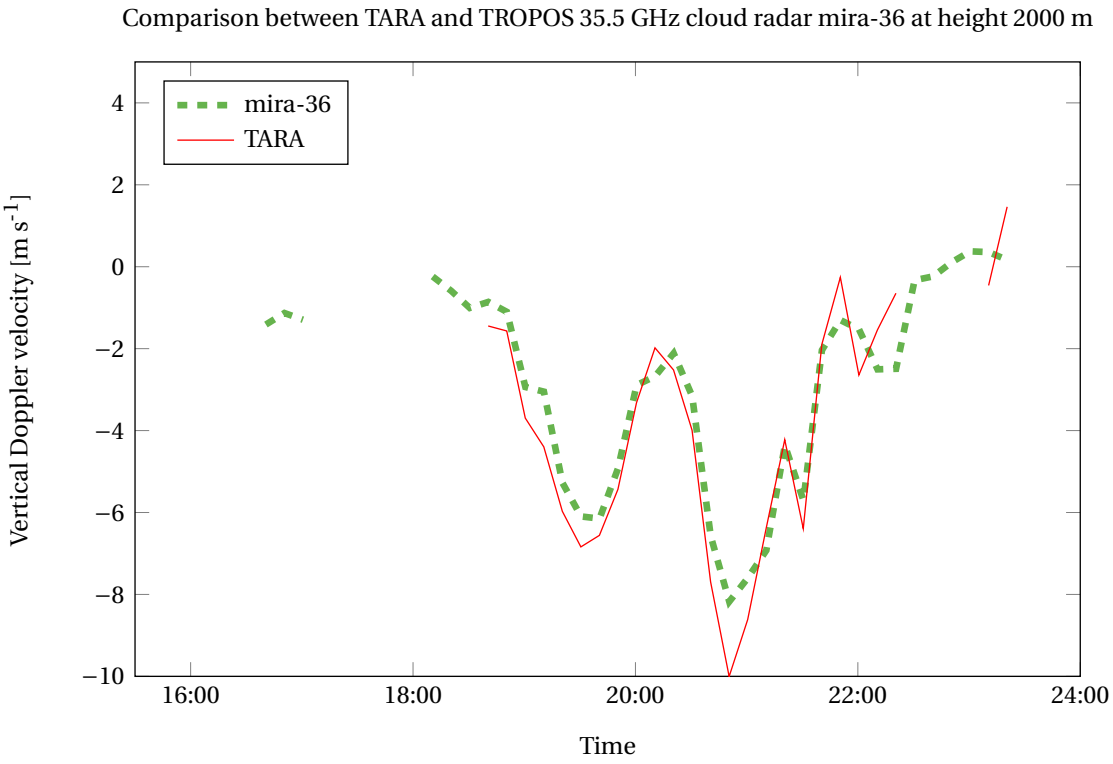

Figure 4.19: Comparison of the vertical velocity between TARA and cloud radar mira36 at Cabauw at height 2000 m.

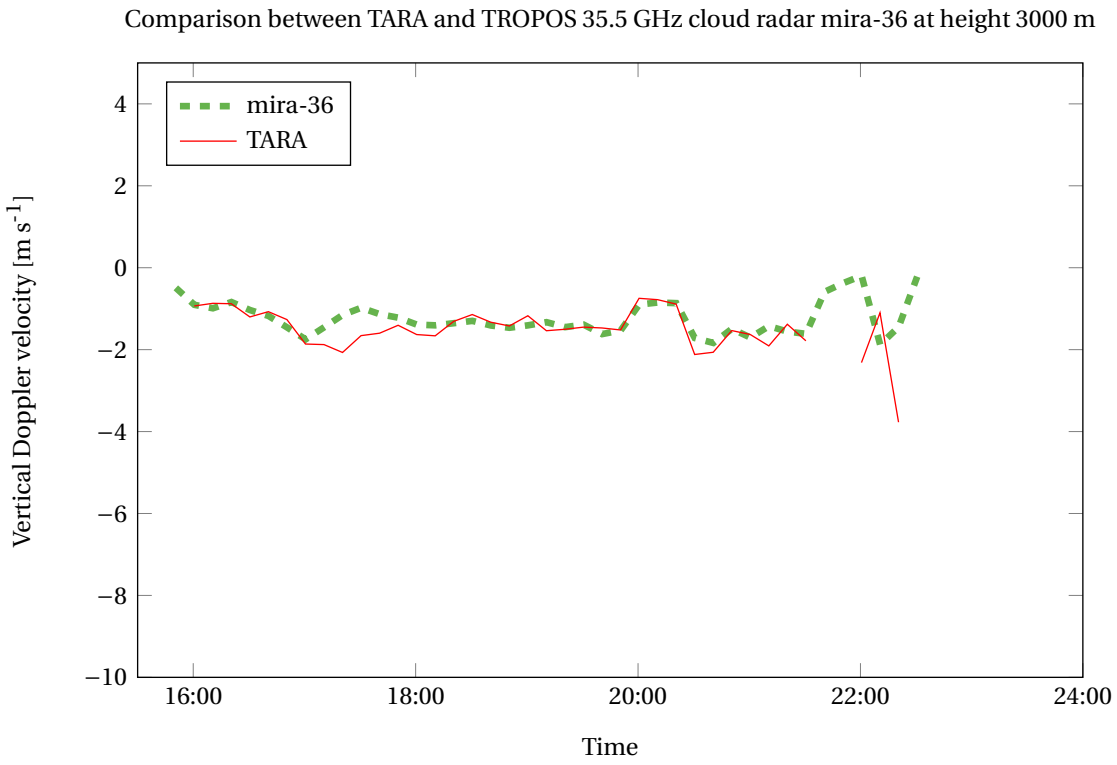

Figure 4.20: Comparison of the vertical velocity between TARA and cloud radar mira36 at Cabauw at height 3000 m.

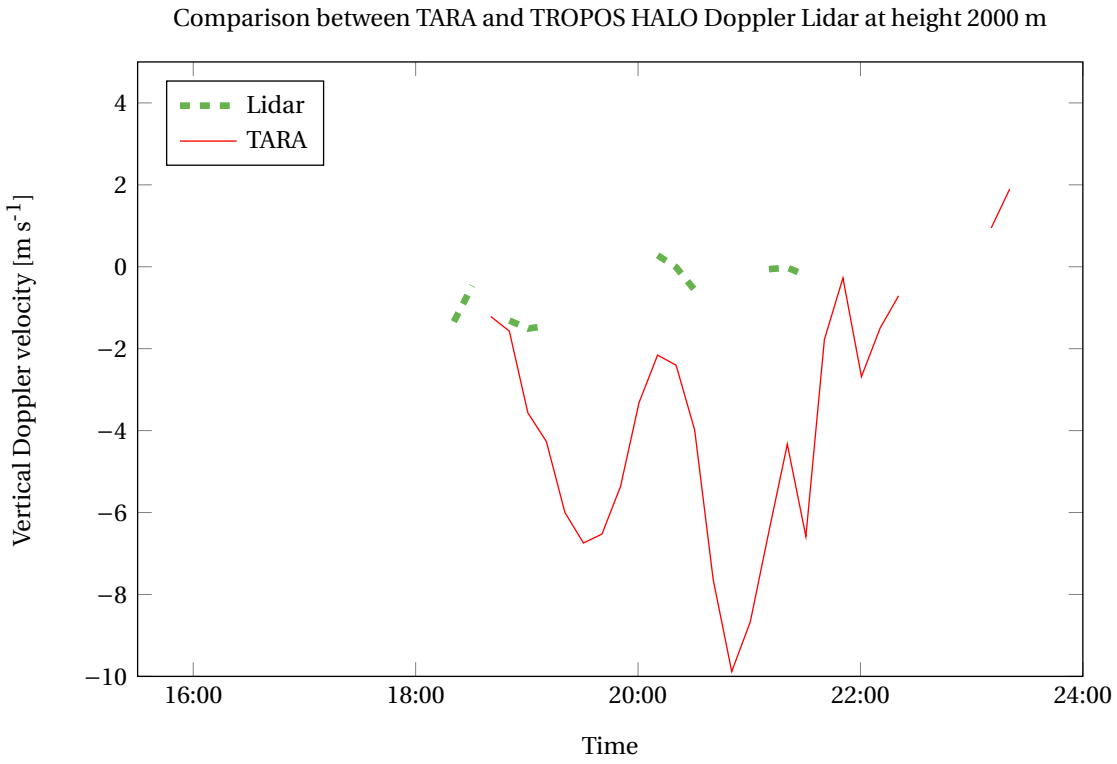

Figure 4.21: Comparison of the vertical velocity between TARA and lidar at Cabauw at height 2000 m.

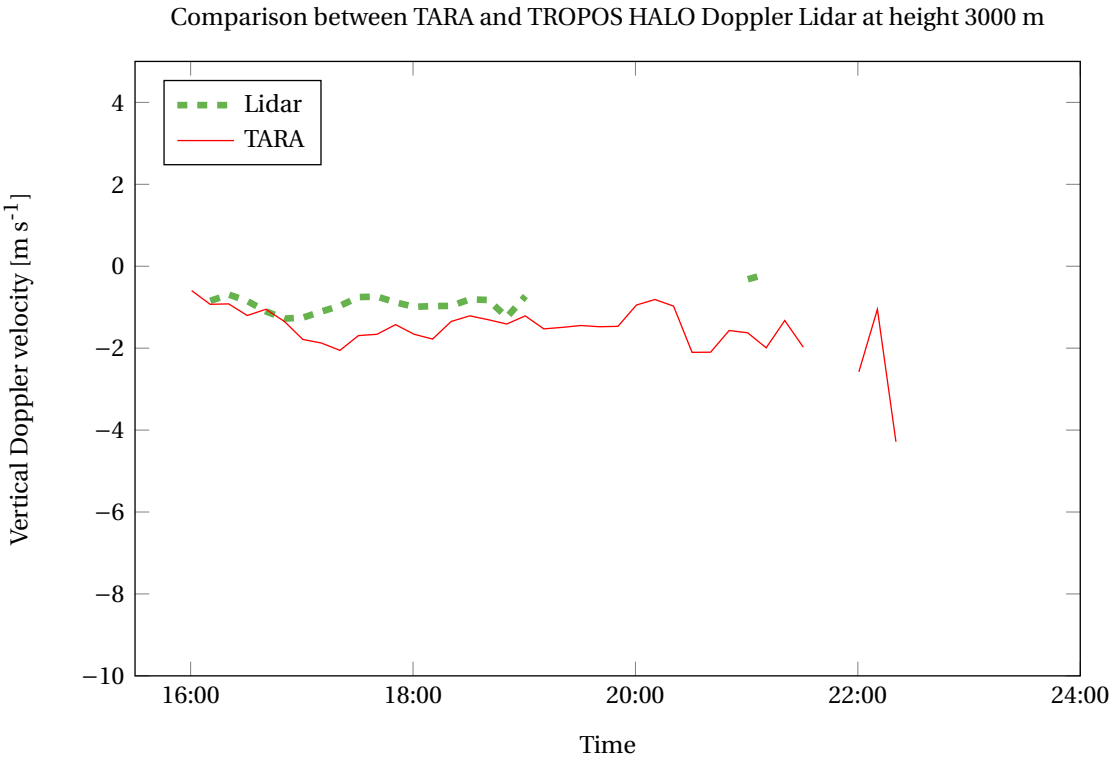

Figure 4.22: Comparison of the vertical velocity between TARA and lidar at Cabauw at height 3000 m.

5

Conclusions and Recommendations

In this chapter the findings of this research are briefly summarized, a conclusion is drawn and recommendations for future research are given.

5.1. Conclusions

The aim of this thesis has been to improve the dealiasing of the offset beams of TARA. Chapter 1 provided an introduction on Doppler FM-CW radar and in particular TARA. Also existing dealiasing techniques were discussed. These techniques could not be used or only partly used due to various reasons; user input required, more than one dimension used, changing the radar measurement specifications and the necessity for polarimetric information.

In chapter 2 the algorithms used for this research were discussed. The dealiasing can be divided into two parts. The first part is the unfolding of every individual Doppler spectrum. Two different approaches for the unfolding were presented; unfold around the maximum or unfold around the minimum of a spectrum. The method using the minimum to unfold around is found to perform better than the one using the maximum. This performance can be improved when an adaptive notch filter is available. The second part of the dealiasing is placing every correctly unfolded spectrum in the right Doppler velocity interval. Using a reference from the main beam of TARA, an estimate is made in which Doppler velocity interval a first spectrum of each of the offset beams should be placed. Then this first spectrum can be used as a reference for the next spectrum of that offset beam. This continues until all spectra are corrected. Checking whether a spectrum is in the right Doppler velocity interval can be done in different ways. Two ways were described:

- Calculating the cross correlation between a reference spectrum and the current spectrum.
- Computing the mean Doppler velocity of both the reference spectrum and the current spectrum. Then, comparing both mean Doppler velocities with each other.

It is found the method using the mean Doppler velocity is performing better than the method using the cross correlation. Especially when not all the noise can be removed, using the mean Doppler velocity is more robust. The mean Doppler velocity method is also easier to implement, adjust and explain.

Furthermore, dealing with gapped spectrograms is covered in chapter 2. When a gap is present in the data of the main beam or in the offset beam under examination (figures 2.18 to 2.21) the dealiasing process is split into two parts. This improves the result of dealiasing in case of high noise and/or clutter between the two parts, or when the two parts are in significantly different Doppler velocity ranges.

Chapter 3 presented the results and unsolved problems. The new algorithm described in chapter 2 definitely improves the dealiasing compared with the old algorithm. Main difference between the old and new algorithm is the use of the main beam as a reference. Some issues still cause the algorithm to fail, including overlapping spectra, a large difference between mean Doppler velocities and clutter.

In chapter 4 a comparison is made between the horizontal wind (velocity and direction) and the vertical Doppler velocity generated by TARA and generated by other sensors located in Cabauw. When dealiasing is successfully applied the results of TARA are comparable to the results of other sensors. The cause of the differences still present are unknown, but include the fact that TARA combines three radar resolution volumes to determine the wind field and the other sensors are looking at different volumes.

Taking all processing results into account using different algorithms, the method implemented now has the best performance. This method consists of the alternative unfolding algorithm (section 2.1.2) and the dealiasing algorithm using the mean Doppler velocity (section 2.2.2). This also answers the first question from section 1.1: How can the dealiasing of the offset beams be improved? Important aspects of the method are that no user input is required and it works in real time.

The second research question (can the main beam be used as a reference?) can be answered positively. In fact, the method discussed in this report depends on a reference taken from the main beam. Without a properly dealiased main beam, the offset beams are less likely to be dealiased correctly.

5.2. RECOMMENDATIONS

In this section some recommendations are given to possibly improve the dealiasing of the offset beams of TARA even further. An easy solution to solve aliasing in Doppler velocity is to change the radar parameters to increase the Nyquist velocity interval. The drawback here is that the maximum unambiguous range is decreased. However, this is not a problem for a S-band radar which profiles the troposphere (up to about 15 km).

On the processing side a closer look at more dimensions should be taken. Two things that might improve the dealiasing considerably are using information from each offset beam to help dealiase the other one, and use the previous spectrogram (in time) to help dealiase the current one. The latter suggestion is difficult to implement for real-time dealiasing, while the current computer system is in place. However, for off line processing it might be a viable option to look at.

Furthermore, a closer look should be taken at is spectrograms where no 'nref' was found in the main beam. Currently no dealiasing is performed when this occurs. No nref does not automatically mean there is no useful information in the main beam. Therefore it might improve the wind field estimations when dealiasing is performed when there is no nref available.

A last recommendation is to include other sensors in the dealiasing of the offset beams of TARA. As shown in chapter 4 it is possible compare sensors after the processing is done. If it is possible to collect data from different sensors in real-time and comparing those data before processing, the dealiasing of the offset beams of TARA can be improved. However, the coupling of different sensors in real-time is not expected in the near future.

BIBLIOGRAPHY

[1] Bargen, D. and Brown, R. (1980). Interactive radar velocity unfolding. In *19th Conference on Radar Meteorology of the American Meteorological Society*, pages 278–283, Miami, Florida. Preprints.

[2] Bergen, W. and Albers, S. (1988). Two- and three-dimensional de-aliasing of Doppler radar velocities. *Journal of Atmospheric and Oceanic technology*, 5:305–319.

[3] Browning, K. and Wexler, R. (1968). The determination of kinematic properties of a wind field using Doppler radar. *Journal of Applied meteorology*, 7:105–113.

[4] Doviak, R. J. and Zrnić, D. (1993). *Doppler Radar and Weather Observations*. Academic Press.

[5] Eilts, M. and Smith, S. (1990). Efficient dealiasing of Doppler velocities using local environment constraints. *Journal of Atmospheric and Oceanic technology*, 7:118–128.

[6] Gong, J., Wang, L., and Xu, Q. (2003). A three-step dealiasing method for Doppler velocity data quality control. *Journal of Atmospheric and Oceanic technology*, 20:1738–1748.

[7] Heijnen, S., Ligthart, L., and Russchenberg, H. (2000). First measurements with TARA; an S-Band transportable atmospheric radar. *Physics and Chemistry of the Earth, Part B: Hydrology, Oceans and Atmosphere*, 25(10-12):995–998.

[8] James, C. and Houze Jr, R. (2001). A real-time four-dimensional Doppler dealiasing scheme. *Journal of Atmospheric and Oceanic technology*, 18:1674–1683.

[9] Janssen, L. and Van Der Spek, G. (1985). The shape of Doppler spectra from precipitation. *Aerospace and Electronic Systems, IEEE Transactions on*, AES-21(2):208–219.

[10] KNMI. Daily weather data of the Netherlands. http://www.knmi.nl/climatology/daily_data/.

[11] Marshall, J. S. and Palmer, W. M. (1948). The distribution of raindrops with size. *Journal of Meteorology*, 5:154–166.

[12] Mori, Y. (1986). Evaluation of several "single-pass" estimators of the mean and the standard deviation of wind direction. *Journal of climate and applied meteorology*, 25(10):1387–1397.

[13] Ray, P. and Ziegler, C. (1977). Dealiasing first moment Doppler estimates. *Journal of Applied Meteorology*, 16:563–364.

[14] Tabary, P., Scialom, G., and Germann, U. (2001). Real-time retrieval of the wind from aliased velocities measured by Doppler radars. *Journal of Atmospheric and Oceanic technology*, 18:875–882.

[15] Unal, C. (2009). Spectral polarimetric radar clutter suppression to enhance atmospheric echoes. *Journal of Atmospheric and Oceanic Technology*, 26(9):1781–1797.

[16] Unal, C., Dufournet, Y., Otto, T., and Russchenberg, H. (2012). The new real-time measurement capabilities of the profiling TARA radar. In *Seventh European Conf. on Radar in Meteorology and Hydrology (ERAD)*, Toulouse, France. Preprints.

[17] Unal, C. and Moisseev, D. N. (2004). Combined Doppler and polarimetric radar measurements: correction for spectrum aliasing and nonsimultaneous polarimetric measurements. *Journal of Atmospheric and Oceanic Technology*, 21(3):443–456.

[18] Warner, J. (1969). The microstructure of cumulus cloud. part I. general features of the droplet spectrum. *Journal of the Atmospheric Sciences*, 26(5):1049–1059.

[19] Xu, Q., Nai, K., Wei, L., Zhang, P., Liu, S., and Parrish, D. (2011). A VAD-based dealiasing method for radar velocity data quality control. *Journal of Atmospheric and Oceanic technology*, 28:50–62.

[20] Zrnić, D. and Mahapatra, P. (1985). Two methods of ambiguity resolution in pulse Doppler weather radars. *Aerospace and Electronic Systems, IEEE Transactions on*, AES-21(4):470–483.

Appendices

A

Maximum Allowed Horizontal Wind Speed

Table A.1: The maximum allowed horizontal wind speed for different directions starting at the x-axis of TARA. With vertical wind velocity $V_z = -10, -5$ and 0 m s^{-1}. When TARA is located in Cabauw, the x-axis is at 246.5° to the North. When the maximum is exceeded, the dealiasing for this beam will fail partly or complete, depending on the horizontal wind speed. The elevation angle α is 45°. When the elevation angle increases, the maximum allowed horizontal wind speed also increases and vice versa. The calculations are done using equations (2.1) and (3.1)

V_z = -10 (m s^{-1})				
V_{MB}	V_{OB1}	V_{OB2}	TARA axis	North
V_{max} (m s^{-1})	V_{max} (m s^{-1})	V_{max} (m s^{-1})	Direction (°)	Direction (°)
53.6	72.7	55.9	0	246.5
61.9	83.9	52.9	30	276.5
107.3	145.4	67.5	60	306.5
inf	inf	147.5	90	336.5
147.3	214.6	441.6	120	6.5
85.0	123.9	112.2	150	36.5
73.6	107.3	75.9	180	66.5
85.0	123.9	71.9	210	96.5
147.3	214.6	91.6	240	126.5
inf	inf	200.3	270	156.5
107.3	145.4	325.2	300	186.5
61.9	83.9	82.6	330	216.5

V_z = -5 (m s^{-1})				
V_{MB}	V_{OB1}	V_{OB2}	TARA axis	North
$V_{\max}$ (m s^{-1})	$V_{\max}$ (m s^{-1})	$V_{\max}$ (m s^{-1})	Direction (°)	Direction (°)
58.6	81.3	60.9	0	246.5
67.7	93.9	57.7	30	276.5
117.3	162.7	73.5	60	306.5
inf	inf	160.7	90	336.5
137.3	197.3	412.5	120	6.5
79.3	113.9	104.8	150	36.5
68.6	98.7	70.9	180	66.5
79.3	113.9	67.2	210	96.5
137.3	197.3	85.6	240	126.5
inf	inf	187.1	270	156.5
117.3	162.7	354.3	300	186.5
67.7	93.9	90.0	330	216.5

V_z = 0 (m s^{-1})				
V_{MB}	V_{OB1}	V_{OB2}	TARA axis	North
$V_{\max}$ (m s^{-1})	$V_{\max}$ (m s^{-1})	$V_{\max}$ (m s^{-1})	Direction (°)	Direction (°)
63.6	90.0	65.9	0	246.5
73.5	103.9	62.4	30	276.5
127.3	180.0	79.6	60	306.5
inf	inf	173.9	90	336.5
127.3	180.0	383.4	120	6.5
73.5	103.9	97.4	150	36.5
63.6	90.0	65.9	180	66.5
73.5	103.9	62.4	210	96.5
127.3	180.	79.6	240	126.5
inf	inf	173.9	270	156.5
127.3	180.0	383.4	300	186.5
73.5	103.9	97.4	330	216.5

B

MEAN DOPPLER VELOCITY PROFILES

In this appendix the mean Doppler velocity profiles are shown using the old algorithm and the new algorithm. Most of the time aliasing can be recognized by colors that are outside the color bar. Velocities aliased on the positive side are colored brown and on the negative side white is outside the color bar. When TARA is in the standard mode the main beam has an elevation angle of 45°. This means offset beam 1 has an elevation of 60° and offset beam 2 43°.

The first example is of data with a gap just above 6000 m. This example is from July 26, 2013. The second example is of data with just a cloud with precipitation. This example is from September 9, 2013. The third example is of a cloud without precipitation. This example is from May 29, 2013.

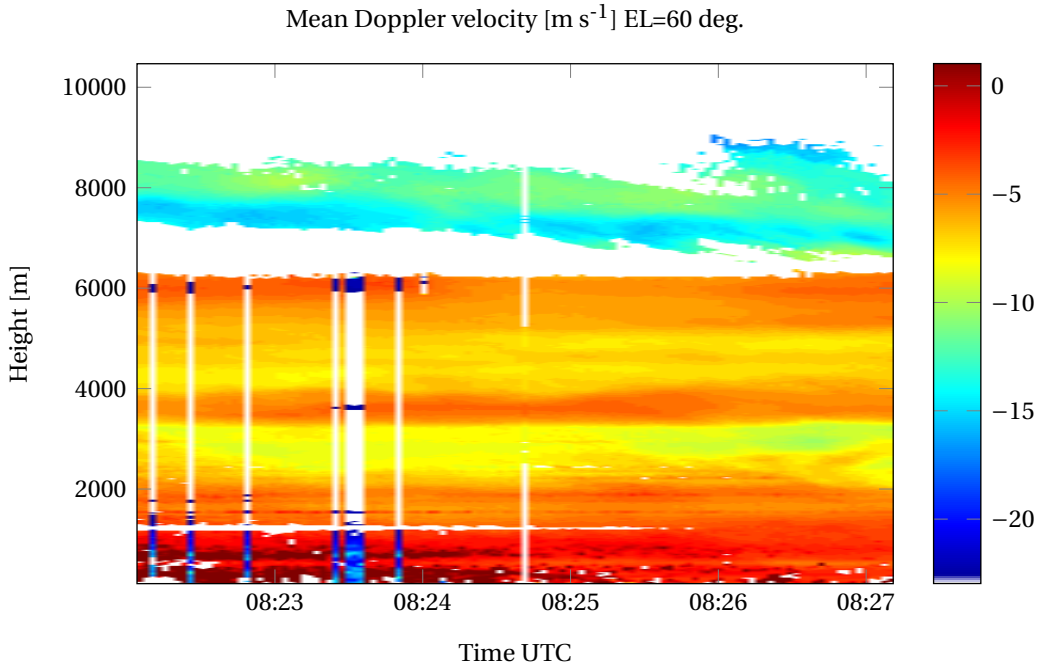

Figure B.1: Profiles of the mean Doppler velocity of offset beam 1 on July 26, 2013. These are the profiles generated with the old dealiasing algorithm. It is clear aliasing occurs in some spectrograms before 08:24. In figure B.2 the profiles generated with the new algorithm are depicted.

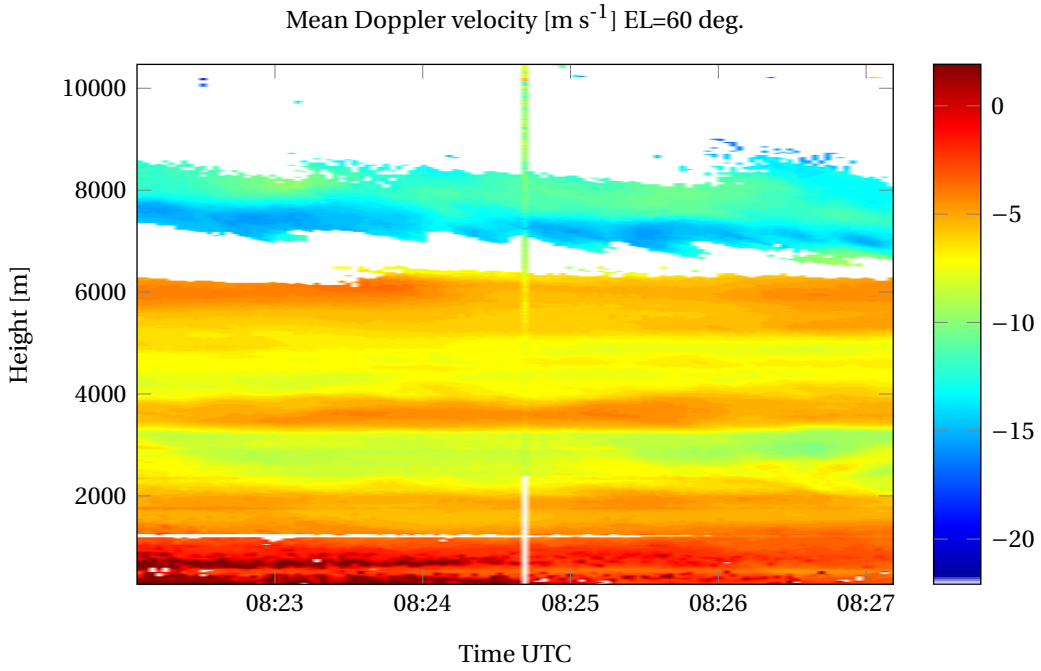

Figure B.2: Profiles of the mean Doppler velocity of offset beam 1 on July 26, 2013. These are the profiles generated with the new dealiasing algorithm. In figure B.1 the profiles generated with the old algorithm are depicted. The aliasing around before 08:24 is solved.

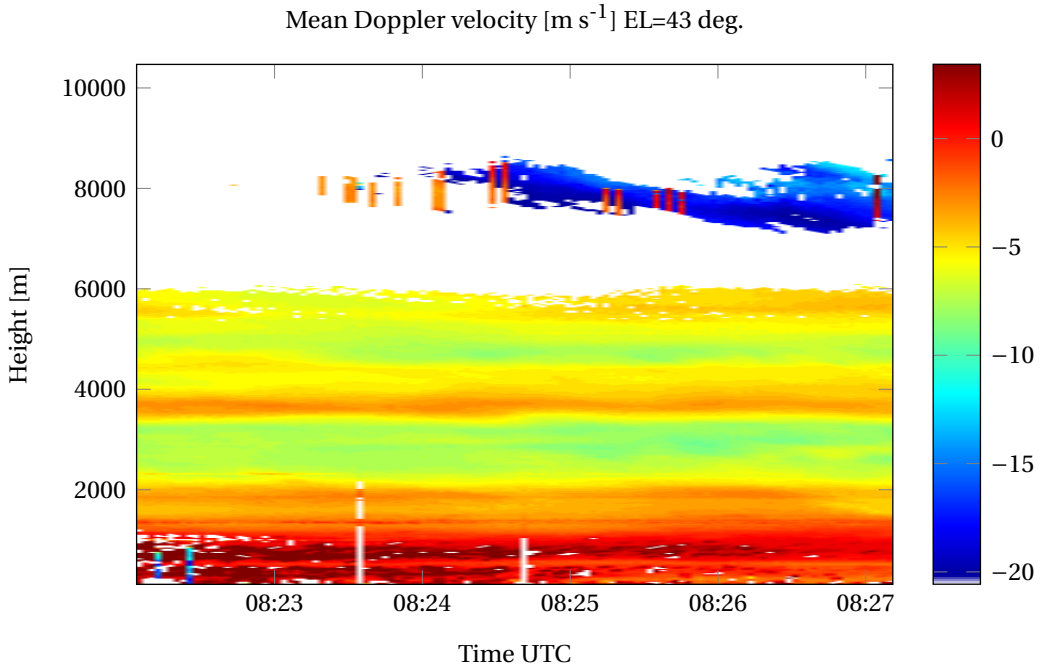

Figure B.3: Profiles of the mean Doppler velocity of offset beam 2 on July 26, 2013. These are the profiles generated with the old dealiasing algorithm. It is clear aliasing occurs in the part around height 8000 m. Note that because the color bar ends just below -20 m s^{-1}, some velocities around height 8000 m are colored white. In figure B.4 the profiles generated with the new algorithm are depicted.

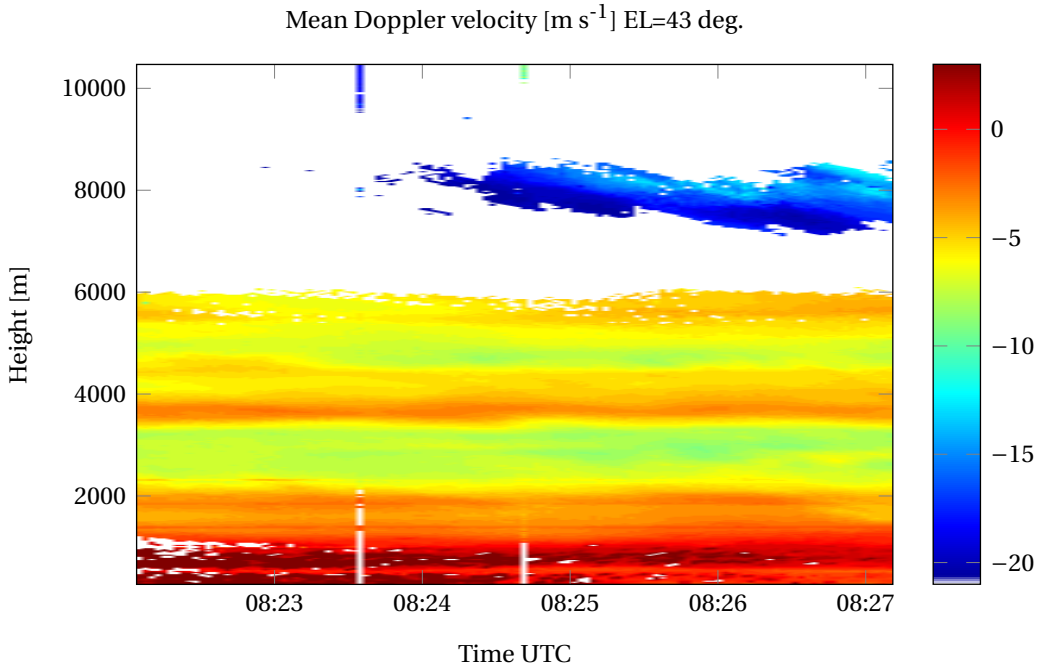

Figure B.4: Profiles of the mean Doppler velocity of offset beam 2 on July 26, 2013. These are the profiles generated with the new dealiasing algorithm. In figure B.3 the profiles generated with the old algorithm are depicted. The aliasing at height around 8000 m is solved.

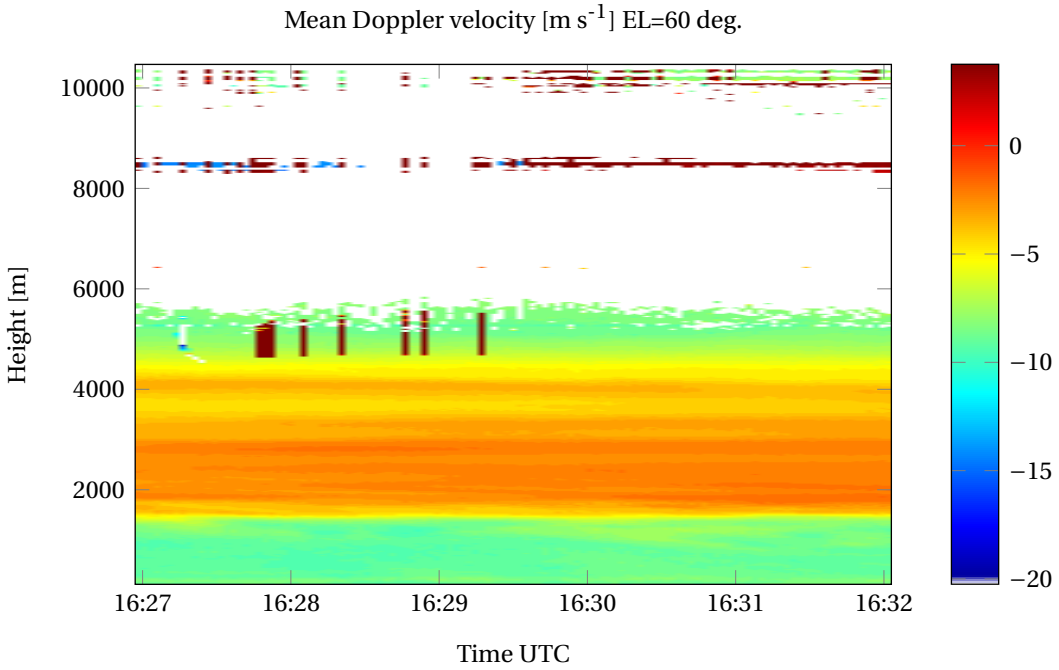

Figure B.5: Profiles of the mean Doppler velocity of offset beam 1 on September 9, 2013. These are the profiles generated with the old dealiasing algorithm. It is clear aliasing occurs in some spectrograms at heights around 5000 m. The velocities at heights 8500 m and 10000 m are radar artifacts (receiver saturation). In figure B.6 the profiles generated with the new algorithm are depicted.

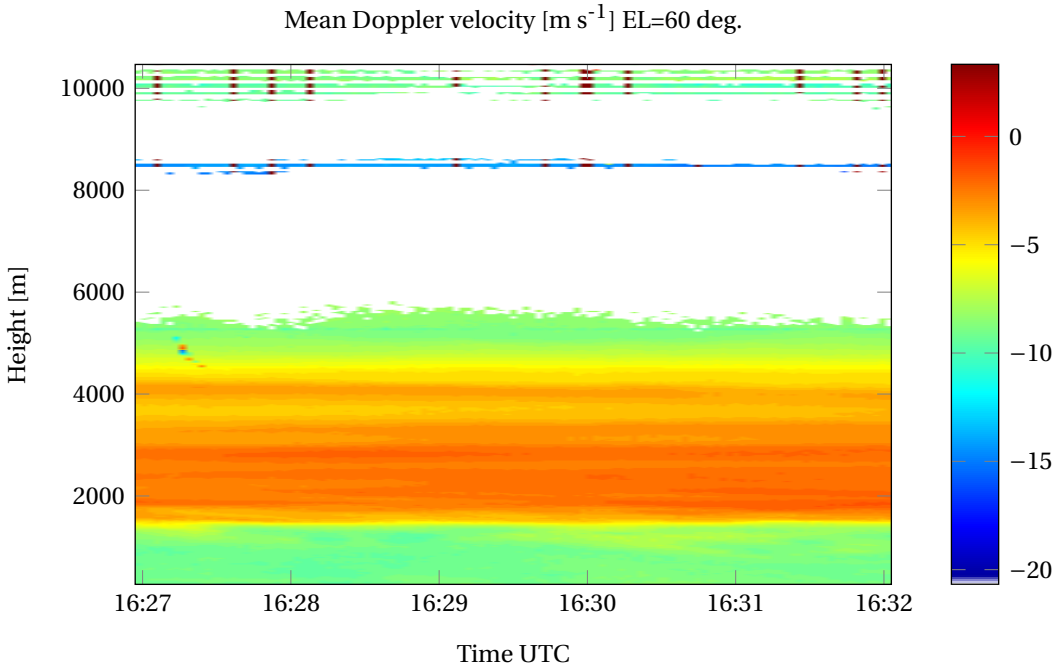

Figure B.6: Profiles of the mean Doppler velocity of offset beam 1 on September 9, 2013. These are the profiles generated with the new dealiasing algorithm. In figure B.5 the profiles generated with the old algorithm are depicted. The aliasing in the parts around 5000 m is solved.

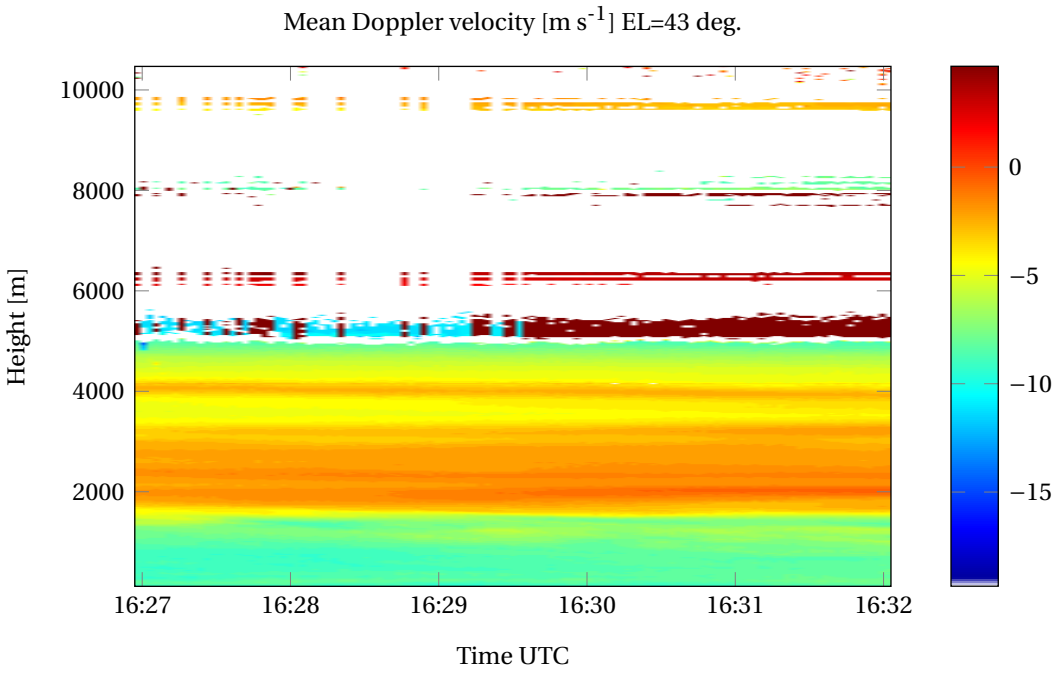

Figure B.7: Profiles of the mean Doppler velocity of offset beam 2 on September 9, 2013. These are the profiles generated with the old dealiasing algorithm. It is clear aliasing occurs a lot in the part around height 5000 m. The velocities around heights 6250 m, 8000 m and 9700 m are radar artifacts. In figure B.8 the profiles generated with the new algorithm are depicted.

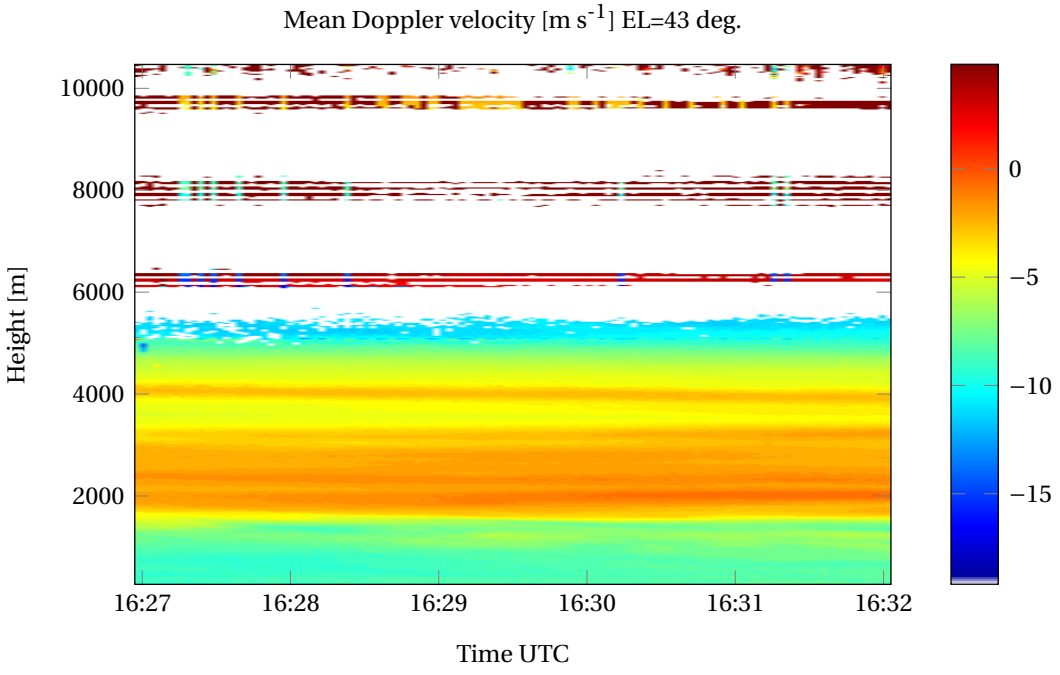

Figure B.8: Profiles of the mean Doppler velocity of offset beam 2 on September 9, 2013. These are the profiles generated with the new dealiasing algorithm. In figure B.7 the profiles generated with the old algorithm are depicted. The aliasing at heights around 5000 m is solved.

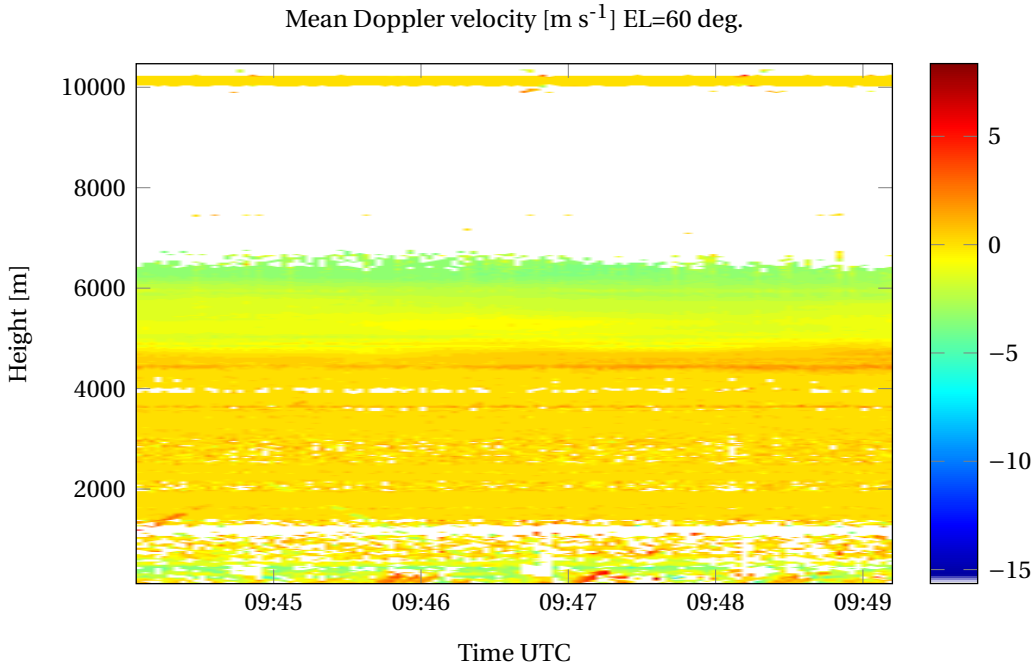

Figure B.9: Profiles of the mean Doppler velocity of offset beam 1 on May 29, 2013. These are the profiles generated with the old dealiasing algorithm. In figure B.10 the profiles generated with the new algorithm are depicted.

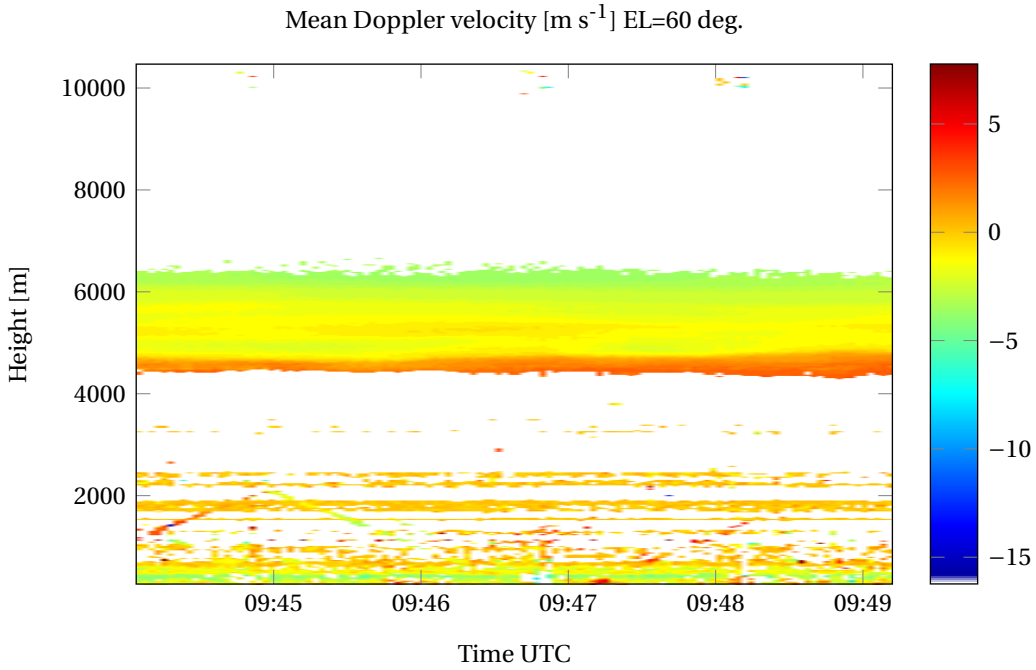

Figure B.10: Profiles of the mean Doppler velocity of offset beam 1 on May 29, 2013. These are the profiles generated with the new dealiasing algorithm. In figure B.9 the profiles generated with the old algorithm are depicted. Because of a higher SNR and the notch filter around 0 m s^{-1} a lot of noise and clutter is removed compared with the old algorithm.

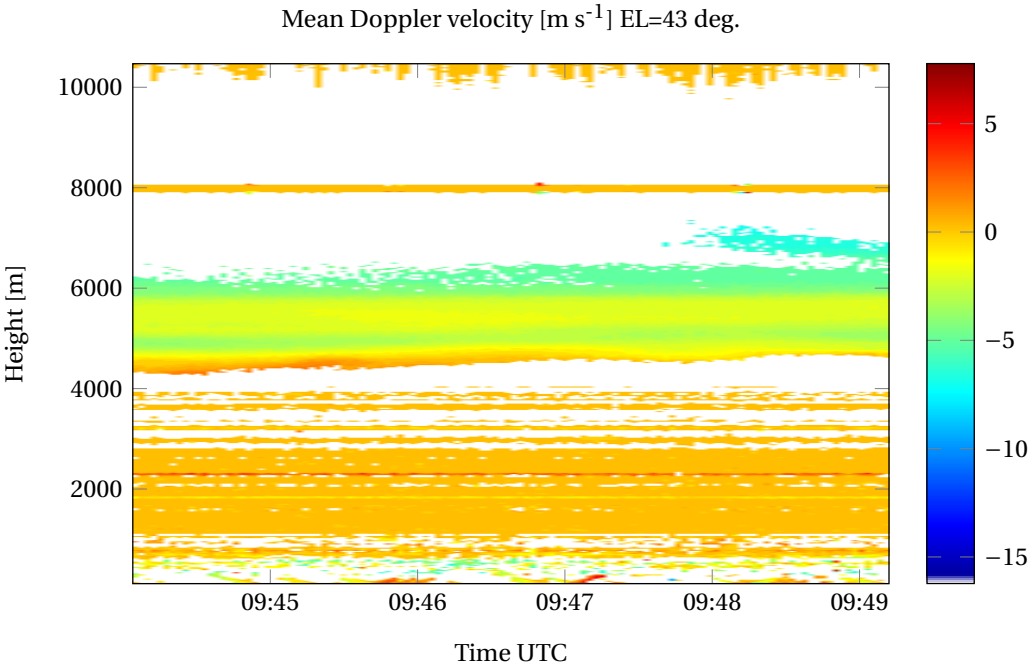

Figure B.11: Profiles of the mean Doppler velocity of offset beam 2 on May 29, 2013. These are the profiles generated with the old dealiasing algorithm. In figure B.12 the profiles generated with the new algorithm are depicted.

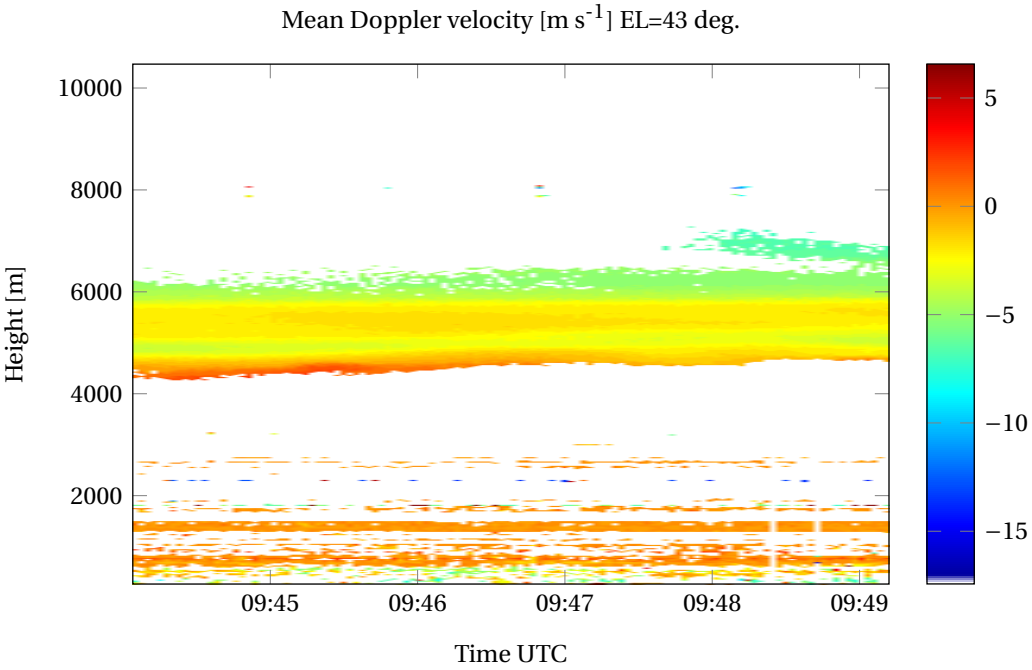

Figure B.12: Profiles of the mean Doppler velocity of offset beam 2 on May 29, 2013. These are the profiles generated with the new dealiasing algorithm. In figure B.11 the profiles generated with the old algorithm are depicted. For OB2 the SNR is not higher compared with the old algorithm, here only the clutter is removed due to the notch filter around 0 m s^{-1}.